

Electronic Thesis and Dissertation Repository

8-10-2017 12:00 AM

Crystal Engineering of Active Pharmaceutical Ingredients with Low Aqueous Solubility and Bioavailability

Jenna M. Skieneh, *The University of Western Ontario*

Supervisor: Sohrab Rohani, *The University of Western Ontario*

A thesis submitted in partial fulfillment of the requirements for the Master of Engineering Science degree in Chemical and Biochemical Engineering

© Jenna M. Skieneh 2017

Follow this and additional works at: <https://ir.lib.uwo.ca/etd>

 Part of the [Medicinal-Pharmaceutical Chemistry Commons](#), and the [Other Chemical Engineering Commons](#)

Recommended Citation

Skieneh, Jenna M., "Crystal Engineering of Active Pharmaceutical Ingredients with Low Aqueous Solubility and Bioavailability" (2017). *Electronic Thesis and Dissertation Repository*. 4708.
<https://ir.lib.uwo.ca/etd/4708>

This Dissertation/Thesis is brought to you for free and open access by Scholarship@Western. It has been accepted for inclusion in Electronic Thesis and Dissertation Repository by an authorized administrator of Scholarship@Western. For more information, please contact wlsadmin@uwo.ca.

Abstract

Approximately 75% of new molecular entities approved by the Food and Drug Administration (FDA) for use in the pharmaceutical industry are found to have poor aqueous solubility. This undesirable attribute leads to consequences such as higher doses required to reach therapeutic levels, greater vulnerability to food effects, lesser fraction absorbed in the small intestine and damage to the environment due to increased quantity of excretion. The addition of an excipient (i.e. a FDA approved inactive ingredient) to the molecular structure of an active pharmaceutical ingredient (API) through intermolecular bonding is of growing interest because the properties of the API can be tuned without further clinical testing. Crystal engineering utilizes the knowledge of intermolecular interactions to design new solids with improved properties (e.g. solubility, stability, bioavailability, dissolution rates). In this thesis, these techniques are applied to increase the solubility of three APIs with low solubility: esomeprazole magnesium, curcumin and rufinamide. Through an extensive screening process, novel solid states were discovered including a water/butanol solvate of esomeprazole magnesium and a co-amorphous mixture comprised of curcumin and folic acid dihydrate. The co-amorphous mixture was found to have increased dissolution rate compared to curcumin and can be repositioned as a prenatal drug. Characterization of these products include powder and single crystal X-ray diffraction, differential scanning calorimetry, thermogravimetric analysis, Fourier Transform infrared spectroscopy, solution nuclear magnetic resonance spectroscopy and dynamic vapour sorption. Screening of rufinamide did not lead to the discovery of any new forms, but the refined molecular structure of the metastable form is reported.

Keywords

Crystallization, co-amorphous mixtures, solvates, eutectics, co-crystals, thermal analysis, solid-state characterization, dissolution studies

Co-Authorship Statement

Chapter 2

Article Title: A Review of Crystal Engineering via Non-Ionic Excipient Addition to Increase Drug Solubility and Bioavailability
Authors: Jenna Skieneh, Sohrab Rohani
Article Status: Submitted to Crystal Growth and Design
Jenna Skieneh conducted the literature review and wrote the manuscript. Prof. Sohrab Rohani supervised the work and reviewed the manuscript.

Chapter 3

Article Title: Crystallization of Esomeprazole Magnesium Water/Butanol Solvate
Authors: Jenna Skieneh, Bahareh Khalili, Stephen Horne, Sohrab Rohani
Article Status: Submitted to Crystal Growth and Design
Jenna Skieneh and Dr. Bahareh Khalili designed and performed the experiments. Jenna Skieneh wrote the manuscript. Molecular structure refinement was performed by Dr. Bahareh Khalili. Prof. Sohrab Rohani and Dr. Stephen Horne supervised the work, provided expertise and reviewed the manuscript.
Skieneh, J.; Khalili Najafabadi, B.; Horne, S.; Rohani, S. <i>Molecules</i> 2016 , <i>21</i> (544), 1–10.

Chapter 4

Article Title: Co-amorphous form of curcumin-folic acid dihydrate with increased dissolution rate
Authors: Jenna Skieneh, Indumathi Sathisaran, Sameer Dalvi, Sohrab Rohani
Article Status: Submitted to Crystal Growth and Design
Jenna Skieneh conducted the research and wrote the manuscript. Indumathi ran DSC and PXRD for co-former screening. Prof. Sohrab Rohani and Prof. Sameer Dalvi supervised the work and reviewed the manuscript.

Chapter 5

Article Title: Efforts to Increase the Solubility of Rufinamide
Authors: Jenna Skieneh, Bahareh Khalili, Sohrab Rohani
Article Status: Submitted to Journal of Crystal Growth Crystal Growth
Jenna Skieneh conducted and designed the experiments and wrote the manuscript. Dr. Bahareh Khalili refined the molecular structure. Prof. Sohrab Rohani supervised the work and reviewed the manuscript.

Acknowledgments

I would like to thank my supervisor, Dr. Sohrab Rohani, for guiding and encouraging me throughout my degree. With his assistance, I could make the most of my time at Western. His direction and patience have been greatly appreciated throughout the last two years. The dedication and enthusiasm he has surrounding his work is truly uplifting.

Next, I would like to thank my lab members at Western University for their experienced opinions and their companionship throughout my degree. I especially send thanks to Bahareh Khalili, not only for her assistance in the lab, but for her valuable friendship. She shared her knowledge of crystallization, taught me how to become a proficient researcher and encouraged me when results seemed hopeless. Without Bahareh, I would not have had nearly as much success in my degree, nor as exciting of a future. I also recognize Hecham Omar, Salman Bukhari and Zhenguo Gao for their advice and accompaniment during my projects, and Allison Crouter for making my time at Western more entertaining and enjoyable. Special thanks to Dr. Paul Boyle for his knowledge and assistance in X-ray crystallography.

I would also like to thank Mitacs and MHRD for awarding me the opportunity to conduct research abroad at IIT Gandhinagar. I am truly grateful that I could work with Prof. Sameer V. Dalvi; I admire his knowledge, the close relationships that he has with his students and his devotion to being involved in their research projects. A special acknowledgment is given to Indumathi Sathisaran and Komal (Didi) Pandey for their assistance and companionship throughout my internship.

Within the department there are numerous thanks that I need to give. Many appreciations go out to Ashley Jokhu and Cole Handsaeme for their assistance and their patience with my frequent questions and casual visits. Thank you to Dr. Barghi, Dr. Briens and Dr. Hudson for being on my examination committee, and I hope that you enjoy reading this work.

Finally, I would like to acknowledge my close family and friends for their reassurance and comfort as I furthered my education. An extremely distinct appreciation goes out to my mother. Without fail, she supported, encouraged and consoled me throughout the ups and downs of this journey.

Table of Contents

Abstract.....	i
Co-Authorship Statement.....	ii
Acknowledgments.....	iv
Table of Contents	v
List of Tables	viii
List of Figures	ix
List of Abbreviations	xiv
Chapter 1	1
1 Introduction.....	1
1.1 Objectives	2
1.2 Motivation.....	2
1.3 Background.....	3
1.3.1 Esomeprazole Magnesium	3
1.3.2 Curcumin.....	5
1.3.3 Rufinamide.....	7
1.4 Thesis Outline	9
1.5 References.....	9
Chapter 2.....	12
2 A Review of Crystal Engineering via Non-Ionic Excipient Addition to Increase Drug Solubility and Bioavailability	12
2.1 Introduction.....	12
2.2 Co-amorphous Mixtures	15
2.3 Co-Crystals	20
2.4 Eutectics	26
2.5 Solvates.....	29

2.6	Excipient Selection and Solid State Screening	34
2.7	Summary	39
2.8	References	41
Chapter 3		51
3	Crystallization of Esomeprazole Magnesium Water/Butanol Solvate	51
3.1	Introduction	51
3.2	Materials and Methods	54
3.3	Results and Discussion	54
3.4	Conclusion	64
3.5	References	65
Chapter 4		68
4	Co-amorphous form of curcumin-folic acid dihydrate with increased dissolution rate	68
4.1	Introduction	68
4.2	Experimental	72
4.2.1	Materials and Instruments	72
4.2.2	Preparation and characterization of curcumin and folic acid dihydrate (CUR-FAD) co-amorphous mixtures	72
4.2.3	Equilibrium solubility and powder dissolution studies	72
4.3	Results and Discussion	73
4.3.1	Solid State Formation	73
4.3.2	Solubility and Dissolution Rate Tests	80
4.3.3	Formation of Curcumin Form II	82
4.4	Conclusion	83
4.5	References	84
Chapter 5		90
5	Efforts to Increase the Solubility of Rufinamide	90

5.1 Introduction.....	90
5.2 Materials and Methods.....	92
5.3 Results and Discussion	92
5.3.1 Rufinamide Modification B	93
5.3.2 Further Screening.....	97
5.3.3 Results from Screening with Citric Acid	99
5.4 Conclusion	102
5.5 References.....	103
Chapter 6.....	105
6 Conclusion and Recommendations	105
6.1 Conclusions.....	105
6.2 Recommendations.....	107
Curriculum Vitae	112

List of Tables

Table 1.1: Some symptoms and complications of GERD.	3
Table 2.1: Preparation of Co-amorphous Systems.	17
Table 2.2: Some Preparation Techniques for Co-Crystal Synthesis.	22
Table 2.3: Cases Representing Some Synthesis Techniques of Eutectic Mixtures.	27
Table 2.4: Cases Representing the Synthesis of Different Types of Solvate Systems.	30
Table 2.5: Inactive Ingredient Search for Approved Drug Products, EPB.	35
Table 2.6: Types of Conclusions from the Selection Committee on GRAS Substances.	36
Table 3.1: Summary of Crystal Data.	56
Table 3.2: IR spectroscopy absorption frequencies and corresponding functional groups. ...	61
Table 4.1: Known Curcumin Co-crystals and Their Intrinsic Dissolution Rates.	71
Table 4.2: Known Curcumin Eutectics and Their Intrinsic Dissolution Rates.	71
Table 4.3: FDA Approved Potential Co-formers for Curcumin Co-crystals.	74
Table 5.1: Some polymorphs of rufinamide.	91
Table 5.2: Summary of Crystal Data of Rufinamide Modification B.	94
Table 5.3: FDA approved co-formers from CSD screening with rufinamide modification B	98
Table 5.4: Attempted acids for synthesis of rufinamide modification B.	102

List of Figures

Figure 1.1: General scheme of possible solid states formation via excipient addition where green is API; blue, yellow and orange are excipients capable of intermolecular bonding; and blue is solvent molecules.	1
Figure 1.2: (a) Nexium, the marketed version of esomeprazole magnesium and (b) the structure of esomeprazole.	4
Figure 1.3: Synthesis for large scale production of esomeprazole magnesium that results in sole presence of (S)-isomer of omeprazole.	4
Figure 1.4: (a) Curcuma longa, also known as turmeric root, is a common spice used in Asian cooking and (b) the chemical structure of curcumin, the principle curcuminoid found in turmeric, in the stable ketol-enol form.	5
Figure 1.5: General synthesis route of curcumin that is widely used.	6
Figure 1.6: (a) Banzel in tablet form (200 or 400 mg) or oral solution, and (b) chemical structure of Rufinamide	7
Figure 1.7: Synthesis routes for rufinamide where schemes (a), (b) and (c) employ (E)-methyl 3-methoxyacrylate, propiolic acids/esters and 2- chloroacrylonitrile, respectively. Routes (b) and (c) rely on amidation in the final step, while route (a) uses hydrolysis.	8
Figure 2.1: BCS used by the FDA where highly soluble is considered when the highest dose strength is soluble in less than 250 mL water over a pH range of 1 to 7.5, and highly permeable is considered when the extent of absorption in humans is determined to be greater than 90% of an administered dose.....	13
Figure 2.2: Representation of (a) crystalline API (green) and excipient (yellow), (b) amorphous API, and (c) co-amorphous API and excipient.	15
Figure 2.3: The PXRD patterns of crystalline curcumin form I (blue), co-amorphous curcumin-artemisinin (purple), and crystalline artemisinin form I (pink).	18

Figure 2.4: Proposed bonding mechanism in the co-amorphous system of curcumin-artemisinin.....	19
Figure 2.5: DSC thermographs of curcumin (black), amorphous curcumin (red), co-amorphous curcumin-artemisinin system (blue) and artemisinin (green). Circled are the glass transition temperatures.....	20
Figure 2.6: Representation of a two-component co-crystal in a 1:1 molar ratio, where both green and orange represent a solid, neutral component.	21
Figure 2.7: Theoretical PXRD patterns of (a) API (b) co-former and (c) their co-crystal.	24
Figure 2.8: Theoretical phase diagram of a binary system capable of co-crystal formation. .	25
Figure 2.9: (a) molecular structures of API (green) and excipient (purple), (b) and (c) are both examples of discontinuous interaction between API and excipient found in eutectic mixtures. These interactions can interact with each other throughout the mixture.	27
Figure 2.10: Theoretical phase diagram of a binary system which forms a eutectic.	28
Figure 2.11: Representation of (a) crystalline API (green) and solvent (blue), (b) stoichiometric or ‘true’ solvate, and (c) non-stoichiometric solvate.....	29
Figure 2.12: Esomeprazole Magnesium solvate with water and 1-butanol. Hydrogen bonding between molecules is shown in blue.	31
Figure 2.13: ¹³ C ssNMR of a non-stoichiometric, channel solvate LY297802 tartrate at (a) ambient conditions, (b) elevated temperature with solvent removal, and (c) elevated temperature with increased solvent removal.....	32
Figure 2.14: Hysteresis shown for an API with the capability to form a solvate. Relative humidity is increased gradually and then reduced	33
Figure 2.15: Hydrogen bonding motifs of (a) carboxylic-carboxylic homosynton and (b) a carboxylic-amide heterosynton.	34

Figure 2.16: Binary phase diagram of an API and excipient incapable of forming intermolecular interactions (physical mixture).	38
Figure 2.17: API (higher melting point) is melted and recrystallized before excipient is brought into contact which creates a zone of mixing.	39
Figure 3.1: The 5-methoxy and 6-methoxy tautomers of omeprazole.....	52
Figure 3.2: A simplified visualization of (a) a “true” solvate vs (b) a non-stoichiometric solvate, where the solvent can be one or more types of solvent.	53
Figure 3.3: Esomeprazole magnesium molecules crystalize in P 6 ₃ spaces group alongside with water and 1-butanol molecules; the molecules of the same colour are symmetry equivalent.	57
Figure 3.4: Two types of coordination around the magnesium centers, hydrogen atoms and non-bonded solvents have been omitted for clarity. Mg: green, S: yellow, O: red, N: blue, C: grey.	58
Figure 3.5: Strong hydrogen bonding between the molecules in the lattice are shown in blue dotted lines; hydrogen atoms have been omitted for more clarity. Mg: green, S: yellow, O: red, N: blue, C: grey.	58
Figure 3.6: X-ray powder diffraction of esomeprazole magnesium water/butanol solvate calculated from single crystal structure and esomeprazole magnesium water/butanol solvate after drying under vacuum.	60
Figure 3.7: TGA of the title sample showing two mass losses. The first loss of 7.6% is desolvation, while the second loss is decomposition of the esomeprazole molecule.	62
Figure 3.8: The DSC curve of esomeprazole magnesium water/1-butanol solvate. The curve was obtained from 25-350 °C at a heating rate of 5 °C/minute. An exotherm characteristic of esomeprazole magnesium is seen at 200 °C as well as an endotherm at 175 °C.....	63
Figure 3.9: Esomeprazole magnesium water/1-butanol adsorption of water at increasing humidity followed by desorption at decreasing humidity. The cycle is repeated to give two isotherms.	64

Figure 4.1: Phase diagram for (a) the physical mixture of curcumin and dextrose and (b) the eutectic mixture of curcumin and suberic acid after grinding at varying molar ratios. Temperatures plotted in blue represent the onset of the first melting peak seen in DSC, while orange represents the temperature of the second peak.....	76
Figure 4.2: PXRD patterns for (a) raw suberic acid, (b) raw curcumin, (c) curcumin form I, (d) form II, (e) form III, (f) 1:1 curcumin:suberic acid (CUR-SUB), (g) 1:2 CUR-SUB, (h) 2:1 CUR-SUB, (i) 1:3 CUR-SUB, (j) 3:1 CUR-SUB, (k) 1:4 CUR-SUB, (l) 4:1 CUR-SUB acid and (m) 4:1 CUR-SUB acid heated to 133°C.	77
Figure 4.3: PXRD patterns for CUR-FAD from LAG after (a) 90 min, (b) 60 min, (c) 30 min, (d) 20 min, (e) 10 min, (g) raw folic acid dihydrate and (h) raw curcumin.....	78
Figure 4.4: DSC thermograph for CUR-FAD from LAG after (a) 90 min, (b) 60 min, (c) 30 min, (d) 20 min, (e) 10 min, (f) raw folic acid dihydrate and (g) raw curcumin.	79
Figure 4.5: solution ¹ H NMR spectra for (a) CUR-FAD, (b) raw folic acid dihydrate and (c) raw curcumin.	79
Figure 4.6: FT-IR spectra for (a) CUR-FAD, (b) raw folic acid dihydrate and (c) raw curcumin.	80
Figure 4.7: Powder dissolution rate studies for CUR-FAD compared with curcumin.	81
Figure 4.8: PXRD pattern of powder from thermodynamic equilibrium solubility.	82
Figure 4.9: Asymmetric unit of Form II curcumin with space group of P ca ₂ 1 formed via slow evaporation from 90% methanol in the presence of dextrose. Hydrogen atoms are omitted for clarity. C: grey; O: red.	83
Figure 5.1: Molecular structure of rufinamide.....	91
Figure 5.2: Molecules of rufinamide modification B in one unit cell. F: green, O: red, N: blue, C: grey and H: white.	96

Figure 5.3: Strong hydrogen bonding between the molecules in the lattice are shown in black dotted lines (labelled a-d); hydrogen atoms have been omitted for more clarity. F: green, O: red, N: blue, C: grey.....	96
Figure 5.4: Intermolecular homosynthons between (a) two and (b) three amide groups from distinct molecules.....	97
Figure 5.5: (a) PXRD patterns and (b) DSC thermographs for rufinamide modification A (black) and rufinamide modification B obtained from solution (purple).	100
Figure 5.6: ¹ H NMR spectra for (a) citric acid, (b) rufinamide modification A and (c) rufinamide modification B in d-DMSO.....	101
Figure A-1: ¹ H NMR of the esomeprazole magnesium solvate.....	101
Figure A-2: FTIR of the esomeprazole magnesium solvate.	101
Figure B-1: Calibration curve and line of best fit for raw folic acid dihydrate in 40% EtOH.	101
Figure B-2: Calibration curve and line of best fit for raw curcumin in 40% EtOH	101
Figure B-3: Calibration curve and line of best fit for coamorphous mixture of curcumin and folic acid dihydrate in 40% EtOH.....	101

List of Abbreviations

API	Active pharmaceutical ingredient
ATP	Adenosine triphosphate
BCS	Biopharmaceutics classification system
CSD	Crystal structure database
CUR-FAD	Curcumin – folic acid dihydrate co-amorphous mixture
DFT	Density functional theory
DSC	Differential scanning calorimetry
DMSO	Dimethylsulfoxide
DVS	Dynamic vapour sorption
EAFUS	Everything added to food in the United States
EEG	Electroencephalographic
EPB	Ethylparaben
EtOH	Ethanol
FDA	US Food and Drug Administration
FT-IR	Fourier Transform infrared
GERD	Gastroesophageal reflux disease
GRAS	Generally regarded as safe
HBA	Hydrogen bond acceptors

HBD	Hydrogen bond donors
ICH	International council for harmonisation of technical requirements for pharmaceuticals for human use
IDR	Intrinsic dissolution rate
IR	Infrared
LAG	Liquid assisted grinding
NME	New molecular entities
NMR	Nuclear magnetic resonance
NR	Not reported
PCA	Principal components analysis
PPI	Proton pump inhibitor
PXRD	Powder X-ray diffraction
RH	Relative humidity
ssNMR	Solid state nuclear magnetic resonance
T _g	Glass transition temperature
TGA	Thermogravimetric analysis
UV	Ultraviolet
XRD	X-ray diffraction

List of Appendices

Appendix A: Supporting Information for Chapter 3.....	107
Appendix B: Calibration Curves for CUR-FAD Dissolution Studies	101

Chapter 1

1 Introduction

Many of the drugs that are currently or about to be introduced to the market are considered to have low water solubility. This leads to some major issues in drug uptake that are costly to both pharmaceutical companies and the environment. Crystal engineering is a concept that relies on one's knowledge of intermolecular interactions and uses this knowledge to design new materials. A technique exploited by crystal engineering to increase the solubility of active pharmaceutical ingredients (APIs) is to incorporate another molecule(s) that disrupts its crystal lattice, as illustrated in Figure 1.1. Co-amorphous mixtures, eutectics and co-crystals can all be formed when the additional molecules are neutral solids, and a solvate occurs solvent molecules are added.

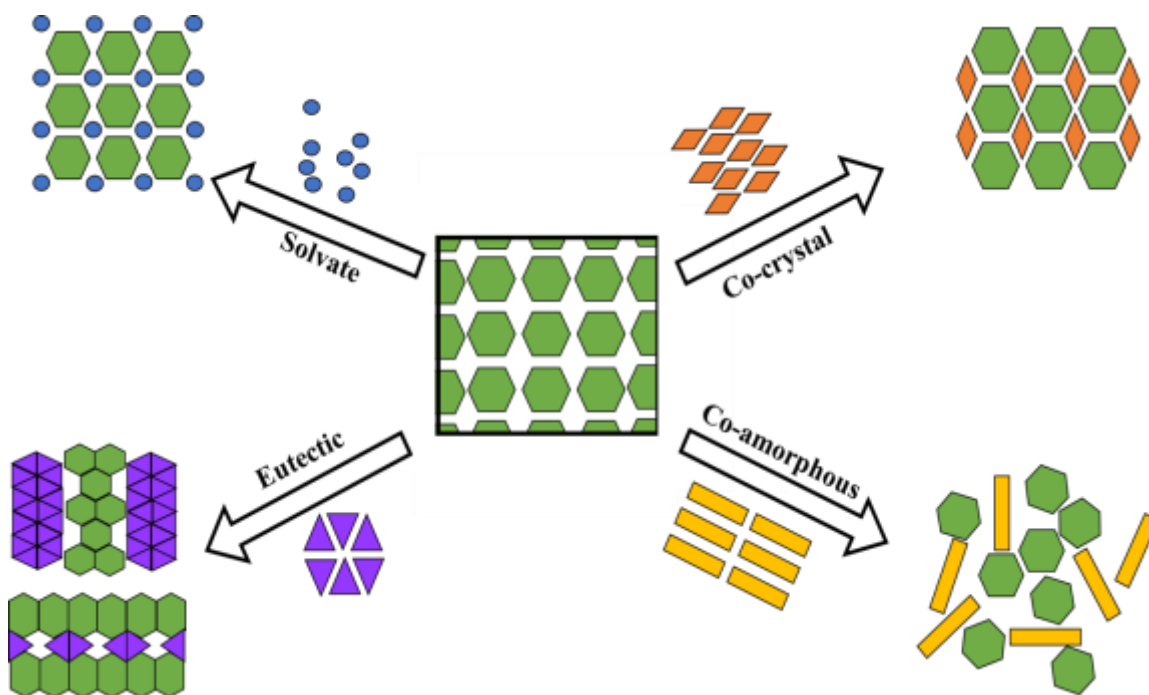


Figure 1.1: General scheme of possible solid states formation via excipient addition where green is API; blue, yellow and orange are excipients capable of intermolecular bonding; and blue is solvent molecules.

Creation of these solid states requires extensive screening, which commonly uses both computer-based and experimental techniques. Computational methods help provide a collection of possible molecules that could be used. Used in parallel with understanding of hydrogen and intermolecular bonding, one can come up with a comprehensive list of drug-approved excipients that would be examined. The next step is to run experiments (e.g. solvent evaporation, grinding, melting, etc.) that will hopefully result in formation of a novel compound. In this thesis, three poorly water soluble APIs (i.e. esomeprazole magnesium, curcumin and rufinamide) are investigated and screened for a solid state with increased solubility. Solvent-based and mechanical techniques are employed for the screening of novel solid states (i.e. eutectics, co-crystals, co-amorphous mixtures and solvates) of these APIs, and the results of these screenings are given in the succeeding chapters.

1.1 Objectives

Esomeprazole magnesium, curcumin and rufinamide are all considered to have low solubility in water. The main questions addressed in this thesis are:

1. How can the crystal structure of an API be engineered to form solid states that will increase thermodynamic equilibrium solubility or kinetic dissolution rate?
2. What methods can be employed to produce these novel solid states?
3. Once formed, how will these solid states be characterized?

1.2 Motivation

The applications for low solubility APIs can be greatly increased if this undesirable characteristic were to be improved. Since higher solubility leads to greater bioavailability and consequently less cost due to lower dosages, the formation of novel solid states is an attractive approach for industry. Also, due to patent laws, pharmaceutical companies are constantly looking for unique forms of name brand drugs that are patented by other companies so that they can also produce them. Incorporating a new molecule that disrupts the lattice of a drug is considered innovative enough to possess its own patent, allowing the pharmaceutical company the ability to legally produce and sell this form of the drug.

Production of this new solid state is often done at a much lower overall cost than if the company were to invent the drug from the beginning stages. For instance, if a novel solid state is formed with an excipient or solvent that is already approved by the FDA, then all-inclusive clinical testing (i.e. that for a novel drug) does not need to be conducted since the therapeutic effects of the API are already known. Not only does this save money, but it will also save the company a lot of time. These techniques are especially helpful for companies that create generic drugs that tend to be sold at a much lower cost.

1.3 Background

1.3.1 Esomeprazole Magnesium

In 2004-2005 alone, \$52,235,910 was spent by the Canadian health care system on patients with a primary diagnosis of esophagus related diseases, including gastroesophageal reflux disease (GERD).¹ GERD often causes chronic heartburn, which can lead to degradation of the lining in the esophagus. Many of the symptoms related to GERD (i.e. those listed in Table 1.1) can be avoided if the disease is treated early enough by the use of a proton pump inhibitor (PPI).² A very common and effective PPI is omeprazole.

Table 1.1: Some symptoms and complications of GERD.²

Common	Uncommon	Complications
Heartburn	Hoarseness and sore throat	Erosive esophagitis
Regurgitation	Difficulties swallowing	Esophageal stricture
Sleep Disturbance	Asthma and sinusitis	Ulceration and bleeding
Early Satiety	Vomiting	Esophageal cancer
Upper abdominal distension	Nausea	Upper respiratory complaints

Esomeprazole (Figure 1.2 (b)), the (S)-isomer of omeprazole, was the first isolated single isomer PPI.³ It is currently marketed by AstraZeneca as the trihydrate form of the magnesium salt under the name Nexium (Figure 1.2 (a)). When compared to other PPIs (i.e. lansoprazole, pantoprazole, omeprazole and rabeprazole), esomeprazole was found to provide more effective control of gastric acid at the standard dose of 40 mg/day.⁴ However, it is considered only slightly soluble in water.

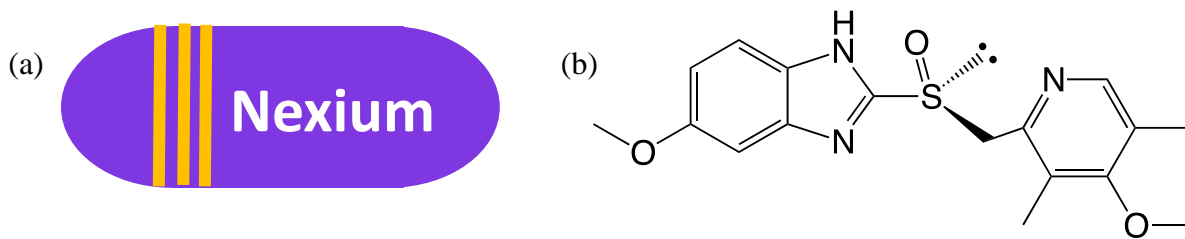


Figure 1.2: (a) Nexium, the marketed version of esomeprazole magnesium and (b) the structure of esomeprazole.

The synthesis of esomeprazole on a large scale involves asymmetric oxidation of the same intermediate in the synthesis of omeprazole. Once coordinated to the Mg center, esomeprazole magnesium is found to contain only the (S)-isomer. The scheme, starting from the intermediate, is given in Figure 1.3.⁵

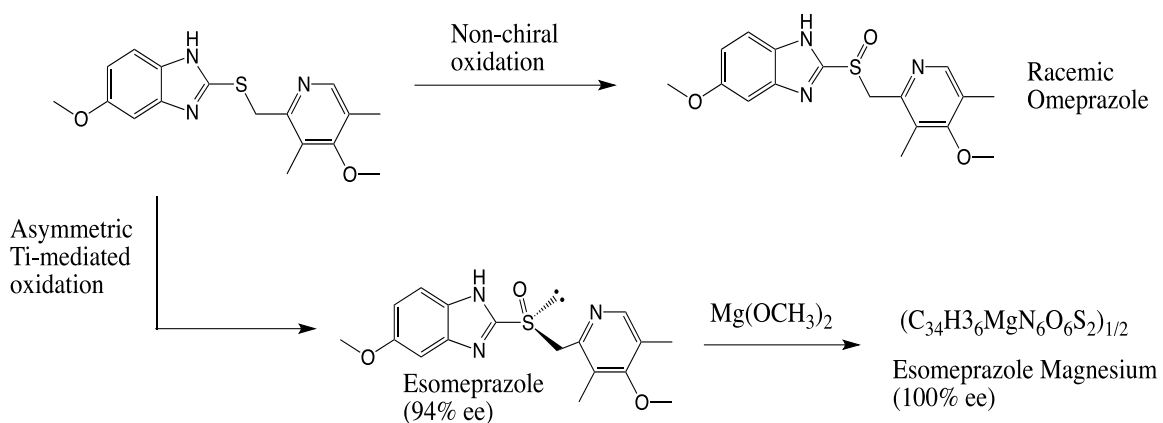


Figure 1.3: Synthesis for large scale production of esomeprazole magnesium that results in sole presence of (S)-isomer of omeprazole.

1.3.2 Curcumin

Turmeric, or *curcuma longa*, is a root belonging to the ginger family and is very common in Asian cuisine (Figure 1.4 (a)). The principal curcuminoid found in turmeric is curcumin; though, desmethoxycurcumin, bis-desmethoxycurcumin and cyclic curcumin are also present. Curcuminoids are very yellow in appearance due to the polyphenols and can be orange if there is conjugation in the chain, which is illustrated by curcumin in Figure 1.4 (b).⁶ Curcumin is a tautomer and is also present in a diketo form, but the ketol-enol tautomer shown below is found to be more stable and is also more effective as a drug.⁷

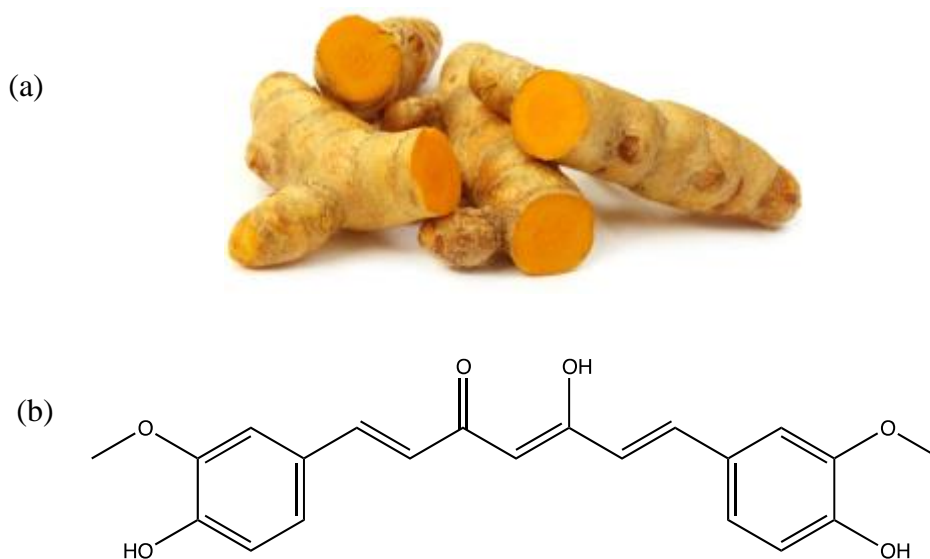


Figure 1.4: (a) *Curcuma longa*, also known as turmeric root, is a common spice used in Asian cooking and (b) the chemical structure of curcumin, the principle curcuminoid found in turmeric, in the stable ketol-enol form.

Curcuminoids make up only 2-9% of the turmeric root, so the extraction process is critical. Curcumin can be extracted from turmeric via many different processes, such as solvent extraction, Soxhlet extraction, microwave extraction, ultrasonic extraction, use of supercritical CO₂, etc. followed by column chromatography. The most frequently employed method is the use of solvent extraction with ethanol (EtOH) due to its capacity to be used in food and pharmaceutical processes as well as curcumin's high solubility in

EtOH. In regions where turmeric is not grown in abundance, a more viable method is to synthesize it. A simple synthesis route is given in Figure 1.5 that has been adopted by many.⁸ This method generally involves reacting 2,4-diketones with substituted aromatic aldehydes. Boron trioxide is employed to form a complex that prevents the keto groups from partaking in condensation reactions. The primary amine is used as a catalyst, while alkyl borate is a water scavenger to increase curcumin yields. Hydrochloric acid (HCl) is the last step to dissociate the boron complex.⁹

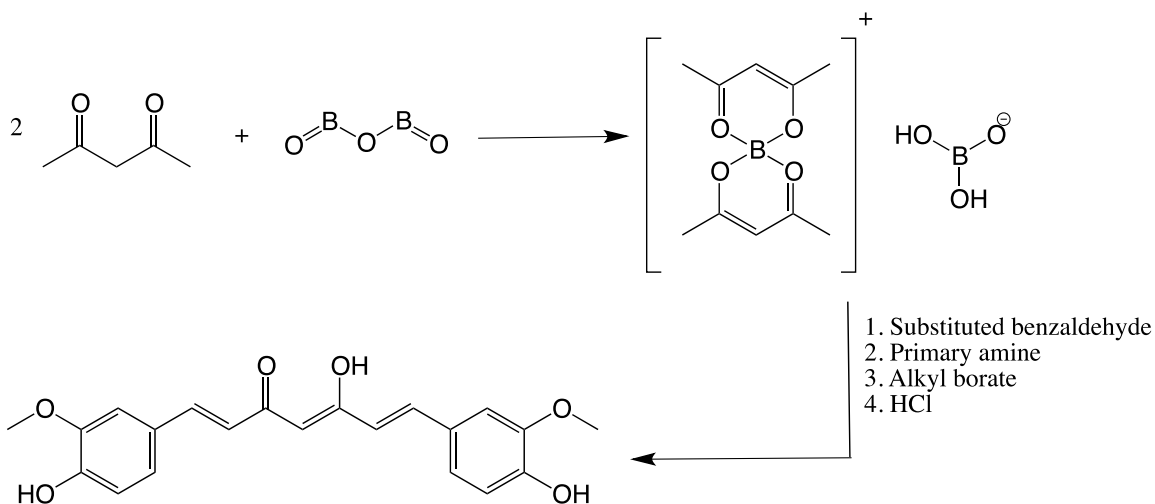


Figure 1.5: General synthesis route of curcumin that is widely used.

Curcumin extract has been shown to have many different uses and valuable health effects. Some of these include antioxidant¹⁰ and anti-inflammatory effects¹¹, use as a colorimetric sensor¹², tumor reducer¹³, prevention of type 2 diabetes¹⁴, etc. Many Asian countries, especially India, see the benefits of using turmeric since it is usually cooked in oil, which acts as a solvent to dissolve curcumin and allows for better uptake. Turmeric is not as common in Western countries, and some are not accustomed to the taste. This often leads to curcumin being taken in pill form, which greatly decreases the bioavailability.¹⁵ If the solubility of this drug could be increased, then its use in various distinct applications would be much more feasible.

1.3.3 Rufinamide

Lennox-Gastaut is a catastrophic form of child epilepsy that has its onset from 1-7 years of age and tends to continue into adulthood. This syndrome and the impact of its seizures requires a group of health professionals to support the child and the family.¹⁶ Though first discovered in the 1930s, Lennox-Gastaut syndrome was later defined as a very severe form of childhood epilepsy characterized by frequent and multiple types of seizures, mental retardation and slow spike-wave electroencephalographic (EEG) patterns.¹⁷ Common drugs that are used to treat these seizures include clobazam, lamotrigine, rufinamide, topiramate and valproate.

Rufinamide, marketed as Banzel by Eisai Co., is a triazole derivative with low aqueous solubility. It is produced as both a tablet and oral solution (Figure 1.6 (a)). The chemical structure is shown in Figure 1.6 (b); there is a lot of potential for intermolecular interactions with rufinamide due to the amide group, aromatic fluorine and lone pair electrons of the triazole ring. This leads to the investigation of possible novel solid states (such as those in Figure 1.1) that is described in Chapter 5.

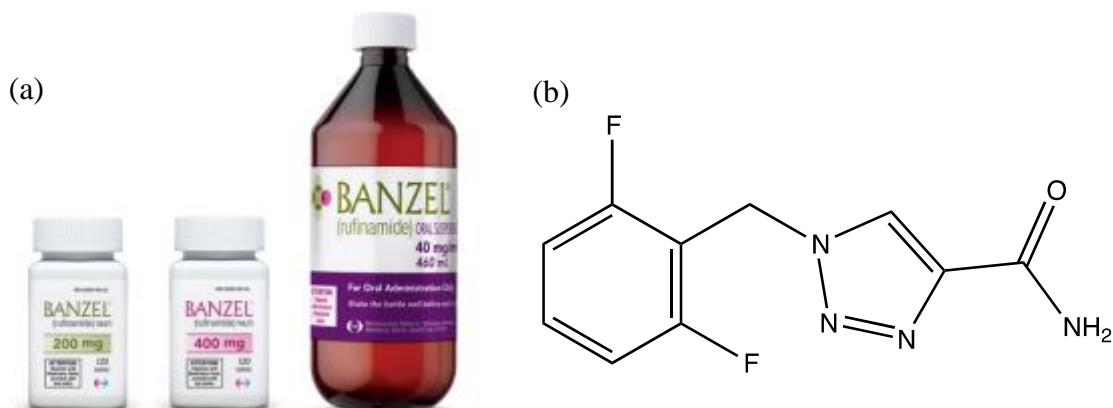


Figure 1.6: (a) Banzel in tablet form (200 or 400 mg) or oral solution, and (b) chemical structure of Rufinamide.²¹

Rufinamide is generally synthesized through one of the three routes depicted in Figure 1.7. To construct the triazole core, all three routes employ 1,3-dipolar Huisgen cycloaddition

of 2,6-difluorobenzylazide with a dipolarophile. Route (c) is commonly used as it uses low cost starting materials, does not require catalyst and can be produced continuously. Rufinamide can also be synthesized using continuous flow copper tubing reactor-catalyzed cycloaddition reaction.¹⁸

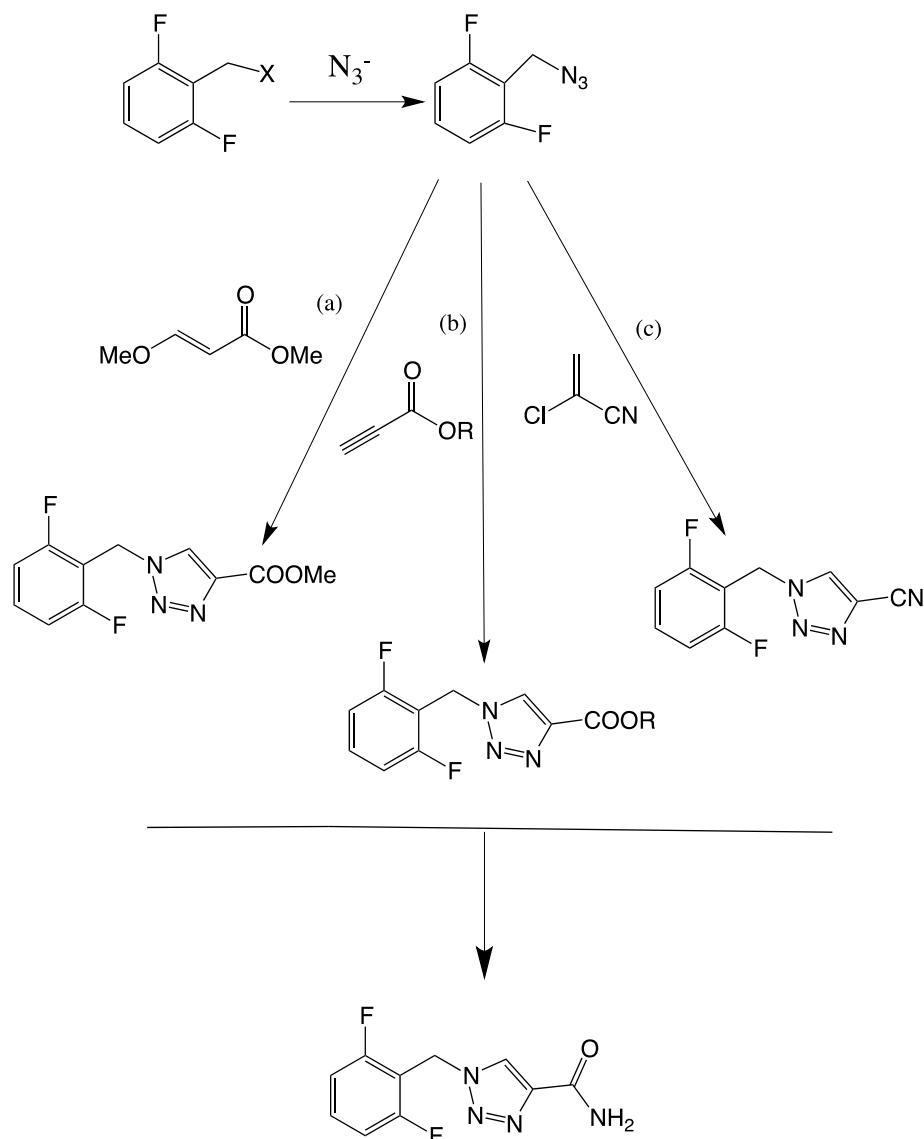


Figure 1.7: Synthesis routes for rufinamide where schemes (a), (b) and (c) employ (E)-methyl 3-methoxyacrylate, propionic acids/esters and 2-chloroacrylonitrile, respectively. Routes (b) and (c) rely on amidation in the final step, while route (a) uses

1.4 Thesis Outline

Chapter one provides a brief introduction to the low solubility APIs addressed in this thesis. The objectives and motivations of the work in this thesis are also given.

A literature review of solid state formation by excipient addition is presented in chapter two. The subject matter included is the formation and characterization of co-amorphous mixtures, co-crystals, eutectics and solvates.

In chapter three, a novel esomeprazole magnesium solvate with water and 1-butanol is described. The molecular structure shows how esomeprazole co-ordinates to magnesium for the first time. Full characterization is given.

Chapter four presents the research conducted on curcumin, including the formation of a novel co-amorphous mixture with folic acid dihydrate that displays increased dissolution rate and has potential as a prenatal drug. Work on solid state screening and formation of form II is also available.

Chapter five highlights the screening conducted with rufinamide. While no novel solid states were presented in this chapter, the molecular structure of modification B is illustrated along with a unique method to produce this metastable form.

The final portion, chapter six, gives a conclusion on the entire thesis and provides recommendations for future works.

1.5 References

- (1) Canadian Institute for Health Information. The Cost of Hospital Stays: Why Costs Vary <https://secure.cihi.ca/estore/productSeries.htm?pc=PCC400> (accessed Jun 14, 2017).
- (2) Fedorak, R. N.; van Zanten, S. V.; Bridges, R. *Can. J. Gastroenterol.* **2010**, *24* (7), 431–434.
- (3) Robins, G. W.; Scott, L. J.; Levy, B. I.; Federatif, I.; Circulation, D. R.; Lariboisiere,

- H. *Drugs* **2002**, *62* (10), 1503–1538.
- (4) Miner, P.; Katz, P. O.; Chen, Y.; Sostek, M. *Am. J. Gastroenterol.* **2003**, *98* (12), 2616–2620.
- (5) Olbe, L.; Carlsson, E.; Lindberg, P. *Nat. Rev. Drug Discov.* **2003**, *2* (2), 132–139.
- (6) Akram, M.; Ahmed, A.; Usmanghani, K.; Hannan, A.; Mohiuddin, E.; Asif, M. *Rom J Biol Plant Biol* **2010**, *55* (2), 65–70.
- (7) Yanagisawa, D.; Shirai, N.; Amatsubo, T.; Taguchi, H.; Hirao, K.; Urushitani, M.; Morikawa, S.; Inubushi, T.; Kato, M.; Kato, F.; Morino, K.; Kimura, H.; Nakano, I.; Yoshida, C.; Okada, T.; Sano, M.; Wada, Y.; Wada, K.; Yamamoto, A.; Tooyama, I. *Biomaterials* **2010**, *31* (14), 4179–4185.
- (8) Priyadarsini, K. I. *Molecules* **2014**, *19*, 20091–20112.
- (9) Pabon, H. J. J. *Recl. des Trav. Chim. des Pays-Bas* **2010**, *83* (4), 379–386.
- (10) Ak, T.; Gülçin, İ. *Chem. Biol. Interact.* **2008**, *174* (1), 27–37.
- (11) Srimal, R. C.; Dhawan, B. N. *J. Pharm. Pharmacol.* **1973**, *25* (6), 447–452.
- (12) Pourreza, N.; Sharifi, H.; Golmohammadi, H. *Microchem. J.* **2016**, *129*, 213–218.
- (13) Soudamini; Kuttan, R. *Indian J. Pharmacol.* **2016**, *20* (2), 95.
- (14) Chuengsamarn, S.; Rattanamongkolgul, S.; Luechapudiporn, R.; Phisalaphong, C.; Jirawatnotai, S. *Diabetes Care* **2012**, *35* (11).
- (15) Prasad, S.; Tyagi, A. K.; Aggarwal, B. B. *Cancer Res. Treat.* **2014**, *46* (1), 2–18.
- (16) Crumrine, P. K. *J. Child Neurol.* **2002**, *17* (1 suppl), S70–S75.
- (17) Wheless, J. W.; Constantinou, J. E. C. *Pediatr. Neurol.* **1997**, *17* (3), 203–211.
- (18) Zhang, P.; Russell, M. G.; Jamison, T. F. **2014**.

- (19) Portmann, R. Process for preparing 1-substituted 4-cyano-1,2,3-triazoles. US 6156907, 2000.
- (20) Attolino, E.; Colombo, L.; Mormino, I.; Allegrini, P. Method for the preparation of rufinamide. US 20100234616 A1, 2010.
- (21) Mudd, W. H.; Stevens, E. P. *Tetrahedron Lett.* **2010**, *51* (24), 3229–3231.
- (22) Kable. Banzel - Treatment for LGS <http://www.drugdevelopment-technology.com/projects/banzel-treatment-for-linnaux-gastaut-syndrome/banzel-treatment-for-linnaux-gastaut-syndrome2.html> (accessed Jun 14, 2017).

Chapter 2

2 A Review of Crystal Engineering via Non-Ionic Excipient Addition to Increase Drug Solubility and Bioavailability

Approximately 75% of the drugs that are being approved for use in the pharmaceutical industry have low aqueous solubility. This leads to issues with drug uptake, higher doses and consequently a negative environmental impact. One approach to improving these active pharmaceutical ingredients (APIs) is to use the crystal engineering technique of adding another molecule that disrupts the crystal lattice of the API. This method relies on the knowledge of the intermolecular bonds that the API can form with the excipient and employs many different synthesis techniques. The formation of a novel solid state is dependent on the strength of the intermolecular bonds formed and the type of synthesis used. Main synthesis routes include a variety of solution crystallization procedures as well as liquid assisted or neat grinding. This review will emphasize the formation of new states by incorporating a distinct molecule through non-ionic bonding with the API. For this reason, polymorphs and salts will be disregarded and the main forms analyzed are co-amorphous materials, co-crystals, eutectics and solvates. Once formed, the proper characterization procedure and the methods of distinguishing these solid forms are discussed. Appropriate choice of excipient as well as screening methods are also given in detail.

2.1 Introduction

Every year the Food and Drug Administration (FDA) approves new molecular entities (NMEs) for pharmaceutical use; as of May 2017, there have already been 20 active pharmaceutical ingredients (APIs) accepted, this year. A biopharmaceutics classification system (BCS), depicted in Figure 2.1 is used by the FDA to classify APIs and reduce unnecessary human testing.¹ The BSC goes as follows: Class I (high permeability, high solubility); Class II (high permeability, low solubility); Class III (low permeability, high solubility); and Class IV (low permeability, low solubility).² When combined with dissolution studies, a biowaiver for in vivo bioavailability and bioequivalence can be

applied for Class I and III drugs, which leads to a less vigorous testing required for these drugs.³

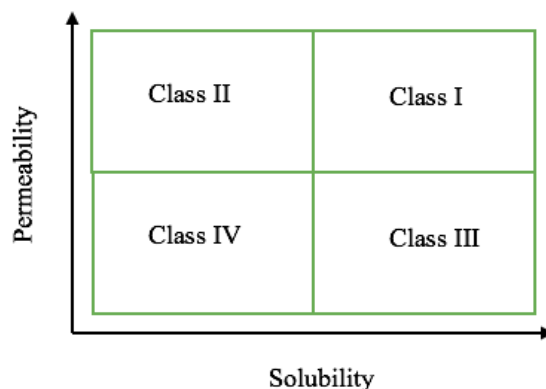


Figure 2.1: BCS used by the FDA where highly soluble is considered when the highest dose strength is soluble in less than 250 mL water over a pH range of 1 to 7.5, and highly permeable is considered when the extent of absorption in humans is determined to be greater than 90% of an administered dose.¹

A simple solution to help pharmaceutical companies with more efficient drug testing (i.e. less clinical testing) would be to stop using drugs that do not belong to Class I and III; however, approximately 75% of NMEs belong to BCS Class II and IV.⁴ This means that majority of effective medicines that are FDA approved drug innovations have a poor solubility in aqueous solutions. Many drugs today are designed using high throughput screening approaches to ensure valuable and successful products. Since the approval process for NMEs takes years, pharmaceutical companies want to guarantee that they have the best contenders. The screening processes tend to result in APIs that are higher in molecular weight and have increased hydrogen-bonding.⁵ Increased molecular size results in greater van der Waals interaction between like molecules, while more hydrogen bonding within the API creates a stronger crystal lattice. Both characteristics lead to a compound that is more difficult to dissolve.

Why are low solubility drugs undesirable? First, they often require high doses to reach required therapeutic plasma concentrations after oral administration, hence patients are ingesting significantly more than necessary. The increase in dose also leads to more costly

medicines, which is unfavourable to consumers and pharmaceutical companies. Poorly soluble APIs are also more vulnerable to food effects (e.g. some drugs are suggested to be taken after a fasting period due to reduced absorption in the presence of food), and slow dissolution can lead to lesser fraction absorbed in the small intestine.⁶ High levels of API excretion due to low absorption are costly to the pharmaceutical industry and can be detrimental to our environment. For instance, carbamezapine, a routine API that is nearly insoluble in water, was found in every sample taken from wastewater treatment plants' effluent of three different rivers in England.⁷ Therefore, not only are Class II and IV drugs more expensive to administer, they also have a lasting effect on the Earth. Taking these factors into account, a strong need to increase the solubility of these drugs is prevalent.

Crystal engineering is defined as: *the understanding of intermolecular interactions in the context of crystal packing and the utilization of such understanding in the design of new solid forms with desired physical and chemical properties.*⁸ Numerous methods are present that involve altering the solid state of Class II and IV APIs to increase water solubility and bioavailability. This altering of states is known as crystal engineering, and some of these approaches include formation of: salt, co-crystal, solvate, eutectic and co-amorphous mixture. The bioavailability of a drug is affected by its aqueous solubility, dissolution rate, permeability, etc. If one can increase the water solubility of Class II drugs, the bioavailability will be greatly improved.⁹

In this chapter, the practices discussed will focus on non-ionic bonding between distinct molecules, so salts and polymorphs will be overlooked. The techniques mentioned involve adding another component called an excipient into the crystal structure; excipients will usually have more ideal physical and chemical characteristics than the API, so the combination will lead to a superior drug product. The beauty of these methods relies on the fact that excipients are already approved by the FDA for use in pharmaceuticals, and thus, the novel solid state of the API will not need to undergo new clinical studies.

2.2 Co-amorphous Mixtures

An amorphous solid, also referred to as a glass, has no long range molecular order of packing nor does it have a distinct molecular conformation.¹⁰ Amorphous materials have properties similar to liquids at a molecular level but are more like solids at a macroscopic level.¹¹ Due to the lack of order and since this form is the most energetic, amorphous compounds have been shown to have increased solubility in comparison to their crystalline counterparts.¹² Consequently, this will also result in an increase in bioavailability, so the formation of an amorphous pharmaceutical compound is an appropriate means to tackle the issues with Class II and IV drugs.

Co-amorphous solids, depicted in Figure 2.2 (c), occur when two components become amorphous due to interaction with one another. Intermolecular bonding between API and excipient impedes the arrangement of individual molecules into separate lattices and results in an amorphous material.¹³ Co-amorphous mixtures are shown to be not only high in solubility, but have a high stability.¹⁴ By adding another component into the system, the problem of low stability in amorphous materials is alleviated in co-amorphous materials. Amino acids are great candidates as excipients in these systems.¹⁵

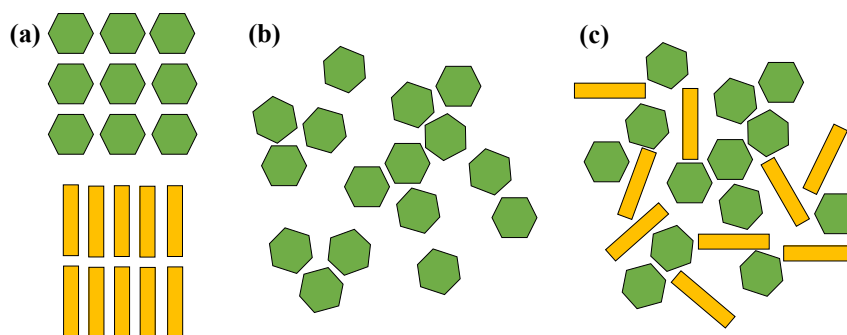


Figure 2.2: Representation of (a) crystalline API (green) and excipient (yellow), (b) amorphous API, and (c) co-amorphous API and excipient.

An amorphous phase composed of a single material can be created through two main routes of production: either a thermodynamic or kinetic disordering processes. Thermodynamic disordering occurs when the loss of long range order symmetry causes disorder in the solid state. It allows for close random packing and is termed thermodynamic disorder due to the breaking of symmetry.¹⁶ Kinetic disordering is referred to when long range disorder is caused by short range order. This process is considered to be continuous and can reduce crystalline material to glassy material.¹⁷ When creating an amorphous state, the thermodynamic pathway involves starting with a thermodynamically stable non-crystalline form, such as a melt or solution. The melt will then undergo quenching, while the drug will be precipitated from solution. Conversely, the kinetic pathway will start with a solid state which is then converted by introducing crystal defects via crushing, milling and continuous shear forces.¹⁸ These pathways are also applicable to the synthesis of co-amorphous systems.

While still quite a new practice in drug formulations, co-amorphous mixtures have been shown to be readily obtained by a variety of procedures. The main procedures are milling and grinding (kinetic disordering) or quenching and solvent evaporation (thermodynamic disordering). Given in Table 2.1 are some instances of co-amorphous mixtures and the methods used to produce them. These are all desirable techniques because not only are they quick to produce, they also only require a small amount of sample; however, not every technique is applicable to every drug-excipient combination. Quenching is not available if degradation occurs at higher temperature, solvent evaporation can prove difficult if there are solubility differences, and milling may not apply enough force to disrupt the lattice.

Table 2.1: Preparation of Co-amorphous Systems.

Drug	Excipient (or drug)	Technique	Experimental
Curcumin	Artemisinin	Solvent Evaporation	A mixture of 1:1 molar ratio of curcumin and artemisinin was dissolved in ethanol. The solution was then rotovaped (fast evaporation under vacuum) to give the co-amorphous product. ¹⁹
β -azelnidipine	Maleic Acid	Grinding (LAG or neat)	β -azelnidipine and maleic acid at molar ratios of 1:1 and 1:2 were placed into a 50 mL stainless steel jar and milled at 30 Hz in a laboratory-scale oscillatory disk mill. This can be done neat or with the addition of ethanol. ²⁰
Indomethacin	Cimetidine	Quenching	Indomethacin–cimetidine physical mixtures were melted on an aluminium foil placed on a preheated hotplate (180°C) for 1 min. The molten liquid was cooled quickly by placing the aluminum foil over ice water. ²¹

To classify a material as amorphous, perhaps the most effective method is to use powder X-ray diffraction (PXRD). Crystalline material will show very distinct and sharp peaks, while amorphous material will appear as one very broad peak termed a halo since it has no defined crystal lattice or symmetry operators. To further examine the characterization of a co-amorphous system, the first example in Table 2.1 will be considered. Curcumin, a poorly water soluble molecule, has been shown to help increase anti-malaria effects when taken in parallel with the API, artemisinin. Instead of prescribing these and taking them separately, a co-amorphous mixture was formed via fast solvent evaporation so that a patient could take them together. The PXRD patterns of the starting materials and the mixture are shown in Figure 2.3.¹⁹ It is clear that the mixture has lost the crystalline nature of the starting materials and is now forming weak intermolecular interactions.

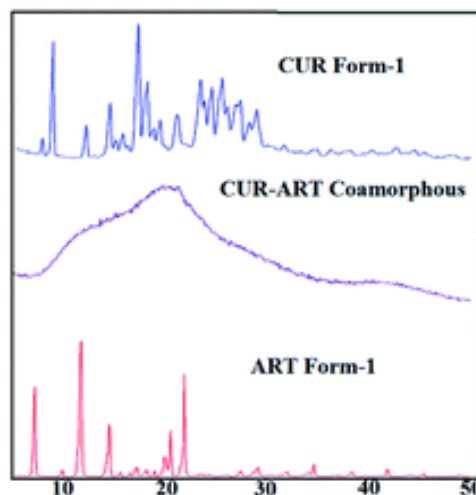


Figure 2.3: The PXRD patterns of crystalline curcumin form I (blue), co-amorphous curcumin-artemisinin (purple), and crystalline artemisinin form I (pink).¹⁹

Depending on the method used for producing the co-amorphous mixture, obtaining an amorphous pattern from PXRD is sufficient for characterization. If prepared via grinding, then the product is usually co-amorphous; however, quenching may lead to degradation and solvent evaporation could lead to a single amorphous state precipitating out first. To ensure that both starting materials are present in the amorphous product, one should perform solution ^1H NMR (nuclear magnetic resonance). If the shifts seen are solely representative of both starting materials, then the product can be said to be co-amorphous. Keeping with the curcumin-artemisinin mixture, it was exhibited that chemical shifts for both starting materials were present in their product.

Solid state NMR (ssNMR) is another method that can be used for the characterization of these systems. ssNMR will usually show broader bands for amorphous material compared to crystalline material due to the increase of molecular orientations.²² There will also be a shift in peaks due to the intermolecular bonding between the drug and excipient.²³ Furthermore, when compared to the ssNMR spectrum of a purely crystalline homogeneous mixture of the starting materials, the amorphous content of the co-amorphous system can

be determined.²⁴ However, this technique often relies on peak integration, which can prove to be difficult when there is an overlap (i.e. broad peaks in amorphous materials often result in overlap). Also, formation of the homogeneous mixture could result in decreased crystallinity that would introduce error. Another method is to compare with both the fully crystalline and fully amorphous spectra of the starting materials. This method uses principal components analysis (PCA) of ssNMR data that is normalized by dividing all PCA scores by the score of the 100% amorphous sample after subtracting the score of the crystalline sample. The profile for rate of co-amorphization can be obtained by plotting the normalized data against mill time.²⁵

For further characterization, Raman and FT-IR (Fourier Transform Infrared Spectroscopy) can be conducted. For both techniques, the spectra will appear as a combination of the starting materials with small shifts in frequencies.²⁶ The peaks that have shifted when compared to the starting materials, are representative of the bonds involved in the intermolecular bonding that stabilizes and causes formation of co-amorphous mixtures.^{27,28} When coupled with ssNMR, these characterization techniques are useful in proposing a bonding mechanism between components of the system. Following the ongoing example, the proposed bonding mechanism of curcumin and artemisinin in Figure 2.4 was determined by analyzing the FT-IR spectrum, which showed a shift in carbonyl stretching of artemisinin and the phenolic alcohol of curcumin.

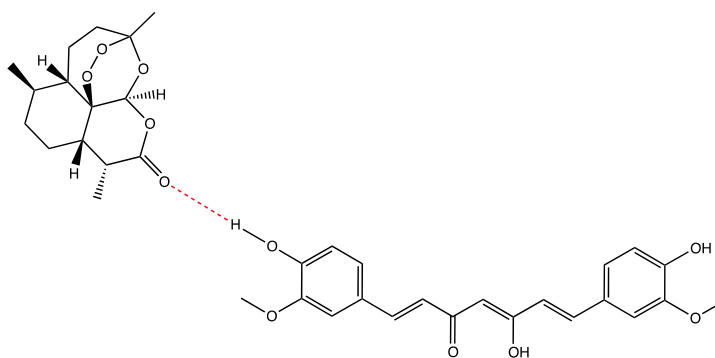


Figure 2.4: Proposed bonding mechanism in the co-amorphous system of curcumin-artemisinin.¹⁹

Fundamental thermal analysis of these systems is done by differential scanning calorimetry (DSC). Amorphous materials will undergo a glass transition at a specified temperature (T_g), above which the material will tend to crystallize.²⁹ The DSC data of a co-amorphous system will vastly differ from that of the starting materials. Once again considering the Curcumin-artemisinin system, the differences can be appreciated in Figure 2.5. The melting of the starting materials is seen in the endothermic peaks, while the co-amorphous system has a broad exotherm. The T_g is highlighted and appears below the melting of both curcumin and artemisinin. When plotting a phase diagram of a binary system using DSC, a “v” shape may appear for co-amorphous mixtures with a single thermal event happening at a particular molar ratio.³⁰ Since co-amorphous systems are not well studied, using DSC alone is not useful as its results are not universal (e.g. the formation of a “v” in the binary phase diagram is an ideal situation).

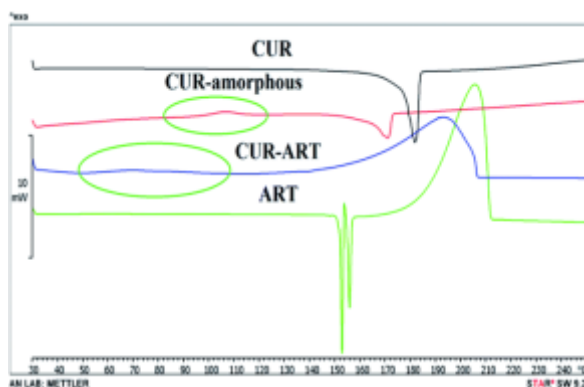


Figure 2.5: DSC thermographs of curcumin (black), amorphous curcumin (red), co-amorphous curcumin-artemisinin system (blue) and artemisinin (green). Circled are the glass transition temperatures.

Since amorphous materials are not crystalline, single crystal XRD cannot be obtained.

2.3 Co-Crystals

Much like co-amorphous systems, a co-crystal is composed of neutral, solid components that interact with each other through intermolecular bonding. A simple depiction of a 1:1 molar ratio co-crystal comprised of two different compounds is given in Figure 2.6. In this

representation, the green component can be the API, while the orange is the excipient. Intriguingly, one of the components can be comprised of a salt or hydrate so long as each component is considered overall neutral.^{31,32} Co-crystals have been known for some time by different names (e.g. addition compounds, mixed binary molecular crystals, molecular complexes, solid-state complexes, heteromolecular crystals, etc.), but have not been of great interest until recently.³³ To avoid being ambiguous between solid states, the FDA gave the following definition to co-crystals: *solids that are crystalline materials composed of two or more molecules in the same crystal lattice.*³⁴ In a pharmaceutical co-crystal, at least one of these components will be an API; the excipient is referred to as the co-crystal former or co-former.³⁵

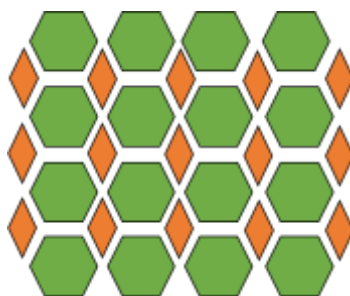


Figure 2.6: Representation of a two-component co-crystal in a 1:1 molar ratio, where both green and orange represent a solid, neutral component.

Co-crystallization occurs when an excipient is introduced that competes with and supersedes the intermolecular bonding of a molecule with itself.³⁶ The most difficult task in co-crystal formation is picking an appropriate co-former, which will be discussed later on. The main intermolecular force behind co-crystal formation is hydrogen bonding, so the co-former should have appropriate hydrogen bond donors (HBD) and acceptors (HBA). There are additional contributing factors to co-crystal formation, and a statistical review of co-crystals in the CSD (Crystal Structure Database) leads to some general assumptions: co-crystals form between molecules of similar shape and polarity, and the number of HBD/HBA is less important than the strength of the potential hydrogen bonding.³⁷ For instance, if an API has multiple functional groups and one is carboxylic, it will tend to have greater potential forming a co-crystal with an excipient containing an amide than with an

excipient that can form multiple weaker bonds. Furthermore, if an API shows potential for intermolecular bonding with an excipient due to matching the HBD and HBA groups, a co-crystal may not form if the shapes do not match (e.g. planar molecules will tend to form co-crystals with planar molecules).

The formation pathways for co-crystallization are comparable to those for co-amorphous mixtures and include liquid assisted (LAG) or dry/neat grinding, solvent evaporation, isothermal slurry conversion, cooling crystallization, anti-solvent crystallization, spray drying and rapid expansion of supercritical fluids. Provided in Table 2.2 is a summary which highlights examples of each method.

Table 2.2: Some Preparation Techniques for Co-Crystal Synthesis.

Drug	Co-former	Technique	Experimental
Theophylline	Citric Acid	Neat Grinding	0.150 g of an equimolar combination of theophylline and citric acid was placed into a 25 mL stainless steel grinding jar and ground for 1 h using two stainless steel balls 7 mm in diameter. The overall temperature of the reaction mixture remained below 35 °C. ³⁸
Adefovir Dipivoxil	Glutaric Acid	LAG	1:1 mole ratio of adefovir dipivoxil and glutaric acid was ground using an agate mortar and pestle for 20–30 min. Methanol was added dropwise over the course of grinding (0.5 mL/mmol cocrystal). ³⁹
Fenofibrate	Nicotinamide	Solvent Evaporation	A mixture of FNO and nicotinamide in 1:1 molar ratio was dissolved in 20 mL of ethanol with sonication (to induce saturation) and was kept overnight to evaporate solvent. The crystals obtained after evaporation of ethanol were dried in air. ⁴⁰
Trospium Chloride	Salicylic Acid	Quenching	A 1:1 physical mixture of trospium chloride with salicylic acid was prepared and heated at 10°C per min under nitrogen purge above eutectic temperature. The mixture was then cooled to room temperature at a cooling rate of 10°C per min. After the mixture stood at

Indomethacin	Saccharin	Anti-solvent Addition	30°C for 60 min, the heating was repeated and the co-crystal was obtained. ⁴¹ In a 1L double jacketed reactor, predetermined amounts of indomethacin and saccharin were fully dissolved in methanol (300 mL), and 150 mL of purified water as anti-solvent was added to the solution using a peristaltic pump. The process was performed for 30 min and the product was filtered and dried under vacuum. ⁴²
Theophylline	Glutaric Acid	Slurry Conversion	Equimolar mixture of theophylline and glutaric acid was added into chloroform to form slurry at 50°C. This slurry was seeded with crystals from co-grinding of theophylline and glutaric acid and co-crystals formed as solvent evaporated. ⁴³
Theophylline	Saccharin	Spray Drying	A 0.9% equimolar solution of theophylline and saccharin in ethanol were spray dried at an inlet temperature of 120°C and outlet temperature of 77°C to give a co-crystal. The feed rate was 5 mL/min, the air flow was 536 L/h and the aspiration was 100%. ⁴⁴

The most advantageous way to characterize a co-crystal is by growing single crystals and running X-ray diffraction. This technique will give the stoichiometric ratio, crystal lattice and intermolecular bonding of the molecular structure.⁴⁵⁻⁴⁸ Single crystal X-ray diffraction method alone is adequate in declaring that there is positive formation of a co-crystal. However, while it is the most useful, obtaining single crystals is an art, and it is not always possible. Since many co-crystals are formed using mechanochemical techniques, single crystals are often not achievable.⁴⁹ Also, changing to conditions necessary to form high quality crystals can sometimes cause components to crystallize independently. In these scenarios, other techniques can be employed to characterize the suspected co-crystal.

ssNMR is a practical characterization technique in helping elucidate the structure of the co-crystal formed. It has even been shown that ssNMR can be used to monitor co-crystal formation in situ.⁵⁰ This method can be used for small amounts of sample, is non-invasive and can adequately analyze multiphase systems.⁵¹ Using 1D and 2D ssNMR techniques

can lead to the determination of the intermolecular bonding sites within the co-crystal.⁵² When coupled with PXRD and density functional theory (DTF) calculations, 1D ssNMR can be employed to determine the molecular structure of a co-crystal. For example, a theophylline-nicotinamide co-crystal has been formed by LAG or slow evaporation with ethanol and is shown to have improved solubility and hygroscopicity than anhydrous API.⁵³ Characterization techniques and crystal engineering knowledge were used to interpret intermolecular bonding sites in the co-crystal. Next, this suggested bonding between API and excipient was refined using DTF method, and the ^{13}C and ^{15}N ssNMR spectra were predicted. These were then compared to the spectra that were obtained experimentally and validated the refined structure of the theophylline-nicotinamide co-crystal.⁵⁴

PXRD is also particularly useful; if a co-crystal is formed then the crystal lattice will change, resulting in a powder pattern that is distinct from the starting materials. This concept can be easily visualized by examining the theoretical PXRD patterns of an API, co-former and their corresponding co-crystal in Figure 2.7. It has also been demonstrated that PXRD can be utilized to help determine the purity of the co-crystal formed. This is done by formation of a calibration curve using known amounts of co-crystal and then monitoring the most intense peak in the PXRD pattern that has the least amount of overlapping.⁵⁵

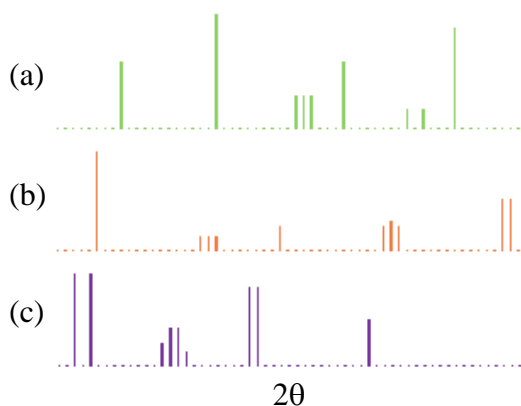


Figure 2.7: Theoretical PXRD patterns of (a) API (b) co-former and (c) their co-crystal.

Thermal analysis is also critical in the analysis of co-crystals.⁵⁶ Akin to the PXRD patterns, DSC thermographs will result in data that is different from the starting materials. The thermographs of co-crystals usually show an endothermic peak for co-crystal melting that is above or below the melting of the API and co-former.⁵⁷ Ideally, the co-crystal will have a lower melting point than the API; this will result in bonds that are easier to break and increase the drug's aqueous solubility.⁵⁸ DSC can also be employed to prepare a phase diagram for the system. When plotting the onset of peak one and the peak temperature of peak two at varying molar ratios, the result is a sort of “w” shape.⁵⁹ The region between the two eutectic peaks is the co-crystal forming region. This phenomenon is more suitably explained with the aid of an image (Figure 2.8).⁶⁰

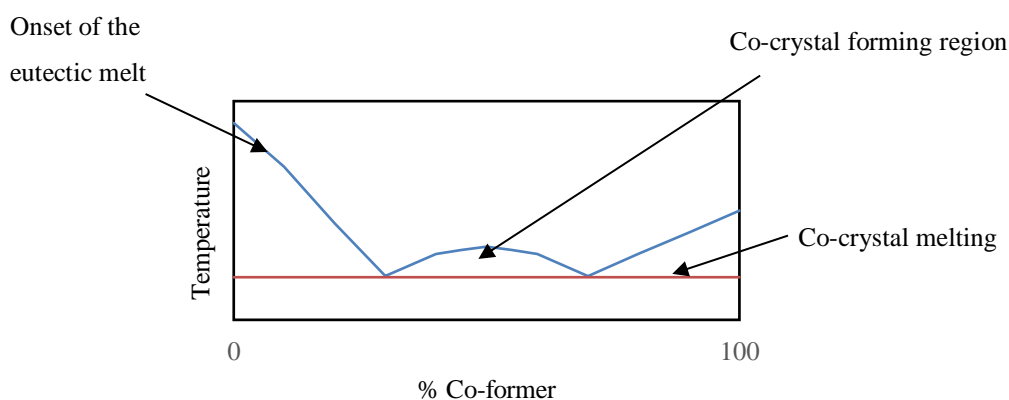


Figure 2.8: Theoretical phase diagram of a binary system capable of co-crystal formation.

Obtaining PXRD and DSC data that validates the presence of a co-crystal is sufficient in claiming co-crystal formation. To acquire the stoichiometric ratio, integration techniques of solution ^1H NMR can be employed.⁶¹ For example, if a single proton in the API is normalized to one and a chemical shift representing three protons in the excipient integrates to three, then the co-crystal ratio is 1:1 API:co-former. If single crystal XRD and/or ssNMR have been attained, then Raman and FT-IR are not necessary. However, if not attained, these techniques will show a change in stretching frequencies which will imply that certain bonds are involved in intermolecular bonding and help to determine what supramolecular synthons (see Section 2.5) are being formed.^{62,63} DSC can be coupled with FT-IR as a very quick and easy means of co-crystal confirmation. By comparing the changes in IR

frequencies as a binary system is heated, one can confidently see where co-crystal formation occurs.⁶⁴ Often times a combination of all or multiple techniques that have been mentioned are used to ensure a complete characterization so that co-crystal formation is irrefutable.

2.4 Eutectics

Like co-crystals and co-amorphous mixtures, eutectics are comprised of multiple components that are neutral at ambient conditions. A pharmaceutical eutectic mixture is comprised of API(s) and excipient(s) that do not interact to form a novel compound, but will impede the crystallization of each other at certain molar ratios.⁶⁵ These interactions are short ordered and are not seen over a long range.⁶⁶ Formation of eutectic mixtures is a useful method for weakening the intermolecular bonding of a crystalline material. This will reduce the melting point of a system, which will ultimately increase the solubility. The solubility is also increased due to the reduction in particle size (and consequently the increase in surface area) found in eutectics compared to the separate crystalline components.⁶⁷ Figure 2.9 is a visualization to help comprehend the concept of eutectics: if the green and purple characters shown in (a) are representative of the crystal structures of API and excipient, then (b) and (c) are ways in which they can interact. These different types of interactions will be found discontinuously within the eutectic mixture and can interact with each other.⁶⁸ The components of a eutectic mixture are miscible in the liquid state, but only slightly in solid state. At a eutectic composition, the API and excipient will crystallize out at the same time, while at any other molecular ratio one component will start to crystallize distinctly.⁶⁹

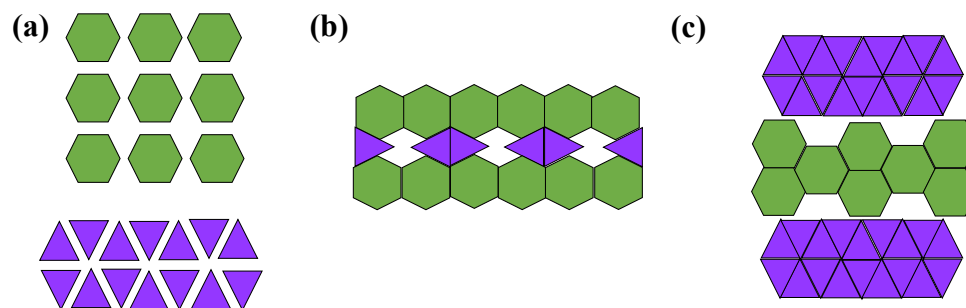


Figure 2.9: (a) molecular structures of API (green) and excipient (purple), (b) and (c) are both examples of discontinuous interaction between API and excipient found in eutectic mixtures. These interactions can interact with each other throughout the mixture.⁶⁸

The synthesis of eutectic mixtures is comparable to that of other solid states. Usually the same techniques are employed and will simply result in a eutectic instead of a co-crystal or co-amorphous mixture due to the strength of the interactions between API and excipient. The most common techniques include melting, grinding and solvent evaporation; some examples are displayed in Table 2.3.

Table 2.3: Cases Representing Some Synthesis Techniques of Eutectic Mixtures.

Drug	Excipient (or drug)	Technique	Experimental
Curcumin	Nicotinamide	Grinding	Curcumin and nicotinamide were taken in a stoichiometric ratio and subjected to solid-state grinding in a mortar-pestle for 15 min. ⁷⁰
Acetaminophen	Caffeine	Melting	A stoichiometric mixture of acetaminophen and caffeine was heated to a temperature 2°C above complete fusion of both compounds. The mixture was stirred, cooled to room temperature and gently ground (using a mortar and pestle). ⁷¹
Aspirin	Paracetamol	Solvent Evaporation	A different proportion of aspirin and paracetamol was dissolved in a methanol:dichloromethane (3:1) solution; the solvent was evaporated rapidly under vacuum. ⁷²

Eutectic mixtures are an emblematic product when screening for pharmaceutical co-crystals; consequently, the same techniques are employed for characterization. The initial step is typically to run PXRD due to its capacity for rapid analysis. The PXRD pattern for a eutectic mixture differs from that of co-crystals and co-amorphous mixtures since they are characterized by a pattern that is a combination of the starting materials (similar to a physical mixture) as opposed to one that is unique.⁷³ This distinguishing characteristic is due to API and excipient retaining their molecular structures while still comprising of intermolecular bonding.

Obtaining a PXRD pattern of this nature is not sufficient for eutectic confirmation as it may simply be a physical mixture of the components; the next step in characterization would be DSC. The thermograph for a eutectic mixture will usually appear as a melting endotherm that occurs at a temperature below both API and excipient melting.⁷⁴ A physical mixture differs and will show two distinct melting points, since the constituents are not interacting.⁷⁵ At a specific ratio, this endotherm will appear as a single peak resembling a co-crystal; however, since the PXRD pattern is not distinct, it is known to be a eutectic and no exothermic events will occur.⁵⁹ Running DSC at different molar ratios and plotting the binary phase diagram (as previously described) will result in a graph that has a “v” shape similar to Figure 2.10.

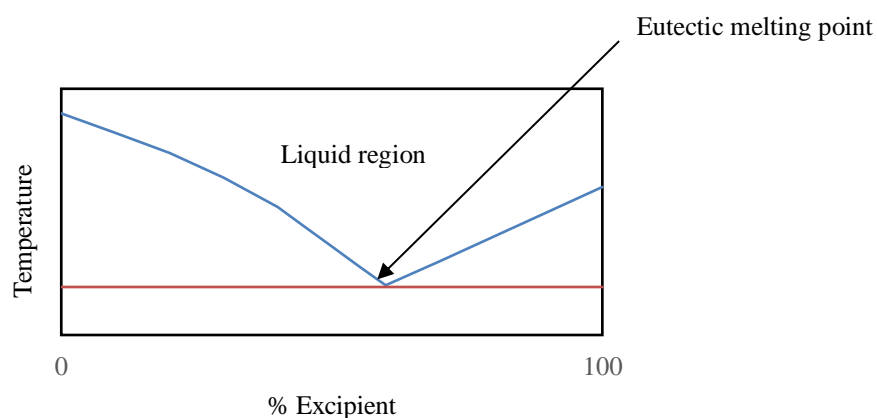


Figure 2.10: Theoretical phase diagram of a binary system which forms a eutectic.

These two techniques, PXRD and DSC, are typically sufficient in determining if a eutectic has formed. Solution ^1H NMR can be run to confirm stoichiometric ratios. FT-IR, Raman and ssNMR will all mirror PXRD in terms of obtaining result that reflect a combination of the starting materials.⁷⁰ Confocal Raman Microscopy has been employed to show discontinuous bonding in eutectic mixtures by monitoring characteristic bonding peaks.⁷⁶

2.5 Solvates

Contrary to the previous solid states that have been discussed and consist exclusively of solid materials at room temperature, a solvate is comprised of multiple components where solvent(s) has been incorporated into the crystal lattice.⁷⁷ A special case, termed a hydrate, occurs when solvent involved is water.⁷⁸ Liquid solvent at ambient conditions can be found in both stoichiometric and non-stoichiometric amounts, as depicted in Figure 2.11.⁷⁹ A solvate is described simply as any crystal composed of a solvent molecule and either a co-former or a cation-anion pair (Figure 2.11(c)). When the components are found in stoichiometric amounts, this is referred to as a “true solvate” (Figure 2.11(b)).⁸⁰

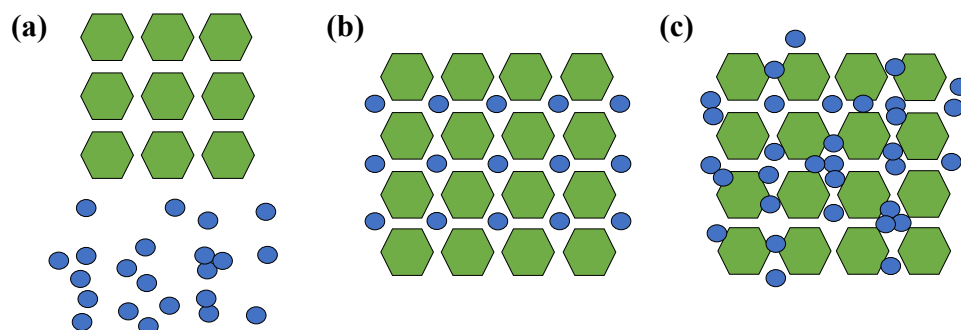


Figure 2.11: Representation of (a) crystalline API (green) and solvent (blue), (b) stoichiometric or “true” solvate, and (c) non-stoichiometric solvate.

Pharmaceutical solvates will contain an API as a co-former or pharmaceutical salt as the cation-anion pair. Solvent can incorporate into the voids of the crystal lattice and is recognized as channel solvent.⁸¹ These types of solvates will retain their crystal structure

if the solvent is removed and can be found in stoichiometric or non-stoichiometric amounts.⁸² Another type involves stronger intermolecular bonding between the solvent and the solid that results in a distinct and more stable crystal lattice. In this scenario, functionality is a more vital factor in solvent inclusion.⁸³ The extent of stabilizing, intermolecular bonding found in these solvates includes: hydrogen bonding, halogen binding, metallic bonding and Van der Waals Interactions.^{84,85}

Since solvent (especially water) is present in many stages of pharmaceutical production, solvates are an interesting means of increasing the solubility and stability of drugs. Water and many other solvents have potential to form strong hydrogen bonding interactions with a variety of molecules that could result in the formation of a crystal lattice with increased stability. Removing solvent can lead to the decomposition of the API or ruin its crystal lattice.⁸⁶ Instead of trying to remove solvent from the system as waste, alternatively, it can be incorporated (so long as it is safe for ingestion).

Synthesis of solvates is usually achieved via cooling and/or evaporative crystallization from solution. Both methods rely on supersaturation to promote crystal growth. Solvates have also been formed via grinding.⁸⁷ A case for the synthesis of each type of solvate is given in Table 2.4.

Table 2.4: Cases Representing the Synthesis of Different Types of Solvate Systems.

Drug	Solvent	Solvate Type	Experimental
Atorvastatin	Isopropanol	Stoichiometric Channel	Atorvastatin was stirred in acetone and isopropanol just below boiling point for over 24 hours. The solution was filtered, water added as anti-solvent and the product is allowed to crystallize in air at room temperature. ⁸⁸
Sitagliptin L-tartrate	Water	Non-stoichiometric Channel	Solvate was crystallized from a 2-propanol:water (8:2, v/v) mixture in air at room temperature. ⁸⁹
Dirithromycin	Cyclohexane	Stoichiometric Lattice Inclusion	Solvate isolated by vapor diffusion of cyclohexane into a toluene solution of Dirithromycin. ⁹⁰

After a solvate has been formed, one needs to properly characterize it. Once again, single crystal XRD is the all-telling technique for characterization. The data obtained will result in the molecular structure which can be used to establish the intermolecular bonding between components, whether a “true solvate” has been formed, if the solvent is located predominantly in the voids, and much more. To explore this method, an Esomeprazole Magnesium solvate, displayed in Figure 2.12 and discussed in detail in Chapter 3, will be investigated. Esomeprazole Magnesium is a poorly soluble pharmaceutical salt with low stability. In this solvate, water is bonded in two distinct modes: strong dative-covalent bonding directly with Mg and in the voids of the crystal lattice. The former water molecules are bonded more powerfully than the latter. The 1-butanol molecules are also found in the channels and can be seen to form hydrogen bonds with water. This compound is determined to be a “true solvate” with respect to the water molecules, and butanol is found in non-stoichiometric amounts.

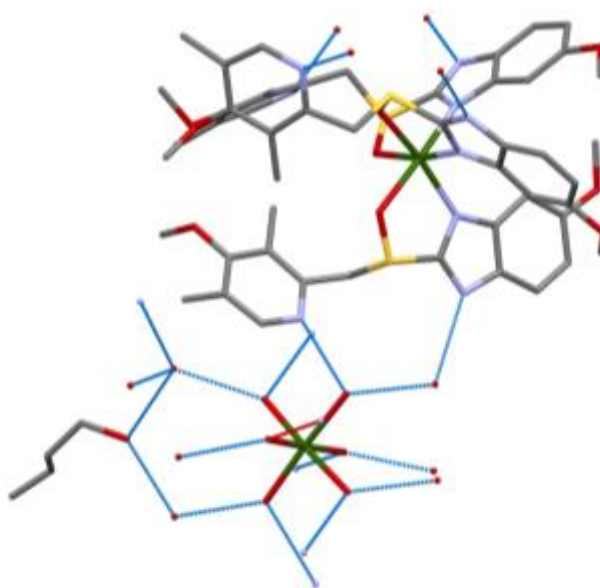


Figure 2.12: Esomeprazole Magnesium solvate with water and 1-butanol. Hydrogen bonding between molecules is shown in blue.⁷⁹

Since single crystals are not easily attainable, there are a variety of other techniques that can be used for characterization. PXRD is particularly useful when the solvate is synthesized via the formation of a new crystal lattice that incorporates the solvent. This will result in a PXRD pattern that is novel in comparison to the API.⁹¹ Conversely, if the solvent is simply filling the voids in the crystal lattice, the PXRD pattern will appear to be analogous to that of the API with very slight differences. In this situation, it is necessary to conduct further analysis, such as ssNMR, to ensure that a solvate has indeed been formed.⁹² An outstanding illustration of this is seen in Figure 2.13; ¹³C ssNMR spectra is taken for a non-stoichiometric solvate where solvent is found in the channels. The solvate is then heated to remove solvent and the resulting spectra are observed, while PXRD patterns showed no differences as the solvent was removed.⁹³

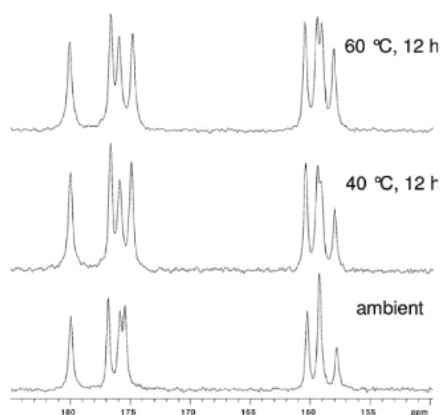


Figure 2.13: ¹³C ssNMR of a non-stoichiometric, channel solvate LY297802 tartrate at (a) ambient conditions, (b) elevated temperature with solvent removal, and (c) elevated temperature with increased solvent removal.⁹³

Dynamic Vapor Sorption (DVS) is another valuable tool in analyzing pharmaceutical solvates. This instrument measures the mass of a sample with respect to changes in relative humidity (RH). For example, if a hydrate-forming API is put into an environment of increasing humidity, a change in mass is seen during hydrate formation. The additional mass will correspond to the ratio of water incorporated into the system, and the graph will

form a hysteresis, such as the one shown in Figure 2.14.⁹⁴ This technique can also be used with other organic vapors to determine solvate formation.⁹⁵ Solvates that can form in multiple ratios or non-stoichiometrically will show multiple hysteresis. If solvate is found to bind only to the surface, it is easily removed and usually appears as a linear increase in mass with increasing RH.⁹⁶ Solvent that is incorporated into the crystal lattice will not instantly be removed; this is illustrated in Figure 2.14, as well. Once the solvate has formed, it takes a significant decrease in humidity to remove it from the lattice.⁹⁷

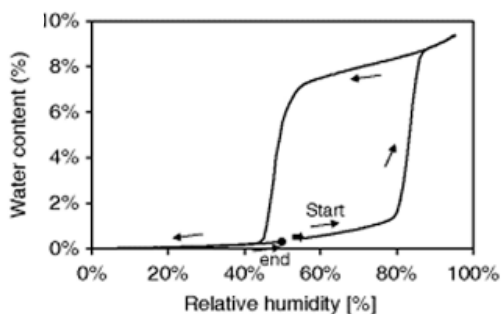


Figure 2.14: Hysteresis shown for an API with the capability to form a solvate. Relative humidity is increased gradually and then reduced.⁹⁴

Solution NMR is not a useful technique to determine the amount of solvent present due to contaminations. Often the solvate is a hydrate, and water is found in many deuterated solvents.⁹⁸ A more appropriate method is to use thermal analysis such as DSC and TGA (thermogravimetric analysis). DSC will show the removal of solvent as an endothermic peak. Due to intermolecular interactions, solvent will evaporate above its boiling point. Channel solvent is usually removed much easier and closer to boiling temperatures. TGA monitors the weight loss as a substance is heated. The percentage lost (assuming the API has not decomposed) will correspond to how much solvent has been removed, which can then be used to calculate the ratio of solvent:API.⁹⁹

2.6 Excipient Selection and Solid State Screening

The excipient that is chosen for inclusion into a drug's solid state should increase the solubility and consequently the bioavailability of the drug. This is mainly done by choosing molecules that are water soluble and have plenty of potential for intermolecular bonding.¹⁰⁰ It is also ideal to pick an excipient with a melting point lower than the API for reasons previously mentioned. The principal approach used in choosing an appropriate molecule is the supramolecular synthon method, which evaluates the potential intermolecular bonds between separate constituents of the multi-component solid state.¹⁰¹ Illustrated in Figure 2.15 are both hetero- and homosynths: one involving a bond that interacts with the same type of bond (e.g. carboxylic-carboxylic) and the latter being dissimilar bond types interacting with each other (e.g. carboxylic-amide). It was reported that heterosynths are more energetically stable; however, homosynths are still a feasible means of intermolecular bonding.¹⁰² The proposed intermolecular bonding should be strong enough to displace the bonding of the single components with themselves in order to synthesize the aforementioned solid states.

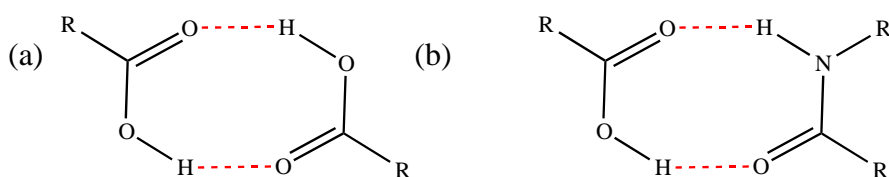


Figure 2.15: Hydrogen bonding motifs of (a) carboxylic-carboxylic homosynthon and (b) a carboxylic-amide heterosynthon.

A database of approved excipients is easily accessible from the FDA.¹⁰³ Table 2.5 is an example of the results for the molecule ethylparaben (EPB). This excipient is pre-approved for use in drugs both orally and topically with potency varying depending on the method administered. If, for example, to form a co-crystal between an API and EPB, it should be in a ratio that will not cause EPB to be administered more than ~0.6 mg per dose.

Table 2.5: Inactive Ingredient Search for Approved Drug Products, EPB

Inactive Ingredient	Route	Dosage Form	CAS Number	UNII	Maximum Potency
Ethylparaben	Oral	Granule, For Oral Solution	120478	14255EXE39	0.6 mg
Ethylparaben	Oral	Powder, For Oral Solution	120478	14255EXE39	0.66 mg
Ethylparaben	Oral	Powder, For Solution	120478	14255EXE39	0.6 mg/2 g
Ethylparaben	Oral	Solution	120478	14255EXE39	0.6 mg/5 mL
Ethylparaben	Oral	Suspension	120478	14255EXE39	2 mg/5 mL
Ethylparaben	Topical	Emulsion, Cream	120478	14255EXE39	NA

Where CAS is Chemical Abstracts Services, UNII is Unique Ingredient Identifier and EPB is ethylparaben.

Another source that researchers can use when choosing excipients is the Generally Regarded as Safe (GRAS) database, which is also published by the FDA.¹⁰⁴ Based on current studies, molecules are given an evaluation from 1-5, and the meanings of these ratings are specified in Table 2.6. Ascorbic acid, also known as vitamin C, is given a conclusion of 1 since it is well studied and known to be safe for consumption. Conclusions 1 and 2 are acceptable excipient choices for solid state modifications. This database, however, can lead to some misleading results (e.g. nutmeg is listed as class 3, but it is ingested frequently in food). Also, since these inactive ingredients are not necessarily approved for use in drug products, new clinical testing may need to be

conducted. The preferred method for excipient choice should be the Inactive Ingredient Search for Approved Drug Products Database.

Table 2.6: Types of Conclusions from the Selection Committee on GRAS Substances

Type of Conclusion	Definition
1	There is no evidence in the available information on [substance] that demonstrates, or suggests reasonable grounds to suspect, a hazard to the public when they are used at levels that are now current or might reasonably be expected in the future.
2	There is no evidence in the available information on [substance] that demonstrates a hazard to the public when it is used at levels that are now current and in the manner now practiced. However, it is not possible to determine, without additional data, whether a significant increase in consumption would constitute a dietary hazard.
3	While no evidence in the available information on [substance] demonstrates a hazard to the public when it is used at levels that are now current and in the manner now practiced, uncertainties exist requiring that additional studies be conducted.
4	The evidence on [substance] is insufficient to determine that the adverse effects reported are not deleterious to the public health should it be used at former levels and in the manner formerly practiced.
5	In view of the almost complete lack of biological studies, the Select Committee has insufficient data upon which to evaluate the safety of [substance] as a [intended use].

Another source for finding excipients is the Everything Added to Food in the United States (EAFUS) lists.¹⁰⁵ As the name states, these lists include chemicals that the FDA has approved for additives in food.¹⁰⁶ It is theorized that if the substance is safe for ingestion, then it can be used to some extent for oral administration.

The databases mentioned above are suitable to use when choosing an appropriate solvent for solvate formation; however, perhaps a more appropriate method is to use the ICH's (International Council for Harmonisation of Technical Requirements for Pharmaceuticals

for Human Use) guideline for residual solvents. Solvents are given a Class 1-3 where Class 1 should be avoided for use in pharmaceutical production, 2 should be limited and 3 has low toxic potential. For solvate formation, one should only consider Class 3 solvents that have a permitted daily exposure of 50 mg or more.¹⁰⁷

The molecule that is added for intermolecular interaction with the API may not always be an inactive ingredient. Recently, drug-drug compounds have become of increasing interest; they have been employed to reduce number of prescriptions, reposition drugs, reduce production cost and increase therapeutic effect.¹⁰⁸ It has been shown that combining antihypertension drugs that display poor aqueous solubility via co-crystal, co-amorphous mixture and eutectic formation leads to increased antihypertension activity.¹⁰⁹ As an outcome, number of prescriptions and production costs should decrease.

Now that an appropriate excipient has been chosen, which is arguably the most difficult task in this approach of crystal engineering, an extensive screening process must commence. While solid state formation procedures are well studied, they are still not necessarily well understood, especially in terms of which combinations will form novel solid states; therefore, proper screening is essential for successful crystal engineering.¹¹⁰ An extremely efficient means of screening involves grinding API and potential excipient together at varying molar ratios and collecting the DSC thermographs at a heating rate of 10K/min. This can only be done when there is no decomposition of the components before their melting.¹¹¹ When done without the presence of solvent (neat grinding), this technique is considered “green” and does not complicate the system with possible solvate formation such as with LAG.¹¹² If the resulting phase diagram gives a “w” shape, then co-crystal formation is possible; if a “v” shape is determined then there is likely a eutectic or co-amorphous product. If the melting endotherms are found not to converge, then the resulting product is merely a physical mixture, such as the illustration in Figure 2.16.¹¹³

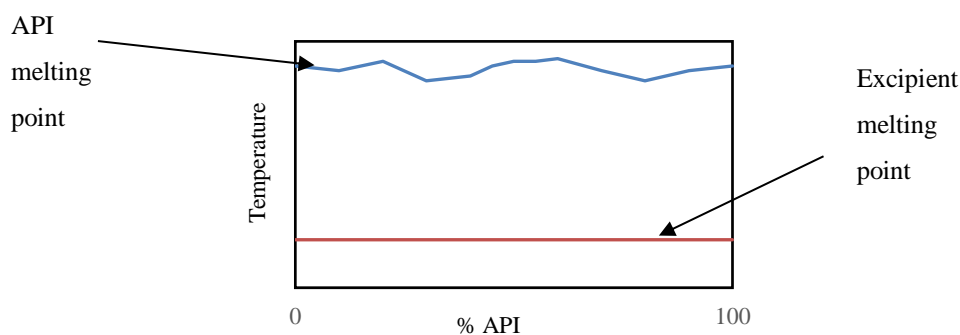


Figure 2.16: Binary phase diagram of an API and excipient incapable of forming intermolecular interactions (physical mixture).

For a more rapid screening, one can merely run the DSC for ground mixtures of 1:1, 1:2 and 2:1 molar ratios of API:excipient.¹¹⁴ One scenario is the presence of a melting endotherm that is distinct from the melting of the starting materials and is found at a consistent temperature in all three ratios. If the PXRD pattern shows novel peaks, then co-crystal formation is possible. Another scenario is the presence of an endothermic peak found lower than the melting temperature of the API or excipient that will alter slightly with varying molar ratio. Running PXRD will indicate if the product is co-amorphous or a eutectic.

While these techniques are both effective and reliable, they are not applicable for solvate formation, and sometimes solvent effects promote the formation of different solid states (e.g. a co-crystal that can be synthesized from solution but not from LAG). Solution methods usually involve dissolving API (and often excipient) in solvent(s) and seeing what product is obtained via slow evaporation and/or cooling. Another technique is to create a suspension/slurry that is allowed to equilibrate at ambient conditions.¹¹⁵ A clear drawback is that crystallization may occur slowly, and solubility issues could lead to single phases crystallizing out. Conceivably, screening with solvent(s) should be run in parallel to the DSC methods mentioned, so multiple solid states can be screened simultaneously. Using solvent mixtures helps decrease the solubility differences between API and excipient and can promote co-crystal over solvate formation if low enough solvent concentrations are employed.¹¹⁶

Another screening method, known as the Kofler technique, employs hot stage microscopy and

is useful for solid state screening. One component is melted and allowed to solidify, then a second molten phase is introduced. This partially solubilizes the first component in the second and a mixing zone is created that contains a concentration gradient (Figure 2.17). In this mixing zone, a novel solid state may form under suitable conditions. Light microscope is used to observe the number of melting points while heating.¹¹⁷ One melt is relevant for co-amorphous and eutectic mixtures, while two melts are seen for co-crystal. Co-crystal formation will result in a crystalline phase at the interface.¹¹⁸

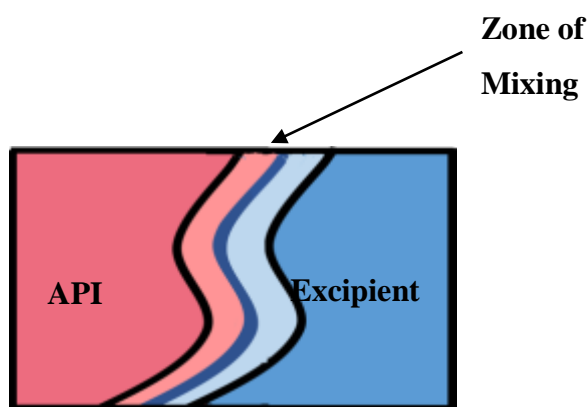


Figure 2.17: API (higher melting point) is melted and recrystallized before excipient is brought into contact which creates a zone of mixing.¹¹⁷

With appropriate screening and sufficient excipient/solvent selection, one can efficiently obtain a novel solid form that will potentially display increased solubility and bioavailability.

Summary

The FDA releases dozens of NMEs per year for pharmaceutical usage, and most of these drugs have very low aqueous solubility (i.e. the highest dose strength is soluble in more than 250 mL water over a pH range of 1 to 7.5). The solubility of Class II and IV drugs can be improved through the crystal engineering technique of adding another molecule into the crystal lattice of the API. This molecule should be pre-approved for use in pharmaceuticals and not interact

with the API. Use of this type of excipient requires no clinical testing, which is very advantageous to industry. Potential excipients can be narrowed down using a computer-based software that statistically analyzes molecular complementarity of the API with a list of common co-formers established from their molecular structure. Another technique, called the molecular synthon approach, will analyze the potential intermolecular bonding of the API and find corresponding excipients. Once a list of excipients is chosen, they should be screened using solvent crystallization in parallel with grinding and DSC techniques.

Should the screening result in the formation of a novel solid state, it is essential that it is appropriately identified. The first step should be to have the proper characterization of both the API and the excipients used; this will lead to an easy comparison and solid state analysis. Next, one should run PXRD on the new product. For the solid states mentioned in this review (i.e. co-amorphous mixtures, co-crystals, eutectics and solvates), there are three different outcomes from the evaluation of the PXRD patterns. If the product's pattern shows no new peaks and appears as a combination of the starting materials, then the result is either a physical mixture or a eutectic. If there are peaks that are distinct from the starting materials (and their polymorphs) or an entirely new pattern is observed, then the resulting solid state could either be a co-crystal or solvate. The final option is to observe a "halo" in which there is simply one very broad peak. This pattern is characteristic of an amorphous material.

A good idea at this point would be to run ^1H NMR on the product and compare it to that of the starting materials. Are the chemical shifts corresponding to the API present? How about the shifts for the excipient or solvent? Solution NMR is a valuable tool to ensure that the API did not decompose and determines what is present in their product. If a PXRD pattern of the product resulted in novel peaks and ^1H NMR revealed that the excipient (or solvent) was present, then the result is most likely a co-crystal (or solvate). Likewise, if the PXRD pattern was amorphous and both starting materials are present in the NMR spectrum, then the product is co-amorphous. ^1H NMR cannot be used to help elucidate physical mixtures from eutectics.

The next step would be to run thermal analysis to validate the formation of a new solid state. If there is a single peak in DSC that is distinct from the melting of the starting materials, then the product is a co-crystal. If there is a mixture of co-crystal and starting material, then three

peaks should be observed: one for eutectic melt, one for co-crystal melt and one for the melting of excess API. The melting point of the co-crystal is usually seen between the melting points of the starting materials. Solvates will often result in a thermograph that shows the evaporation of solvent in the lattice above its boiling point, followed by the melting of the API. TGA should be run on potential solvates to see if the weight loss corresponds to solvent loss. Co-amorphous mixtures are not predictable in their DSC thermographs but will often not show the melting of the starting materials, and an exothermic peak will be present. Physical mixtures will simply show the melting of each starting material in DSC, while eutectics will melt below the lower melting point starting material (usually excipient). DSC is also useful to plot phase diagrams. Eutectics and co-amorphous systems will give a “v” shape, while co-crystals will result in a “w” shape. The melting points in physical mixtures will not converge, so no such shape will be present.

These techniques are usually sufficient in determining what solid state is formed, but they can be aided by ssNMR, FT-IR and Raman. The ultimate tool would be to determine the molecular structure from single crystal XRD, but often it is difficult to grow crystals of appropriate quality. After a novel solid state is formed, the rate that dissolves should be determined and compared with that of the API through intrinsic or powder dissolution rate studies. If the novel product is found to have an increased solubility compared to the API, then a viable alternative to the API has been synthesized. The same can be said if the dissolution rate is increased, since the API will have only a limited time in solution (i.e. in the body). The pharmaceutical company can now investigate patenting and eventually distributing this form.

References

- (1) Rautio, J.; Kumpulainen, H.; Heimbach, T.; Oliyai, R.; Oh, D.; Järvinen, T.; Savolainen, J. *Nat. Rev. Drug Discov.* **2008**, 7 (3), 255–270.
- (2) FDA. The Biopharmaceutics Classification System (BCS) Guidance <https://www.fda.gov/aboutfda/centersoffices/officeofmedicalproductsandtobacco/cder/ucm128219.htm> (accessed Apr 13, 2017).

- (3) Lindenberg, M.; Kopp, S.; Dressman, J. B. *Eur. J. Pharm. Biopharm.* **2004**, *58* (2), 265–278.
- (4) Di, L.; Kerns, E. H.; Carter, G. T. *Curr. Pharm. Des.* **2009**, *15* (19), 2184–2194.
- (5) Lipinski, C. A. *J. Pharmacol. Toxicol. Methods* **2000**, *44* (1), 235–249.
- (6) Di, L.; Fish, P. V.; Mano, T. *Drug Discov. Today* **2012**, *17* (9), 486–495.
- (7) Zhou, J. L.; Zhang, Z. L.; Banks, E.; Grover, D.; Jiang, J. Q. *J. Hazard. Mater.* **2009**, *166* (2), 655–661.
- (8) Desiraju, G. R. (Gautam R. . *Crystal engineering : the design of organic solids*; Elsevier, 1989.
- (9) Savjani, K. T.; Gajjar, A. K.; Savjani, J. K. *ISRN Pharm.* **2012**, *2012*, 195727.
- (10) Yu, L. *Adv. Drug Deliv. Rev.* **2001**, *48* (1).
- (11) Shah, N.; Sandhu, H.; Duk Soon, C.; Chokshi, H.; Malick, W. *Amorphous Solid Dispersions : Theory and Practice*.
- (12) Hancock, B. C.; Parks, M. *Pharm. Res.* **2000**, *17* (4), 397–404.
- (13) Yamamura, S.; Gotoh, H.; Sakamoto, Y.; Momose, Y. *Eur. J. Pharm. Biopharm.* **2000**, *49* (3), 259–265.
- (14) Laitinen, R.; Löbmann, K.; Strachan, C. J.; Grohgan, H.; Rades, T. *Int. J. Pharm.* **2013**, *453* (1), 65–79.
- (15) Kasten, G.; Grohgan, H.; Rades, T.; Löbmann, K. *Eur. J. Pharm. Sci.* **2016**, *95*, 28–35.
- (16) Bates, S.; Zografi, G.; Engers, D.; Morris, K.; Crowley, K.; Newman, A. *Pharm. Res.* **2006**, *23* (10), 2333–2349.
- (17) Keen, D. A.; Dove, M. T. *Mineral. Mag.* **2000**, *64* (3).

- (18) Dengale, S. J.; Grohganz, H.; Rades, T.; Löbmann, K. *Adv. Drug Deliv. Rev.* **2016**, *100*, 116–125.
- (19) Suresh, K.; Mannava, M. K. C.; Nangia, A. *RSC Adv.* **2014**, *4* (102), 58357–58361.
- (20) Han, Y.; Pan, Y.; Lv, J.; Guo, W.; Wang, J. *Powder Technol.* **2016**, *291*, 110–120.
- (21) Lim, A. W.; Löbmann, K.; Grohganz, H.; Rades, T.; Chieng, N. *J. Pharm. Pharmacol.* **2016**, *68* (1), 36–45.
- (22) Lefort, R.; De Gusseme, A.; Willart, J.-F.; Danède, F.; Descamps, M. *Int. J. Pharm.* **2004**, *280* (1), 209–219.
- (23) Schantz, S.; Hoppu, P.; Juppo, A. M. *J. Pharm. Sci.* **2009**, *98* (5), 1862–1870.
- (24) Shah, B.; Kakumanu, V. K.; Bansal, A. K. *J. Pharm. Sci.* **2006**, *95* (8), 1641–1665.
- (25) Jensen, K. T.; Larsen, F. H.; Cornett, C.; Löbmann, K.; Grohganz, H.; Rades, T. *Mol. Pharm.* **2015**, *12* (7), 2484–2492.
- (26) Yamamoto, K.; Kojima, T.; Karashima, M.; Ikeda, Y. *Chem. Pharm. Bull. (Tokyo)*. **2016**, *64* (12), 1739–1746.
- (27) Chieng, N.; Aaltonen, J.; Saville, D.; Rades, T. *Eur. J. Pharm. Biopharm.* **2009**, *71* (1), 47–54.
- (28) Allesø, M.; Chieng, N.; Rehder, S.; Rantanen, J.; Rades, T.; Aaltonen, J. *J. Control. Release* **2009**, *136* (1), 45–53.
- (29) Widmann, G. *Thermochim. Acta* **1987**, *112* (1), 137–140.
- (30) Löbmann, K.; Laitinen, R.; Grohganz, H.; Gordon, K. C.; Strachan, C.; Rades, T. *Mol. Pharm.* **2011**, *8* (5), 1919–1928.
- (31) Chieng, N.; Hubert, M.; Saville, D.; Rades, T.; Aaltonen, J. *Cryst. Growth Des.* **2009**, *9* (5), 2377–2386.

- (32) Grifasi, F.; Chierotti, M. R.; Gaglioti, K.; Gobetto, R.; Maini, L.; Braga, D.; Dichiarante, E.; Curzi, M. *Cryst. Growth Des.* **2015**, *15* (4), 1939–1948.
- (33) Vishweshwar, P.; McMahon, J. A.; Bis, J. A.; Zaworotko, M. J. *J. Pharm. Sci.* **2006**, *95* (3), 499–516.
- (34) FDA; CDER. Guidance for Industry Guidance for Industry Regulatory Classification of Pharmaceutical Co-Crystals <http://www.fda.gov/Drugs/GuidanceComplianceRegulatoryInformation/Guidances/default.htm> (accessed May 30, 2017).
- (35) Aitipamula, S.; Banerjee, R.; Bansal, A. K.; Biradha, K.; Cheney, M. L.; Choudhury, A. R.; Desiraju, G. R.; Dikundwar, A. G.; Dubey, R.; Duggirala, N.; Ghogale, P. P.; Ghosh, S.; Goswami, P. K.; Goud, N. R.; Jetti, R. R. K. R.; Karpinski, P.; Kaushik, P.; Kumar, D.; Kumar, V.; Moulton, B.; Mukherjee, A.; Mukherjee, G.; Myerson, A. S.; Puri, V.; Ramanan, A.; Rajamannar, T.; Reddy, C. M.; Rodriguez-Hornedo, N.; Rogers, R. D.; Row, T. N. G.; Sanphui, P.; Shan, N.; Shete, G.; Singh, A.; Sun, C. C.; Swift, J. A.; Thaimattam, R.; Thakur, T. S.; Kumar Thaper, R.; Thomas, S. P.; Tothadi, S.; Vangala, V. R.; Variankaval, N.; Vishweshwar, P.; Weyna, D. R.; Zaworotko, M. J. *Cryst. Growth Des.* **2012**, *12* (5), 2147–2152.
- (36) Etter, M. C. *J. Phys. Chem.* **1991**, *95* (12), 4601–4610.
- (37) Fábíán, L. *Cryst. Growth Des.* **2009**, *9* (3), 1436–1443.
- (38) Shyam Karki, †; Tomislav Friščić, †; William Jones, *, † and; Motherwell‡, W. D. **S. 2007.**
- (39) Sungyup, J.; Insil, C.; Won II, K. *Crystals* **2015**, *5*, 583–591.
- (40) Shewale, S.; Shete, A. S.; Doijad, R. C.; Kadam, S. S.; Patil, V. A.; Yadav, A. V. *Indian J. Pharm. Sci.* **2015**, *77* (3), 328–334.

- (41) Sládková, V.; Cibulková, J.; Eigner, V.; Štunc, A.; Kratochvíl, B.; Rohlíček, J. *Cryst. Growth Des.* **2014**, *14* (6), 2931–2936.
- (42) Lee, M.-J.; Chun, N.-H.; Wang, I.-C.; Liu, J. J.; Jeong, M.-Y.; Choi, G. J. *Cryst. Growth Des.* **2013**, *13* (5), 2067–2074.
- (43) Zhang, S. *Physical Properties and Crystallization of Theophylline Co-crystals*, KTH Chemical Science and Engineering, 2010.
- (44) Hadi, K. *Spray Drying of Cocrystals for Engineering Particle Properties*, Uppsala Universitet, 2015.
- (45) Peterson, M. L.; Stanton, M. K.; Kelly, R. C.; Staples, R.; Cheng, A.; Pople, J. A.; Gordon, M. S.; Roberts, J.; Wells, M.; Bostick, T.; King, A.; Neervannan, S.; Ostovic, D.; Koparkar, A.; Surapaneni, S.; Tamir, R.; Zhu, J.; Treanor, J. J. S.; Norman, M. H. *CrystEngComm* **2011**, *13* (4), 1170–1180.
- (46) Khorasani, S.; Fernandes, M. A.; Hutter, J.; Leventis, D. C.; Li, N.-Y.; Abrahams, B. F. *Chem. Commun.* **2017**, *53* (36), 4969–4972.
- (47) Srirambhatla, V. K.; Kraft, A.; Watt, S.; Powell, A. V. *Cryst. Growth Des.* **2012**, *12* (10), 4870–4879.
- (48) Meng, F.; Li, Y.; Liu, X.; Li, B.; Wang, L. *Cryst. Growth Des.* **2015**, *15* (9), 4518–4525.
- (49) Lapidus, S. H.; Stephens, P. W.; Arora, K. K.; Shattock, T. R.; Zaworotko, M. J. *Cryst. Growth Des.* **2010**, *10* (10), 4630–4637.
- (50) Mandala, V. S.; Loewus, S. J.; Mehta, M. A. *J. Phys. Chem. Lett.* **2014**, *5* (19), 3340–3344.
- (51) Tishmack, P. A.; Bugay, D. E.; Byrn, S. R. *J. Pharm. Sci.* **2003**, *92* (3), 441–474.
- (52) Vogt, F. G.; Clawson, J. S.; Strohmeier, M.; Edwards, A. J.; Pham, T. N.; Watson, S. A. *Cryst. Growth Des.* **2009**, *9* (2), 921–937.

- (53) Lu, J.; Rohani, S. *Org. Process Res. Dev.* **2009**, *13* (6), 1269–1275.
- (54) Li, P.; Chu, Y.; Wang, L.; Wenslow, R. M.; Yu, K.; Zhang, H.; Deng, Z.; Qian, S.; Cherryman, J. C.; Docherty, R. *CrystEngComm* **2014**, *16* (15), 3141–3147.
- (55) Padrela, L.; de Azevedo, E. G.; Velaga, S. P. *Drug Dev. Ind. Pharm.* **2012**, *38* (8), 923–929.
- (56) Qiao, N.; Li, M.; Schlindwein, W.; Malek, N.; Davies, A.; Trappitt, G. *Int. J. Pharm.* **2011**, *419* (1–2), 1–11.
- (57) Srinivasulu Aitipamula; K. Mapp, L.; H. Wong, A. B.; Shan Chow, P.; H. Tan, R. B. *CrystEngComm* **2015**, *17* (48), 9323–9335.
- (58) Nayak, A.; Pedireddi, V. R. *Cryst. Growth Des.* **2016**, *16* (10), 5966–5975.
- (59) Yamashita, H.; Hirakura, Y.; Yuda, M.; Teramura, T.; Terada, K. *Pharm. Res.* **2013**, *30* (1), 70–80.
- (60) Tilborg, A.; Leyssens, T.; Norberg, B.; Wouters, J. *Cryst. Growth Des.* **2013**, *13* (6), 2373–2389.
- (61) Li, Z.; Matzger, A. *J. Mol. Pharm.* **2016**, *13* (3), 990–995.
- (62) Nugrahani, I.; Bahari, M. U. *J. Chem. Biochem.* **2014**, *2* (2), 117–137.
- (63) Elbagerma, M. A.; M Edwards, H. G.; Munshi, T.; Hargreaves, M. D.; Matousek, P.; Scowen, I. J. **2010**, *10*, 2360–2371.
- (64) Lin, H.-L.; Hsu, P.-C.; Lin, S.-Y. *Asian J. Pharm. Sci.* **2013**, *8* (1), 19–27.
- (65) Al-Saidan, S. M. *J. Control. Release* **2004**, *100* (2), 199–209.
- (66) Stoler, E.; Warner, J. C. *Molecules* **2015**, *20*, 14833–14848.
- (67) Law, D.; Wang, W.; Schmitt, E. A.; Qiu, Y.; Krill, S. L.; Fort, J. J. *J. Pharm. Sci.* **2003**, *92* (3), 505–515.

- (68) Cherukuvada, S.; Nangia, A. *Chem. Commun.* **2014**, 50 (8), 906–923.
- (69) Leuner, C.; Dressman, J. *Eur. J. Pharm. Biopharm.* **2000**, 50 (1), 47–60.
- (70) Goud, N. R.; Suresh, K.; Sanphui, P.; Nangia, A. *Int. J. Pharm.* **2012**, 439 (1), 63–72.
- (71) Bi, M.; Hwang, S.-J.; Morris, K. R. *Thermochim. Acta* **2003**, 404 (1), 213–226.
- (72) Jain, H.; Khomane, K. S.; Bansal, A. K. *CrystEngComm* **2014**, 16 (36), 8471.
- (73) Cherukuvada, S.; Guru Row, T. N. *Cryst. Growth Des.* **2014**, 14 (8), 4187–4198.
- (74) Campanella, L.; Micieli, V.; Tomassetti, M.; Vecchio, S. *J. Therm. Anal. Calorim.* **2010**, 99, 887–892.
- (75) Fathy, M.; Hassan, M. A.; Mohamed, F. A. *Pharmazie* **2002**, 57 (12), 825–828.
- (76) Figueirêdo, C. B. M.; Nadvorny, D.; de Medeiros Vieira, A. C. Q.; Soares Sobrinho, J. L.; Rolim Neto, P. J.; Lee, P. I.; de La Roca Soares, M. F. *Int. J. Pharm.* **2017**, 525 (1), 32–42.
- (77) Griesser, U. J. In *Polymorphism*; Wiley-VCH Verlag GmbH & Co. KGaA: Weinheim, FRG, 2006; pp 211–233.
- (78) Khankari, R. K.; Grant, D. J. W. *Thermochim. Acta* **1995**, 248, 61–79.
- (79) Skieneh, J.; Khalili Najafabadi, B.; Horne, S.; Rohani, S. *Molecules* **2016**, 21 (544), 1–10.
- (80) Grothe, E.; Meekes, H.; Vlieg, E.; ter Horst, J. H.; de Gelder, R. *Cryst. Growth Des.* **2016**, 16 (6), 3237–3243.
- (81) Parkin, S. R.; Behrman, E. J. *Acta Crystallogr. Sect. C Cryst. Struct. Commun.* **2011**, 67 (8), o324–o328.

- (82) Brittan, H. G. *Polymorphism in Pharmaceutical Solids, Second Edition*; CRC Press, 2009.
- (83) Bērziņš, A.; Skarbulis, E.; Reķis, T.; Actiņš, A. *Cryst. Growth Des.* **2014**, *14* (5), 2654–2664.
- (84) Nerenberg, P. S.; Jo, B.; So, C.; Tripathy, A.; Head-Gordon, T. *J. Phys. Chem. B* **2012**, *116* (15), 4524–4534.
- (85) Mukherjee, A.; Tothadi, S.; Desiraju, G. R. *Acc. Chem. Res.* **2014**, *47* (8), 2514–2524.
- (86) Bauer, J. F. *J. Valid. Technol.* **2009**, *15* (2), 49–56.
- (87) Crowley, K. J.; Zografi, G. *J. Pharm. Sci.* **2002**, *91* (2), 492–507.
- (88) Chadha, R.; Kuhad, A.; Arora, P.; Kishor, S. *Chem. Cent. J.* **2012**, *6* (1), 114.
- (89) Tieger, E.; Kiss, V.; Pokol, G.; Finta, Z.; Dušek, M.; Rohlíček, J.; Skořepová, E.; Brázda, P. *CrystEngComm* **2016**, *18*, 3819.
- (90) Stephenson, G. A.; Stowell, J. C.; Toma, P. H.; Dorman, D. E.; Greene, J. R.; By, S. R. *J. Am. Chem. Soc.* **1994**, *116*, 5766–5773.
- (91) Aitipamula, S.; Chow, P. S.; Tan, R. B. H. *CrystEngComm* **2012**, *14* (2), 691–699.
- (92) Othman, A.; Evans, J. S. O.; Evans, I. R.; Harris, R. K.; Hodgkinson, P. *J. Pharm. Sci.* **2007**, *96* (5), 1380–1397.
- (93) Hilfiker, R.; Blatter, F.; Raumer, M. von. In *Polymorphism*; Wiley-VCH Verlag GmbH & Co. KGaA: Weinheim, FRG, 2006; pp 1–19.
- (94) Beckmann, W. *Crystallization : basic concepts and industrial applications*; Wiley-VCH, 2013.
- (95) Florence, A. T. (Alexander T.; Siepmann, J. *Modern pharmaceuticals. Volume 1, Basic principles and systems*; Informa Healthcare USA, 2009.

- (96) Templeton, A. C.; Byrn, S. R.; Haskell, R. J.; Prisinzano, T. E. *Discovering and developing molecules with optimal drug-like properties*; 2014.
- (97) Cui, P.; Yin, Q.; Guo, Y.; Gong, J. *Ind. Eng. Chem. Res.*, **2012**, *51* (39), 12910–12916.
- (98) Fulmer, G. R.; M Miller, A. J.; Sherden, N. H.; Gottlieb, H. E.; Nudelman, A.; Stoltz, B. M.; Bercaw, J. E.; Goldberg, K. I.; Beckman, M. **2010**.
- (99) Neville, G. A.; Becksteadlf, H. D.; Cooney, J. D. *Fresenius J Anal Chem* **1994**, *349*, 746–750.
- (100) Shaw, L. R.; Irwin, W. J.; Grattan, T. J.; Conway, B. R. *Drug Dev. Ind. Pharm.* **2005**, *31* (6), 515–525.
- (101) Desiraju, G. R. *Angew. Chemie Int. Ed. English* **1995**, *34* (21), 2311–2327.
- (102) Adalder, T. K.; Sankolli, R.; Dastidar, P. *Cryst. Growth Des.* **2012**, *12* (5), 2533–2542.
- (103) FDA. Inactive Ingredient Search for Approved Drug Products. <https://www.accessdata.fda.gov/scripts/cder/iig/index.cfm> (accessed May 26, 2017).
- (104) SCOGS (Select Committee on GRAS Substances). GRAS Substances Database <https://www.accessdata.fda.gov/scripts/fdcc/?set=SCOGS> (accessed May 29, 2017).
- (105) Schultheiss, N.; Newman, A. *Cryst. Growth Des.* **2009**, *9* (6), 2950–2967.
- (106) FDA. Everything Added to Food in the United States (EAFUS) <https://www.accessdata.fda.gov/scripts/fcn/fcnNavigation.cfm?rpt=eafuslisting> (accessed Jun 6, 2017).
- (107) International Council for Harmonisation of Technical Requirements for Pharmaceuticals for Human Use. Impurities: Guidline for Residual Solvents Q3C(R6)

https://www.ich.org/fileadmin/Public_Web_Site/ICH_Products/Guidelines/Quality/Q3C/Q3C_R6__Step_4.pdf (accessed Jun 6, 2017).

- (108) Sekhon, B. S. *Daru* **2012**, *20* (1), 45.
- (109) Haneef, J.; Chadha, R. *AAPS PharmSciTech* **2017**.
- (110) Yadav, A. V.; Shete, A. S.; Dabke, A. P.; Kulkarni, P. V.; Sakhare, S. S. *Indian J. Pharm. Sci.* **2009**, *71* (4), 359–370.
- (111) Berry, D. J.; Steed, J. W. *Adv. Drug Deliv. Rev.* **2017**.
- (112) Bag, P. P.; Kothur, R. R.; Malla Reddy, C. *CrystEngComm* **2014**, *16* (22), 4706.
- (113) de Oliveira, G. G. G.; Feitosa, A.; Loureiro, K.; Fernandes, A. R.; Souto, E. B.; Severino, P. *Saudi Pharm. J. SPJ Off. Publ. Saudi Pharm. Soc.* **2017**, *25* (1), 99–103.
- (114) Lu, E.; Rodríguez-Hornedo, N.; Suryanarayanan, R. *CrystEngComm* **2008**, *10* (6), 665.
- (115) Zhang, G. G. Z.; Henry, R. F.; Borchardt, T. B.; Lou, X. *J. Pharm. Sci.* **2007**, *96* (5), 990–995.
- (116) Rager, T.; Hilfiker, R. *Cryst. Growth Des.* **2010**, *10* (7), 3237–3241.
- (117) Berry, D. J.; Seaton, C. C.; Clegg, W.; Harrington, R. W.; Coles, S. J.; Horton, P. N.; Hursthouse, M. B.; Storey, R.; Jones, W.; Friščić, T.; Blagden, N. *Cryst. Growth Des.* **2008**, *8* (5), 1697–1712.
- (118) McNamara, D. P.; Childs, S. L.; Giordano, J.; Iarriccio, A.; Cassidy, J.; Shet, M. S.; Mannion, R.; O'Donnell, E.; Park, A. *Pharm. Res.* **2006**, *23* (8), 1888–1897.

Chapter 3

Crystallization of Esomeprazole Magnesium Water/Butanol Solvate

The molecular structure of esomeprazole magnesium derivative in the solid-state is reported for the first time along with a simplified crystallization pathway. The structure was determined using single crystal X-ray diffraction technique to reveal the bonding relationships between esomeprazole heteroatoms and magnesium. The esomeprazole crystallization process was carried out in 1-butanol and water was utilized as anti-solvent. This compound proved to be esomeprazole magnesium tetrahydrate with two 1-butanol molecules that crystallized in $P6_3$ space group, in a hexagonal unit cell. Complete characterization of a sample after drying was conducted by the use of powder X-ray diffraction (PXRD), ^1H nuclear magnetic resonance spectroscopy (NMR), thermogravimetric analysis (TGA), differential scanning calorimetry (DSC), infrared spectroscopy (IR), and dynamic vapor sorption (DVS). Investigation by ^1H NMR and TGA has shown that the solvent content in the dried sample consists of two water molecules and 0.3 butanol molecules per one esomeprazole magnesium molecule. This is different from the single crystal X-ray diffraction results and can be attributed to the loss of some water and 1-butanol molecules stabilized by intermolecular interactions. The title compound, after drying, is a true solvate in terms of water; conversely, 1-butanol fills the voids of the crystal lattice in non-stoichiometric amounts.

Introduction

Esomeprazole, the (S)-enantiomer of omeprazole, is the first single optical isomer proton pump inhibitor.¹ This enantiomer forms an active inhibitor achiral sulphenamine when in the acidic compartment of the parietal cell. The activated form of omeprazole prevents the formation of gastric acid by blocking the enzyme H^+/K^+ -ATPase, which is accountable for the formulation of gastric acid and is found in the secretory membranes of the parietal cell.² The stability of this active pharmaceutical ingredient (API) is a function of pH and acidic conditions must be avoided. In acidic conditions, omeprazole can degrade to form at least

five distinct impurities. These degradants do not inhibit the production of gastric acid and reduce the competence of the pharmaceutical.³ Omeprazole has been documented to decompose up to 10% in air due to moisture.⁴ Esomeprazole has been presented in various forms of alkaline salts as a means of increasing stability. The salt of interest is esomeprazole magnesium, which has a half-life of 19 hours at 25 °C and 8 hours at 37 °C while at pH 6.⁵

Omeprazole possesses a single stereogenic center on the sulfur atom and is by definition a racemic mixture of the (R) and (S) enantiomers. The (S)-enantiomer of this API is found in higher concentrations in plasma membrane compared to the (R)-enantiomer because it is more slowly and less variably metabolized. The intrinsic clearance is three times lower for esomeprazole, meaning longer resonance time *in vivo*. The active inhibitor formed is the same for both isomers and as a result they have the same effect on the body⁶. Shown in Figure 0.1, esomeprazole displays tautomerism of the benzimidazole N-H hydrogen atom, resulting in 5-methoxy and 6-methoxy tautomers. In solution, both tautomers are present but the 6-methoxy derivative is favoured nearly 2:1.⁷ According to ¹H and ¹³C NMR studies, the 6-methoxy tautomer is the only form present in the solid state.⁸ It has also been confirmed through crystallographic analysis that the 6-methoxy derivative is more stable.⁹ This combination of chirality and tautomerism allows for a wide range of possible crystalline structures of this API.

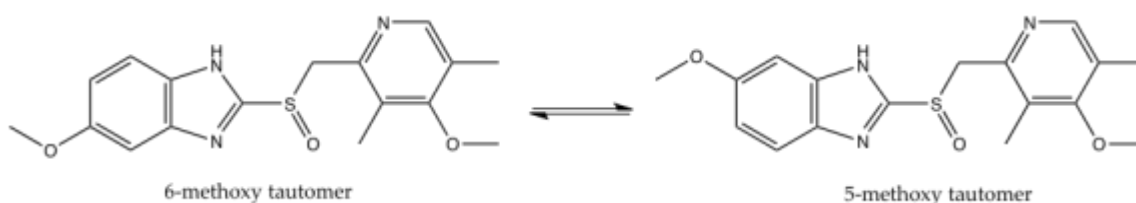


Figure 0.1: The 5-methoxy and 6-methoxy tautomers of omeprazole.

A potential technique to stabilize esomeprazole is to form a solvate by incorporating solvent molecules into the crystal lattice of the API via intermolecular forces. In a “true” solvate, Figure 0.2 (a), the solvent molecules become included in the unit cell in stoichiometric amounts. The crystal structure will collapse when solvent is removed from these solvates. Alternatively, solvent molecules can fill the voids and channels of the

crystal structure in non-stoichiometric amounts. These types of solvates, shown in Figure 0.2 (b), will remain crystalline when solvent is removed.¹⁰ When forming a solvate, one must be vigilant in ensuring that the incorporated solvent is not toxic to the consumer at a given dosage.¹¹ Minimal research articles have been published exploring the possibility of esomeprazole solvates, though a crystalline form of omeprazole sodium ethanol solvate has been reported.^{12,13}

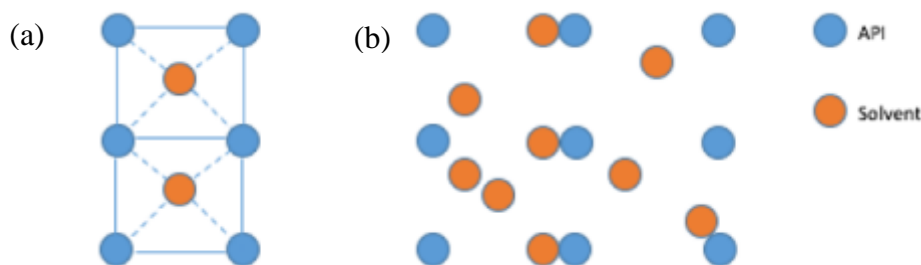


Figure 0.2: A simplified visualization of (a) a “true” solvate vs (b) a non-stoichiometric solvate, where the solvent can be one or more types of solvent.

Analogous to many prospective APIs, the instability of esomeprazole poses concerns for industry in manufacturing and storage.¹⁴ Since water is present throughout many industrial processes, one attempt at stabilization is through the investigation of possible pseudopolymorphs, such as hydrates. Pharmaceutical hydrates occur when water becomes incorporated into the crystal lattice of an API by means of intermolecular bonding.¹⁵ The small size relative to most pharmaceuticals, as well as the hydrogen bonding ability of water, make it an ideal molecule to incorporate into the crystal lattice.¹⁶ To date, there are patented examples of esomeprazole magnesium in tetrahydrate, trihydrate, dihydrate, monohydrate and hemihydrate forms.^{17,18} In a study of esomeprazole magnesium hydrates, it was found that the stability order in water is trihydrate > dihydrate form A > tetrahydrate > dihydrate form B. The solubility order in water was determined to be dihydrate form B > tetrahydrate > dihydrate form A > trihydrate.¹⁹

Materials and Methods

Esomeprazole magnesium (MW= 713.12 g/mol) was provided by Apotex Pharmachem Inc. and kept in an inert environment when in storage. 1-butanol was purchased from Fischer Scientific and used in crystallization. All ^1H NMR spectra were obtained from solutions in $\text{DMSO-}d_6$ purchased from Sigma Aldrich.

A Bruker Apex II Diffractometer with Mo X-ray radiation was used to obtain the crystal structure of the title compound. Powder X-ray Diffraction was obtained from a Rigaku Miniflex instrument with Cu X-ray radiation. Scans were run at a speed of $1.00^\circ/\text{minute}$ for 2θ values of $2.00\text{-}40.00^\circ$. Thermogravimetric analysis and differential scanning calorimetry were conducted on the Mettler-Toledo STAR^e 851^e and 822^e instruments, respectively, at a heating rate of $5^\circ\text{C}/\text{minute}$ from $25\text{-}350^\circ\text{C}$. ^1H NMR spectrum was collected on a Mercury VX 400 MHz machine. IR results were obtained over 32 scans from 4000 cm^{-1} to 500 cm^{-1} using a Nicolet 6700 FT-IR spectrometer. DVS-1000, from Surface Measurement Systems Ltd., was used to obtain results for dynamic vapor sorption. The esomeprazole magnesium water/butanol solvate was obtained by dissolving 0.750 g of amorphous esomeprazole magnesium in 7.0 mL of 1-butanol. Once in solution, it was filtered to obtain a clear solution, then 1.0 mL of distilled water was added and stirred until miscible. The solution was kept overnight at 5.0°C . Crystalline powder was formed which was filtered and washed with 1-butanol. Surface solvent was removed by heating under vacuum at $50\text{-}55^\circ\text{C}$ for up to 16 hours. The single crystal sample was obtained by dissolving 0.700g of amorphous esomeprazole magnesium in 40.0 mL of 1-butanol. To the clear solution, 2.0 mL of distilled water was added. The solution was then left at 5.0°C for 2-3 weeks until single crystals had formed.

Results and Discussion

In the present work, a novel form of esomeprazole magnesium has been characterized by single crystal X-Ray diffraction, powder X-ray diffraction (PXRD), ^1H NMR spectroscopy, infrared spectroscopy (IR), thermogravimetric analysis (TGA), differential scanning calorimetry (DSC) and dynamic vapour sorption (DVS). The trihydrate form is known to be soluble in methanol, ethanol and 1-butanol.²⁰ The solubility in ethanol is low,

and methanol is toxic to humans. Since 1-butanol is on the FDA approved list of solvents/excipients, the esomeprazole magnesium water/1-butanol solvate was further investigated. Additionally, crystallization of this solvate was particularly simple and moderately short.

Existing literature contains the single crystal structures for omeprazole and toluene hemisolvate piperazinium esomeprazolate.^{9,21,22} To better understand the bonding and structure of esomeprazole derivatives, various efforts were made at forming single crystals. Plate like single crystals were formed from a solution of amorphous esomeprazole magnesium in 1-butanol in the presence of water at 5 °C after approximately three weeks. The sample was mounted on a Mitegen polyimide micromount with a small amount of Paratone N oil. All X-ray measurements were made on a Bruker Kappa Axis Apex2 diffractometer at a temperature of 110 K. The unit cell dimensions were determined from a symmetry constrained fit of 9907 reflections with $6.4^\circ < 2\theta < 46.62^\circ$. The data collection strategy was a number of ω and ϕ scans which collected data up to 51.468° (2θ). The frame integration was performed using SAINT.²³ The resulting raw data was scaled and absorption corrected using a multi-scan averaging of symmetry equivalent data using SADABS.²⁴ The structure was solved by using a dual space methodology using the SHELXT program.²⁵ All non-hydrogen atoms were obtained from the initial solution. All hydrogen atoms except for water molecules were introduced at idealized positions and were allowed to ride on the parent atom. The hydrogen atoms on the water molecules were added considering hydrogen bonding with nitrogen or oxygen atoms around them. The structural model was fit to the data using full matrix least-squares based on F^2 . The calculated structure factors included corrections for anomalous dispersion from the usual tabulation. The structure was refined using the SHELXL-2014 program from the SHELXTL suite of crystallographic software.²⁶ Graphic plots were produced using the Mercury program suite (Summary of crystal data in Table 0.1).²⁷ CCDC 1468173 contains the supplementary crystallographic data for this paper. These data can be obtained free of charge from The Cambridge Crystallographic Data Centre via www.ccdc.cam.ac.uk/data_request/cif.

Table 0.1: Summary of Crystal Data.

Formula	$C_{126}H_{198}Mg_3N_{18}O_{36}S_6$
Formula Weight (<i>g/mol</i>)	2806.30
Crystal Dimensions (<i>mm</i>)	$0.185 \times 0.142 \times 0.092$
Crystal System	Hexagonal
Space Group	P 6 ₃
Temperature, K	110
<i>a</i> , Å	14.701(4)
<i>b</i> , Å	14.701
<i>c</i> , Å	39.123(11)
α , °	90
β , °	90
γ , °	120
<i>V</i> , Å ³	7323(5)
<i>Z</i>	2
F(000)	3000
ρ (<i>g/cm</i>)	1.273
λ , Å, (MoK α)	0.71073
μ , (<i>cm</i> ⁻¹)	0.185
R ₁	0.0674
wR ₂	0.1733
GOF	1.032
Maximum shift/error	0.000
Min & Max peak heights on final ΔF Map (<i>e</i> /Å)	-0.497, 0.487

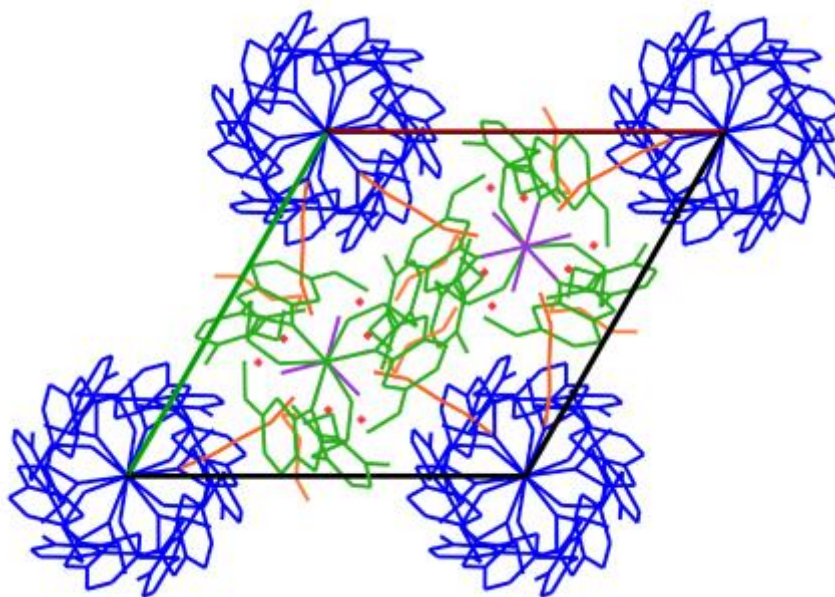


Figure 0.3: Eesomeprazole magnesium molecules crystallize in P 6₃ spaces group alongside with water and 1-butanol molecules; the molecules of the same colour are symmetry equivalent.

Molecules of esomeprazole magnesium crystallize in the space group P 6₃, with $Z = 2$, alongside four water and two 1-butanol molecules ($C_{126}H_{198}Mg_3N_{18}O_{36}S_6$) (Figure 0.3). As it is shown in Figure 0.4, coordination around the magnesium centers is octahedral. For every Mg center that has six water molecules around it, there are two magnesium centers that are coordinated with three esomeprazole ligands. All of the esomeprazole molecules act as chelating ligands and coordinate the Mg centers with one oxygen as well as one nitrogen atom. This agrees with previous DFT calculations, where omeprazole was shown to favour coordination with Co(II) and Fe(III) through the sulfoxide oxygen and the benzimidazolic nitrogen.²⁸ All of the six water molecules that are coordinated to the magnesium center show hydrogen bonding either with other water molecules in the lattice or the nitrogen atoms in the esomeprazole ligands (Figure 0.5). 1-Butanol molecules fill the voids in this lattice and are also hydrogen bonded to the water molecules in the lattice.

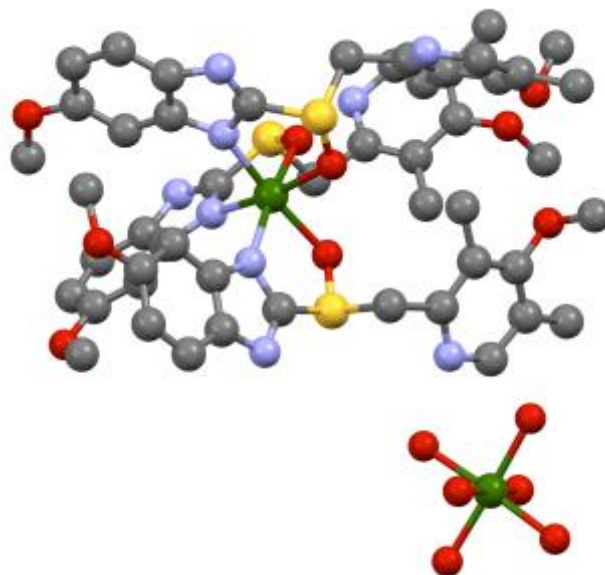


Figure 0.4: Two types of coordination around the magnesium centers, hydrogen atoms and non-bonded solvents have been omitted for clarity. Mg: green, S: yellow, O: red, N: blue, C: grey.

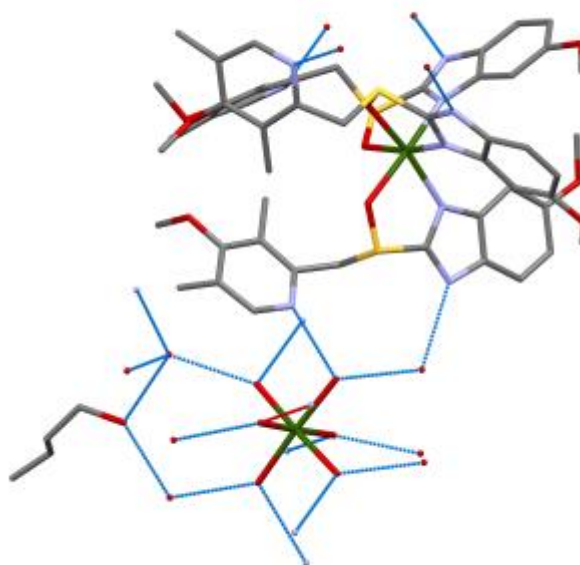


Figure 0.5: Strong hydrogen bonding between the molecules in the lattice are shown in blue dotted lines; hydrogen atoms have been omitted for more clarity. Mg: green, S: yellow, O: red, N: blue, C: grey.

From the single crystal structure, the powder pattern was simulated and is shown in Figure 0.6. This pattern is different than that of the crystals which have been dried under vacuum. In the pattern of the dried sample, the peaks at $2\theta = 7^\circ$ and 8° are much lower in intensity. As well, the simulated peak at $2\theta = 4.5^\circ$ has shifted to 5.1° ; however, the peak at $2\theta = 18.5^\circ$ is consistent in both simulated and experimental powder pattern. Some solvent molecules have been removed from the lattice, and as a result, a different polymorph according to the PXRD pattern is formed. This is further proved by other characterization techniques that are discussed below. As seen in the single crystal analysis, water is found in the channels of the lattice along with being bonded to the magnesium cation. The dative covalent bonding of water to the magnesium is much stronger than the hydrogen bonding displayed by the channel water molecules. The change in PXRD pattern shows that the crystal lattice has changed by removing some of the water and 1-butanol molecules. The pattern obtained of the solvate after drying is comparable to that of esomeprazole magnesium dihydrate form A, with equivalent peaks at $2\theta = 5^\circ$ and 18° .²⁹ The X-ray pattern was consistent for the sample after drying under vacuum at 50°C for two hours and up to 16 hours. The powder diffraction also remained the same for samples that were exposed to air. Since esomeprazole is known to be chemically unstable in air, the ability of the esomeprazole magnesium water/1-butanol solvate to remain crystalline in air highlights a potential advantage for its use in pharmaceutical solid dosage forms.

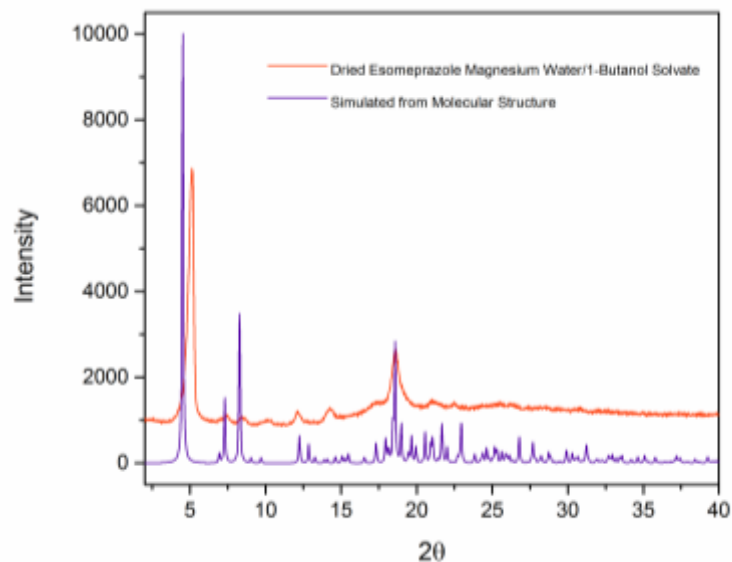


Figure 0.6: X-ray powder diffraction of esomeprazole magnesium water/butanol solvate calculated from single crystal structure and esomeprazole magnesium water/butanol solvate after drying under vacuum.

In order to confirm the occurrence of 1-butanol in the crystal lattice after drying, ^1H NMR data was collected from the dry sample in DMSO- d_6 solution (see Appendix A, Figure A-1). The presence of water and 1-butanol is clear by analysis of the spectrum; esomeprazole: ^1H NMR δ 8.25 (m, 1H), 7.37 (d, $J=8.6$ Hz, 1H), 7.02 (d, $J=2.6$ Hz, 1H), 6.60 (dd, $J=2.5$ Hz, 8.4 Hz, 1H), 4.72 and 4.46 [d (AB system, $J=12.7$ Hz, 2H)], 3.75 (s, 3H), 3.70 (s, 3H) 2.21(s, 6H); 1-butanol: ^1H NMR δ 4.30 (t, 2H), 3.38 (q, 1H), 1.39 (m, 2H) 1.30 (m, 2H) and 0.83 (t, 3H); Water: ^1H NMR δ 3.3 (s, 2H).^{30,31} Since it was assumed that all surface water and solvent are removed after sufficient drying, the characteristic peaks were integrated to determine the 1-butanol content. As previously stated, esomeprazole will demonstrate tautomerism in solution. DMSO- d_6 , a slow exchange solvent, was utilized in an effort to help reduce these effects in solution.³² The multiplet occurring at 8.25 ppm is characteristic of esomeprazole, unaffected by tautomerism, and signifies a single proton, while the triplet at 0.84 ppm is representative of the methylene protons of 1-butanol. Integrating these peaks confirmed that there are still 0.3 1-butanol molecules per esomeprazole magnesium in the dried sample. Water, seen at 3.33 ppm, cannot be accurately quantified in this method due

to inevitable impurities in the NMR solvent. These impurities arise from DMSO's affinity for water; it cannot be dried completely over molecular sieves.³³

The structure of esomeprazole magnesium dihydrate/1-butanol solvate contains many different functional groups. IR spectroscopy was utilized to help confirm the presence of esomeprazole, water and 1-butanol after a sample had been dried under vacuum (see Appendix A, Figure A -2). Table 0.2 shows the absorption frequencies for these functional groups. The peaks presented are characteristic of esomeprazole with a broad peak at approximately 3000 cm^{-1} from the O-H stretching in water and 1-butanol. The peak representative of the N-H in the benzimidazole, usually seen around 3400 cm^{-1} , is not observed. This is due to overlapping with the frequencies of the O-H stretching from coordinated and non-coordinated solvent molecules. Compared to free esomeprazole, no change in frequency is seen for the pyridinic nitrogen. This agrees with the molecular structure determined with single crystal XRD, where esomeprazole is coordinating through benzimidazolic nitrogen and sulfoxide oxygen. The frequencies observed are in close agreement with the calculated IR spectra for omeprazole co-ordinated to different metal centers.²⁸

Table 0.2: IR spectroscopy absorption frequencies and corresponding functional groups.

Functional Group	Absorption Frequency (cm^{-1})	Type of Vibration
sulfoxide	1076	S=O stretching ³⁴
methoxy	1199	C-O stretching ³⁴
methoxy	1228	C-O stretching ³⁴
amine	1409	N-H bending ²⁸
pyridine	1569	C=N stretching ²⁸
benzimidazole	1612, 1588	C=N stretching ²⁸
aromatic	2970	C=C-H asymmetric stretching ³⁴
alcohol/water	3100-2800	O-H stretching ³⁵

In an attempt to confirm the total solvent content in the crystal lattice, thermogravimetric analysis (TGA) was performed. The TGA results revealed two mass losses for this solvate. The first step can be attributed to the loss of solvent in the lattice, while the second step can be accredited to the decomposition of the sample. The desolvation resulted in a loss of 7.6% of the total mass. These results are consistent with the ^1H NMR analysis of 0.3 1-butanol and two water molecules per esomeprazole magnesium. The spectrum obtained from TGA confirms that the esomeprazole magnesium water/1-butanol solvate loses solvent from the lattice when dried under vacuum. TGA was also conducted after heating the sample to 120 °C under vacuum, and the same results were acquired. The second mass loss begins at 200 °C, typical for the decomposition of esomeprazole magnesium.²⁹

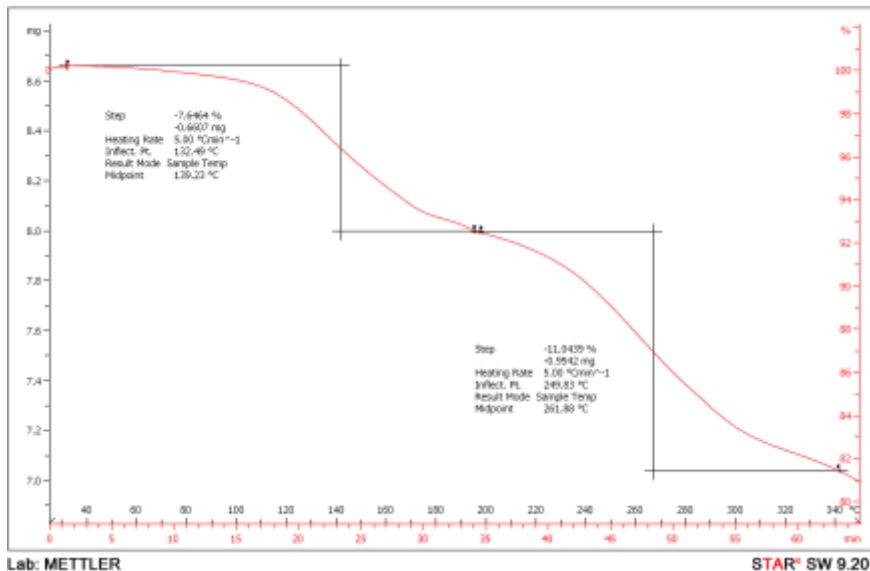


Figure 0.7: TGA of the title sample showing two mass losses. The first loss of 7.6% is desolvation, while the second loss is decomposition of the esomeprazole molecule.

Differential scanning calorimetric analysis was performed on the esomeprazole magnesium water/1-butanol solvate as well (Figure 0.8). The pattern shown can be described as an exothermic melting via decomposition. Amorphous esomeprazole magnesium is known to display an exothermic peak at approximately 200 °C.³⁶ When DSC was run on the starting material, the exothermic peak was seen at 181 °C. From Figure 0.8, the water/1-butanol solvate decomposes at 200 °C. This increase in decomposition

temperature implies an increase in stability. The peak shown below is broader than that of the amorphous API; the width at half height is 13.3 °C, while the width is 5.8°C for amorphous esomeprazole magnesium. The broadening agrees with the results from TGA and ^1H NMR that show solvent is still present in the lattice. In addition to this peak, the DSC curve of the title compound also shows an endotherm at 175 °C. This curve matches known results for esomeprazole magnesium dihydrate, which aids in validating the assumption that some of the solvent is being removed after vacuum drying, leaving esomeprazole magnesium dihydrate with some 1-butanol molecules.¹⁷

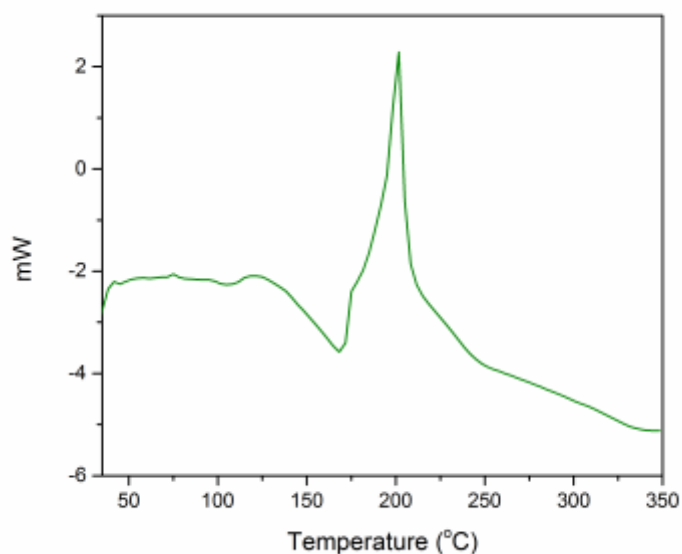


Figure 0.8: The DSC curve of esomeprazole magnesium water/1-butanol solvate. The curve was obtained from 25-350 °C at a heating rate of 5 °C/minute. An exotherm characteristic of esomeprazole magnesium is seen at 200 °C as well as an endotherm at 175 °C.

The stability of this compound is further investigated by DVS; the subsequent isotherm is shown in Figure 0.9. In sorption cycles 1 and 2, there is a 5.3% mass increase. The adsorption/desorption of water is a reversible process in the title compound. Since the sample reverted to the initial mass, the water adsorbed can be said to be on the surface of

the API. The behaviour of this isotherm implies that the structure of the title compound is highly crystalline.

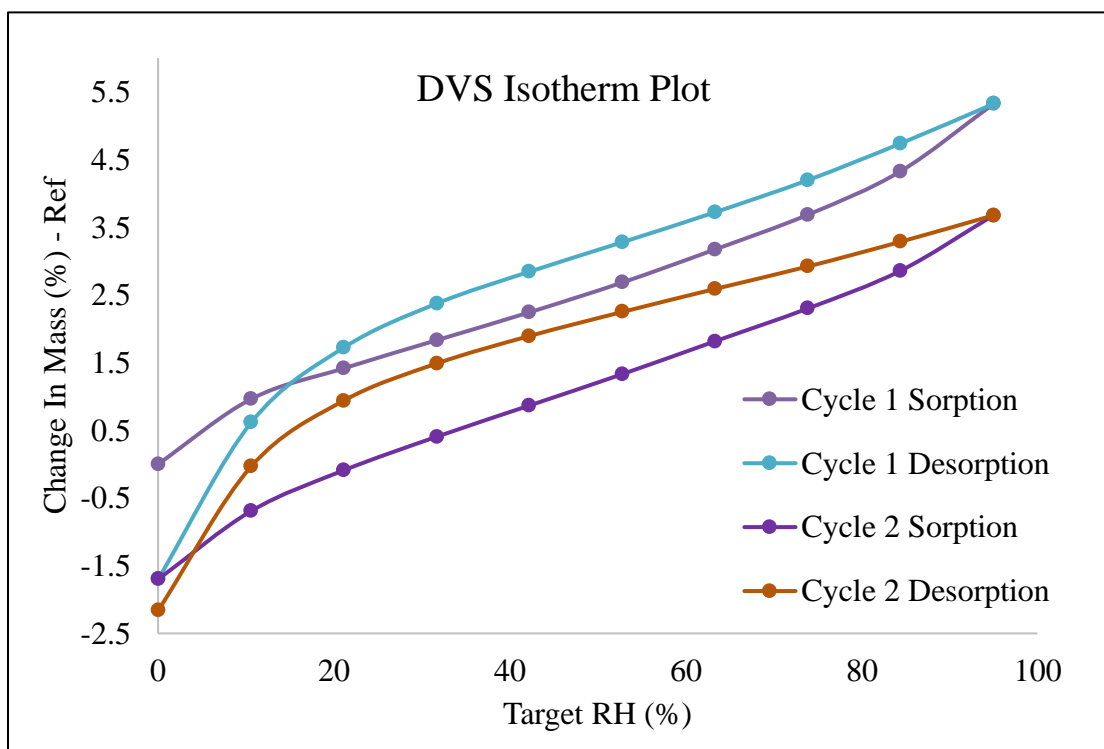


Figure 0.9: Esomeprazole magnesium water/1-butanol adsorption of water at increasing humidity followed by desorption at decreasing humidity. The cycle is repeated to give two isotherms.

Conclusion

This is the first single crystal structure reported that displays esomeprazole coordinated to a metal center. Analysis of the crystal structure shows that water is bound to magnesium cation as well filling the channels of the lattice. The covalently bonded waters are much more strongly kept in the lattice than those maintained by hydrogen bonding. The discovery of this esomeprazole magnesium solvate could have applicability to the development of improved pharmaceutical solid dosage forms.

References

- (1) Robins, G. W.; Scott, L. J.; Levy, B. I.; Federatif, I.; Circulation, D. R.; Lariboisiere, H. *Drugs* **2002**, *62* (10), 1503–1538.
- (2) Lindberg, P.; Nordberg, P.; Alminger, T.; Braendstroem, A.; Wallmark, B. *J. Med. Chem.* **1986**, *29* (8), 1327–1329.
- (3) Nalwade, S. U.; Reddy, V. R.; Rao, D. D.; Morisetti, N. K. *J. Pharm. Biomed. Anal.* **2012**, *57*, 109–114.
- (4) Davidson, A. G.; McCallum, A. *Drug Dev. Ind. Pharm.* **1996**, *22* (12), 1173–1185.
- (5) AstraZeneca. Nexium
http://www.accessdata.fda.gov/drugsatfda_docs/label/2007/021153s027s028,021689s008s011bl.pdf (accessed Nov 9, 2015).
- (6) Andersson, T.; Hassan-Alin, M.; Hasselgren, G.; Röhss, K.; Weidolf, L. *Clin. Pharmacokinet.* **2001**, *40* (6), 411–426.
- (7) Claramunt, R. M.; López, C.; Alkorta, I.; Elguero, J.; Yang, R.; Schulman, S. *Magn. Reson. Chem.* **2004**, *42* (8), 712–714.
- (8) Claramunt, R. M.; López, C.; Elguero, J. *Arkivoc* **2005**, *2006* (5), 5.
- (9) Bhatt, P. M.; Desiraju, G. R. *Chem. Commun.* **2007**, No. 20, 2057.
- (10) Brittan, H. G. *Polymorphism in Pharmaceutical Solids, Second Edition*; CRC Press, 2009.
- (11) P. A. Pangarkar, A. M. Tayade, S. G. Uttarwar, R. S. W. *Int. J. Pharm. Technol.* **2012**, *5* (1), 2374–2402.
- (12) Savanovic Lidija Vranicar, Zoran Ham, J. R. Crystalline solvate of omeprazole sodium, December 14, 2006.
- (13) Dharmaraj Ramachandra Rao, Srinivas Laxminarayan Pathi, Rajendra Narayanrao Kankan, P. A. C. Esomeprazole potassium polymorph and its preparation, September 2, 2010.

- (14) Gonikberg, E. *United States Pharmacop.* **2011**.
- (15) Khankari, R. K. *Thermochim. Acta* **248**, 61–79.
- (16) Lee, A. Y. *Annu Rev Chem Biomol Eng.* **2011**, *2*, 259–280.
- (17) Casar, R. T. Process for the preparation of esomeprazole magnesium in a stable form, January 21, 2010.
- (18) Hanna Cotton, Anders Kronström, Anders Mattson, E. M. Form of S-omeprazole, April 9, 2002.
- (19) Lin Quin, Lu Jei, Wu Danhui, Z. X. *Chinese J. Pharm.* **2014**, *45* (4), 377–380.
- (20) Bhesaniya, K.; Baluja, S. *Russ. J. Phys. Chem. A* **2013**, *87* (13), 2187–2190.
- (21) Ohishi, H.; In, Y.; Ishida, T.; Inoue, M.; Sato, F.; Okitsu, M.; Ohno, T. *Acta Crystallogr. Sect. C Cryst. Struct. Commun.* **1989**, *45* (12), 1921–1923.
- (22) Brüning, J.; Bolte, M.; Schmidt, M. U. *J. Chem. Crystallogr.* **2008**, *39* (4), 256–260.
- (23) Bruker-AXS, Madison, WI 53711, U. 2013.
- (24) Bruker-AXS, Madison, WI 53711, U. **2012**.
- (25) Sheldrick, G. M. *Acta Crystallogr. Sect. A, Found. Adv.* **2015**, *71* (Pt 1), 3–8.
- (26) Sheldrick, G. M. *Acta Crystallogr. Sect. C Struct. Chem.* **2015**, *71* (1), 3–8.
- (27) C. F. Macrae, I. J. Bruno, J. A. Chisholm, P. R. Edgington, P. McCabe, E. Pidcock, L. Rodriguez-Monge, R. Taylor, J. van de S. and P. A. W. *J. Appl. Cryst* **2008**, *41*, 466–470.
- (28) Russo, M. G.; Vega Hissi, E. G.; Rizzi, A. C.; Brondino, C. D.; Salinas Ibañez, Á. G.; Vega, A. E.; Silva, H. J.; Mercader, R.; Narda, G. E. *J. Mol. Struct.* **2014**, *1061*, 5–13.
- (29) Koilpillai, J. P.; Kulkarni, P. B.; Dabe, A. D.; Khan, M. A. Process for the preparation of esomeprazole magnesium dihydrate. US20100267959 A1, October 21, 2010.
- (30) Seenivasaperumal, M.; Federsel, H.-J.; Szabo, K. J. *Adv. Synth. Catal.* **2009**, *351*

- (6), 903–919.
- (31) Jones, I. C.; Sharman, G. J.; Pidgeon, J. *Magn. Reson. Chem.* **2005**, *43* (6), 497–509.
- (32) Thomas, S. *J. Chem. Phys.* **1966**, *44* (8), 3148.
- (33) Mohan, J. *Organic Analytical Chemistry: Theory and Practice*; Alpha Science International Limited, 2003.
- (34) Jain, A.; Ravi Teja, M.; Pariyani, L.; Balamuralidhara, V.; Gupta, N. V. *Trop. J. Pharm. Res.* **2013**, *12* (3), 299–304.
- (35) Doroshenko, I.; Pogorelov, V.; Sablinskas, V. *Dataset Pap. Chem.* **2013**, *2013* (Article ID 329406), 6.
- (36) Vijayabhaskar Bolugoddu, Jaydeepkumar Dahayabhai Lilakar, Koilkonda, Ramchandra Reddy Pingili, Amarnath Reddy Lekkala, Venkata Rambabu Kammili, Swarupa Reddy Dudipala, Sharat Pandurang Srinivasa Rao Malina, R. A. Process for preparing amorphous salts. WO2006096709 A2, September 14, 2006.

Chapter 4

Co-amorphous form of curcumin-folic acid dihydrate with increased dissolution rate

Curcumin is a naturally occurring pharmaceutical derived from turmeric. Despite its many medicinal properties, such as being an antioxidant, anti-inflammatory, tumor reducer, etc., applications of curcumin are restricted due to its low aqueous solubility and consequently its poor bioavailability. By converting the solid state of poorly water soluble active pharmaceutical ingredients to co-amorphous mixtures, solvates, co-crystals and eutectics, the solubility can be significantly improved. In this study, US Food and Drug Administration (FDA) approved excipients were screened for their ability to form novel solid states with curcumin to increase its aqueous solubility. Excipients were screened based on their molecular complementarity with curcumin that was determined using Mercury software. From this screening, it was found that a co-amorphous mixture can be formed between curcumin and folic acid dihydrate that has potential as a prenatal or a women's health drug due to its use in preeclampsia and ovarian cancer treatments. This mixture was found to have an increased dissolution rate when compared with curcumin. After one hour, 175 mg/L of curcumin was dissolved from the co-amorphous mixture, while only 45 mg/L was dissolved from curcumin Form I. The co-amorphous mixture is stable as it was shown to keep its amorphous behavior after 24 hours in solution at elevated temperatures. Eutectics were found to form between curcumin and biotin, carbamazepine, ethyl paraben, paracetamol, suberic acid, succinic acid and L-tyrosine. Screening with other excipients led to no novel solid state formation; however, an improved synthesis method for curcumin Form II in the presence of dextrose is presented.

Introduction

Curcumin, with many potential applications as an antioxidant¹, anti-inflammatory², colourmetric sensor³, tumor reducer⁴, holds a high level of interest in food and pharmaceutical industries. Though it is safe for ingestion up to 8000 mg/day⁵, curcumin is limited in function due to its extremely low water solubility (<0.1 mg/mL), which leads to inadequate bioavailability.⁶ Curcumin is unstable and known to decompose in neutral and

basic conditions. Degradation products include trans-6-(4'-hydroxy-3'-methoxyphenyl)-2,4-dioxo-5-hexenal as the major product, while vanillin, ferulic acid and feruloyl methane are the minor products.⁷ Vanillin has been shown to have its own pharmaceutical applications, but since its concentration is extremely low as a degradation product, it cannot be claimed as the reason for curcumin's bioactivity.⁸ All of these products have low toxicity, but degradation occurs rapidly. In order to increase its prevalence in commercial use, the stability and solubility issues of this naturally occurring active pharmaceutical ingredient (API) need to be addressed.

Changing the solid form of the API as a means of increasing its solubility is a very popular technique in the pharmaceutical industry. Common solid forms include salts, solvates, eutectic mixtures, co-crystals and co-amorphous mixtures. Salts occur from the formation of ionic bonds between an API and one or more excipients. A solvate occurs when solvent molecules are incorporated into the lattice during crystallization through intermolecular bonding. A eutectic mixture is composed of fine crystals of each component that are mixed very closely, and when an API forms a eutectic with a water soluble compound, the dissolution rate of the drug increases.^{9,10} Co-crystals, which have been steadily gaining interest in the pharmaceutical industry¹¹, are more comparable to solvates. They are composed of two or more components, termed API and co-former(s), that are intermolecularly bonded (mainly hydrogen bonding) to form a crystal lattice. All components of a co-crystal are found in stoichiometric amounts and should be overall neutral and solid at ambient conditions.

Co-amorphous solids occur when two components become amorphous due to interaction with one another. Intermolecular bonding between API and excipient impedes the arrangement of individual molecules into separate lattices and results in an amorphous material.¹² Amorphous pharmaceutical compounds have been shown to have increased solubility in comparison to their crystalline counterparts. For instance, indomethacin, glucose, glibenclamide, griseofluvin, iopanoic acid and polythiazide were all experimentally shown to have solubility ratios (amorphous:crystalline) ranging from 1.4 to 24.¹³⁻¹⁸ Since the amorphous form is the most energetic, this solid state should greatly increase solubility and bioavailability.¹³ However, compounds that are amorphous have been shown to have low stability and will tend to crystallize if exposed to moisture.¹⁹ Co-

amorphous mixtures are shown to be not only high in solubility, but also possess high stability and are easily formed via grinding or milling. Co-amorphous systems have shown to not only increase the dissolution rates relative to crystalline materials, but also compared to their individual amorphous components.²⁰ Co-amorphous mixtures of naproxen, indomethacin, simvastatin, carbamezapine, ritonavir and lurasidone hydrochloric acid with various excipients show increases in dissolution rate up to 200-fold when compared to starting materials.²¹⁻²⁸ Various amino acids have been displayed to form co-amorphous mixtures with low solubility APIs and were stable up to 4-6 months at 40 °C/0% relative humidity, which is much longer than most amorphous drugs.

Since co-crystals have shown the ability to enhance solubility and bioavailability of Class II and IV drugs²⁹⁻³⁸, attempts were made to produce co-crystals of curcumin using several co-formers. Before choosing potential co-formers for co-crystallization, a thorough literature review was carried out to understand current state of the art. Curcumin has been reported to form co-crystals with several co-formers listed in Table 0.1. However, formation of co-crystals is not always successful and sometimes results in eutectic mixtures; some known curcumin eutectics have been listed in Table 0.2. Curcumin, which has an intrinsic dissolution rate (IDR) of 0.0061 (mg/cm²)/min³⁹, showed an increase in IDR for all of these solid forms (reported in Tables 4.1 and 4.2). The most successful co-crystal is with pyrogallol, showing well over a tenfold increase in IDR and nearly five times as soluble in 40% ethanol.⁴⁰ There is also a drug-drug co-amorphous mixture of curcumin and artemisinin with an IDR that is 2.6 times faster than curcumin in 60% EtOH.⁴¹ The next most successful solid state, with IDR of 0.0647 IDR (mg/cm²)/min, is the eutectic mixture of curcumin with nicotinamide.³⁹ Some co-formers that simply resulted in a physical mixture include: L-maleic acid³⁹, catechol⁴⁰ and orcinol.⁴⁰

Table 0.1: Known Curcumin Co-crystals and Their Intrinsic Dissolution Rates.

Co-former	IDR (mg/cm ²)/min	Co-former	IDR (mg/cm ²)/min
2-aminobenzimidazole ⁴¹	0.023	nicotinamide ²³	0.040
4-4'-bipyridine-N,N'-dioxide ⁴²	NR	phloroglucinol ⁴³	0.0166
caffeine ^{a, 44}	NR	piperazine ⁴⁴	NR
ibuprofen sodium ⁴⁴	NR	piperidine ⁴⁴	NR
isonicotinamide ⁴⁴	NR	L-proline ^{a,44}	NR
L-lysine ⁴¹	0.029	pyrogallol ⁴⁰	0.09364
methylparaben ⁴⁵	NR	resorcinol ⁴⁰	0.03761
naproxen sodium ⁴⁴	NR		

^aAPI is the curcumin derivative bisdesmethoxycurcumin

IDR = Intrinsic dissolution rate

NR = not reported

Table 0.2: Known Curcumin Eutectics and Their Intrinsic Dissolution Rates.

Co-former	IDR (mg/cm ²)/min
ferulic acid ³⁹	0.0412
hydroquinone ³⁹	0.0344
p-hydroxybenzoic acid ³⁹	0.0270
nicotinamide ³⁹	0.0647
l-tartaric acid ³⁹	0.0132

In addition to increasing the bioavailability, co-crystals, as well as co-amorphous and eutectic mixtures have also been employed to increase therapeutic effect, reduce the number of prescriptions and reposition drugs by means of drug-drug combinations.⁴⁶ Since curcumin is known to be anti-inflammatory, it could be combined with another anti-inflammatory drug to increase potency or combined with a drug that is usually prescribed alongside an anti-inflammatory drug to reduce the number of prescriptions. In this work, we have made attempts to prepare new solid forms of curcumin, including drug-drug

mixtures. While the main aim was to produce co-crystals, eutectics have been formed along with a co-amorphous form of curcumin and folic acid dihydrate (CUR-FAD) with enhanced dissolution rate.

Experimental

Materials and Instruments

Succinic acid, L-tyrosine and ethanol were purchased from Fisher Scientific (Mumbai, India), Alfa Aesar (Hyderabad, India) and Chemcon Specialty Chemicals Pvt Ltd (Vadodara, India), respectively. All other chemicals purchased were from Sigma Aldrich Chemicals Pvt Ltd (Bangalore, India).

DSC analyses of solid samples were carried out on a NETZSCH STA 449F3 Jupiter (NETZSCH-Gerätebau GmbH; Selb, Germany) from 25-350°C at a heating rate of 10K/min, unless otherwise stated. Phase diagrams were obtained from plotting both the onset of the first endotherm and the peak temperature of the second endotherm. Powder X-ray Diffraction (PXRD) studies were carried out using a Rigaku Miniflex instrument with Cu X-ray radiation. Scans were run at a speed of 1.00°/minute for 2 θ values of 2.00-40.00°. Infrared (IR) Spectroscopy results were obtained over 32 scans from 4000 cm⁻¹ to 500 cm⁻¹ using a Vector 22 FT-IR spectrometer (Bruker; Milton, Canada).

Preparation and characterization of curcumin and folic acid dihydrate (CUR-FAD) co-amorphous mixtures

Liquid assisted grinding (LAG) with 5 drops of methanol was executed on equimolar amounts of curcumin and folic acid dihydrate using mortar and pestle for varying amounts of time.

Equilibrium solubility and powder dissolution studies

UV-Vis (ultraviolet visible) spectrophotometer (Agilent Cary 60 UV-Vis Spectrophotometer, Agilent Technologies, Santa Clara, USA) was used for estimation of

equilibrium solubility and powder dissolution rates. Three calibration curves (see Appendix B) were constructed using known concentrations of curcumin, folic acid dihydrate and CUR-FAD so the amount of curcumin and folic acid dihydrate released could be determined. The extinction coefficients were determined to be 45.4, 28.0 and 39.1 L/mmol cm, respectively. Thermodynamic solubility was estimated by adding an excess of CUR-FAD (~20 mg) into 2 mL of 40% EtOH solution. The suspended solutions were allowed to stir at 37°C for over 24 hours. This was done in triplicate and concentration was determined using calibration curves.

To estimate dissolution kinetics, nine samples were prepared by adding excess (determined from thermodynamic solubility) CUR-FAD, which had been sieved through a 150 μ m mesh, into 4 mL of 40% EtOH solution. The solutions were stirred at 3.2 Hz and 37 °C for a specified amount of time. Each sample was filtered using Arodisc 25 mm syringe filters with 0.45 μ m Supor membrane (Pall Corporation; Port Washington, USA), immediately diluted and concentration was estimated using UV-Vis spectroscopy. Powder dissolution studies were conducted in triplicate and the average values have been reported.

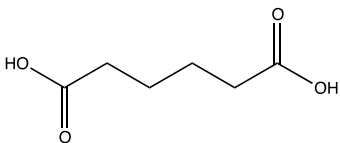
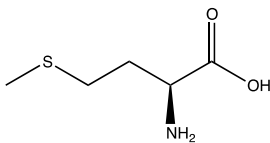
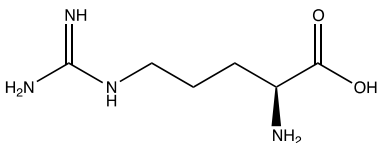
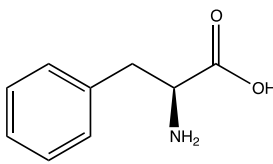
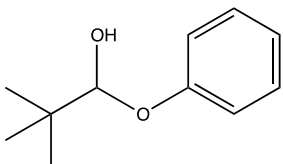
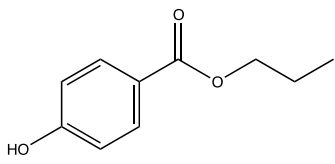
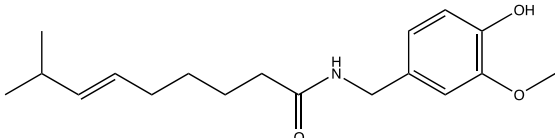
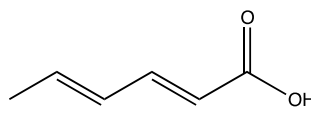
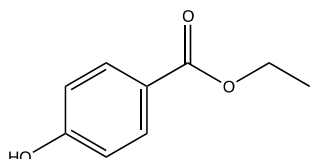
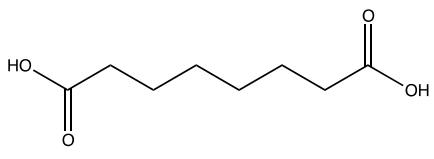
Results and Discussion

Solid State Formation

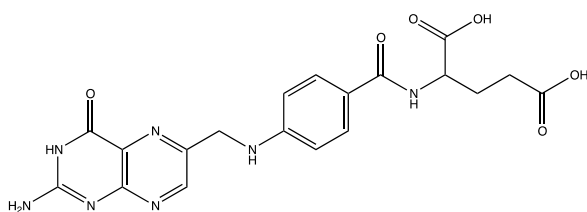
To increase the amount of curcumin absorbed by the body and improve its applications in the pharmaceutical industry, several co-formers were screened to explore their ability to form different solid states with curcumin. The excipients investigated should be safe for human ingestion to have feasible pharmaceutical and food applications. Critical to successful screening is the choice of appropriate co-formers that will form strong intermolecular bonds. Using the molecular complementarity tool in Mercury,⁴⁷ which takes into account factors such as molecular shape and polarity, a list of potential co-formers was constructed based on the molecular structure of Form I curcumin, the stable form.⁴⁸ It should be noted that, like the successful co-formers that form solid states with curcumin, Mercury predicted success with heterosynthons (e.g. curcumin with carboxylic and amine functional groups), utilizing the enol as the strongest probable intermolecular bonding site. The list shown in Table 0.3, was then condensed to only include compounds suitable for

pharmaceutical applications. Analyzing the list, comparing it to the known co-crystals of curcumin and using the compounds present in the laboratory, led to the screening of succinic acid, suberic acid, ibuprofen, paracetamol, oxalic acid, l-tyrosine, N-acetyltryptophan, carbamazepine, ethylparaben, folic acid, biotin and dextrose.

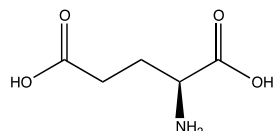
Table 0.3: FDA Approved Potential Co-formers for Curcumin Co-crystals.

Co-former	Co-former
Adipic acid 	L-methionine 
L-arginine 	L-phenylalanine 
t-butylhydroxyanisole 	Propylparaben 
Capsaicin 	Sorbic acid 
Ethylparaben 	Suberic acid 

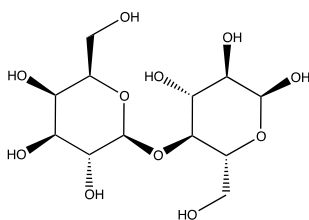
Folic acid



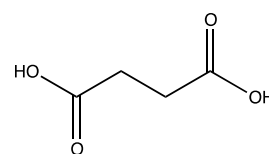
L-glutamic acid



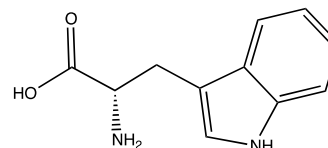
Lactose



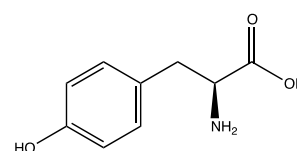
Succinic acid



L-tryptophan



L-tyrosine



A recognized co-crystal screening technique uses DSC (differential scanning calorimetry) as a rapid method for assessing potential co-formers. In this technique, DSC is run for three different ratios (1:1, 1:2 and 2:1) of the components.⁴⁹ This should result in two endotherms representing the eutectic melt and melting of the co-crystal; each endotherm should be distinct from the melting of the API and co-former. Using this screening process, one can usually surmise if an API and co-former have capability of forming a co-crystal or eutectic. In case of ambiguous results, a phase diagram should be constructed. After running DSC for samples ground at varying molar ratios of curcumin and co-former, it was determined whether co-crystal formation was viable or if a eutectic would form. These results are confirmed with PXRD which will show new peaks for co-crystals, a combination of the peaks of the starting materials for eutectic and physical mixtures, or an amorphous pattern for co-amorphous mixtures. From analysis of PXRD and DSC, it was determined that physical mixtures were formed with dextrose, *N*-acetyltryptophan, and ibuprofen. This can be seen by the example with dextrose given in Figure 0.1 (a), where there is clearly no

converging in the phase diagram. Eutectics formed with biotin, carbamazepine, ethyl paraben, paracetamol, suberic acid, succinic acid and L-tyrosine. A phase diagram for the eutectic with suberic acid is given in Figure 0.1 (b). When combined with the PXRD shown in Figure 0.2, it is made clear that the product is a eutectic and not a co-crystal or co-amorphous mixture. None of the screened co-formers were found to form crystals with curcumin; however, a co-amorphous mixture with folic acid dihydrate (CUR-FAD) was formed.

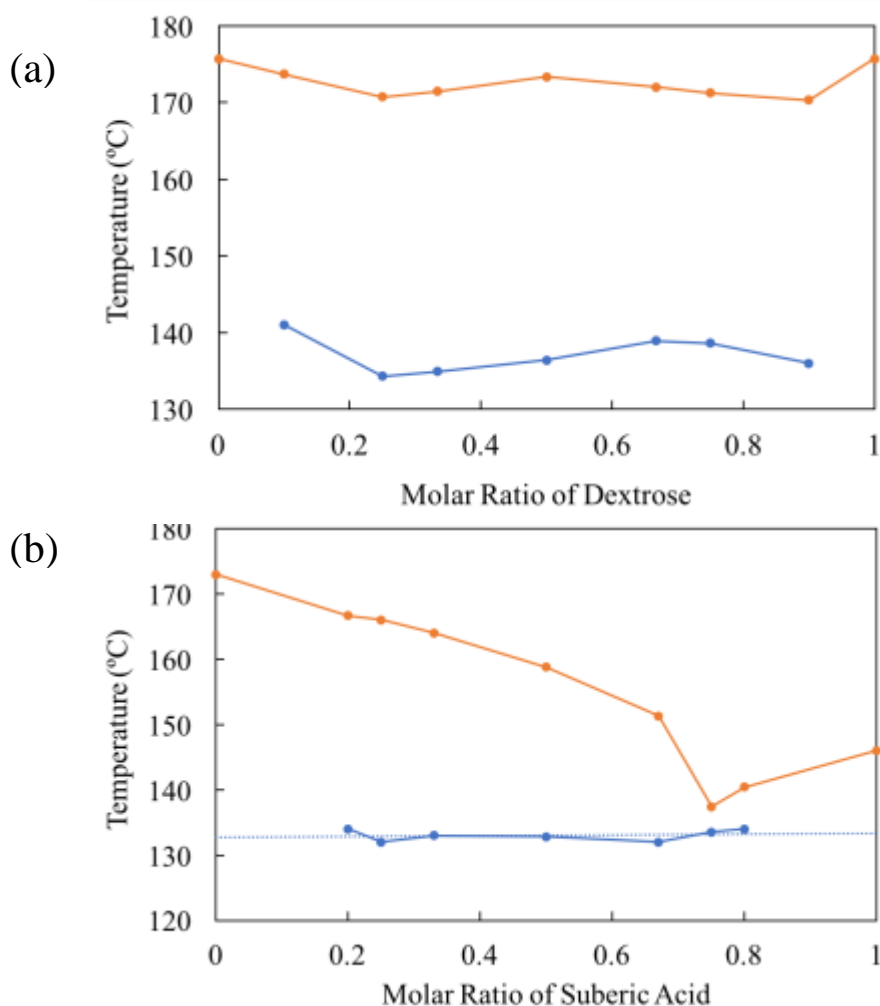


Figure 0.1: Phase diagram for (a) the physical mixture of curcumin and dextrose and (b) the eutectic mixture of curcumin and suberic acid after grinding at varying molar ratios. Temperatures plotted in blue represent the onset of the first melting peak seen in DSC, while orange represents the temperature of the second peak.

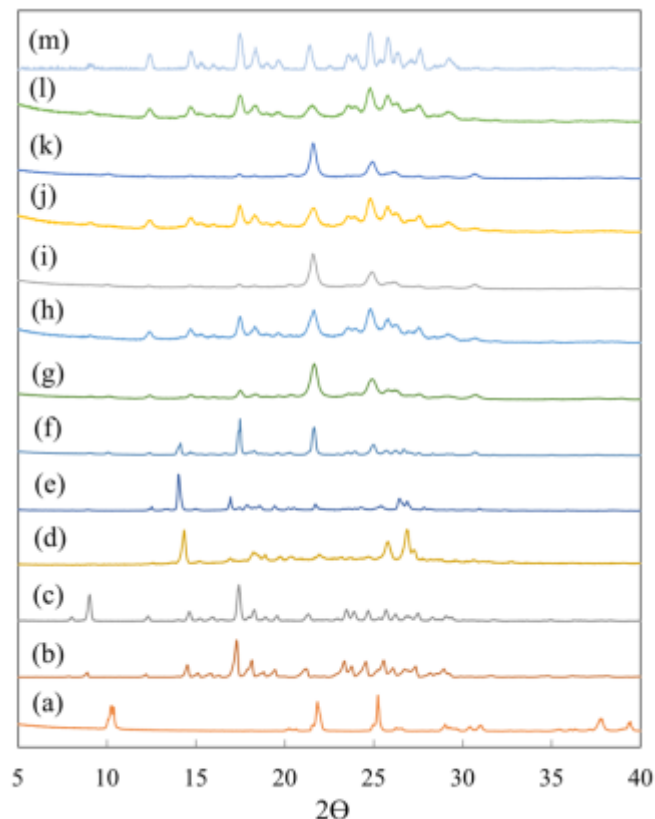


Figure 0.2: PXRD patterns for (a) raw suberic acid, (b) raw curcumin, (c) curcumin form I, (d) form II, (e) form III, (f) 1:1 curcumin:suberic acid (CUR-SUB), (g) 1:2 CUR-SUB, (h) 2:1 CUR-SUB, (i) 1:3 CUR-SUB, (j) 3:1 CUR-SUB, (k) 1:4 CUR-SUB, (l) 4:1 CUR-SUB acid and (m) 4:1 CUR-SUB acid heated to 133°C.

Following the screening protocol, curcumin and folic acid dihydrate were initially ground, and PXRD patterns were recorded for 10, 20, 30, 60 and 90 minute intervals of liquid assisted grinding. As shown in Figure 0.3, the final product remained amorphous after grinding for 90 minutes. The PXRD patterns clearly show the loss of crystallinity, which is different when compared with the PXRD patterns of raw curcumin and folic acid dihydrate. In addition to PXRD, DSC heating experiments were also conducted throughout the grinding process. **Error! Reference source not found.** shows DSC thermographs for ground samples and those for curcumin and folic acid dihydrate. It is observed that the melting endotherm of curcumin at around 180°C is not present in the ground product and instead there is an exothermic peak (seen in **Error! Reference source not found.** (a) and

(b)). The magnitude of the peak corresponding to curcumin melting decreases gradually with heating, which indicates transition to an amorphous phase by grinding. These results clearly indicate that liquid assisted grinding (LAG) of curcumin with folic acid dihydrate results in a co-amorphous solid.

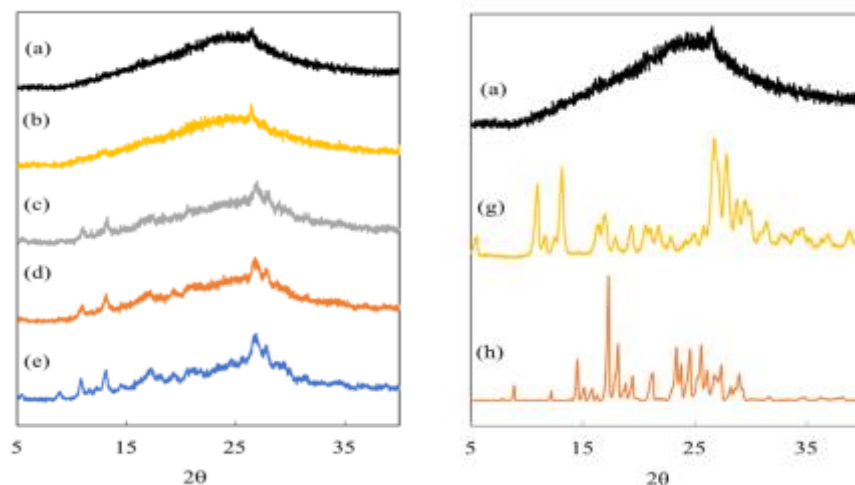


Figure 0.3: PXRD patterns for CUR-FAD from LAG after (a) 90 min, (b) 60 min, (c) 30 min, (d) 20 min, (e) 10 min, (g) raw folic acid dihydrate and (h) raw curcumin.

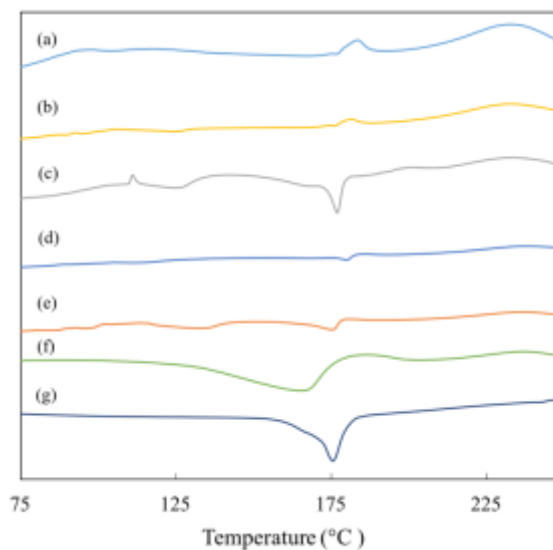


Figure 4.4: DSC thermograph for CUR-FAD from LAG after (a) 90 min, (b) 60 min, (c) 30 min, (d) 20 min and (e) 10 min (f) raw folic acid dihydrate and (g) raw curcumin.

To ensure that there is no decomposition of the starting materials and that a co-amorphous mixture is forming, both ^1H NMR and FT-IR spectra were obtained for the ground samples. It is clear from Figure 0.5 that the solution NMR spectrum of CUR-FAD in DMSO-d_6 shows the characteristic peaks of curcumin as well as folic acid dihydrate. Also, there is no excess peak that would correspond to the decomposition of curcumin nor folic acid dihydrate.

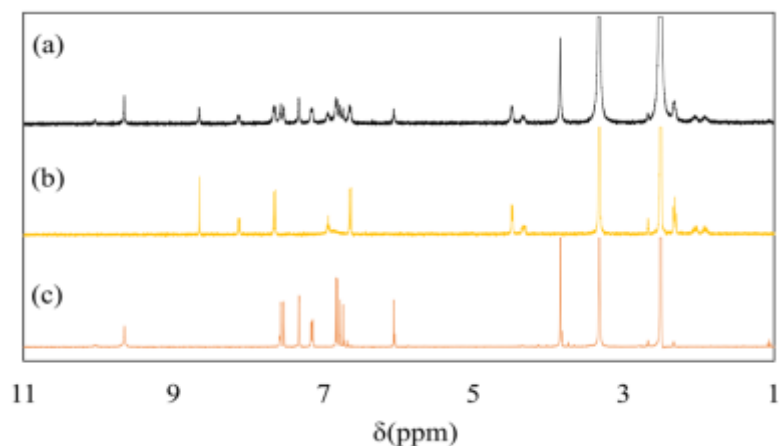


Figure 0.5: solution ^1H NMR spectra for (a) CUR-FAD, (b) raw folic acid dihydrate and (c) raw curcumin in DMSO-d_6 .

Normalized FT-IR spectra are shown in Figure 0.6, and analysis suggests interactions between curcumin and folic acid dihydrate but no decomposition. It should be noted that the peaks in the $3500\text{--}3200\text{ cm}^{-1}$ for the N-H stretching in folic acid dihydrate lose their intensity; this is most likely due to the involvement of weak intermolecular bonding with the API. The peak for the phenolic O-H stretching in curcumin⁵⁰ at 3509 cm^{-1} is not seen in the spectrum of the co-amorphous product, and the carbonyl stretching⁵¹ at 1691 cm^{-1} of folic acid dihydrate is shifted to 1697 cm^{-1} for CUR-FAD. There is also a shift in the carbonyl stretching of curcumin from 1627 cm^{-1} to 1623 cm^{-1} , implying that it is involved in the interaction, too. No indication of degradation during grinding in addition to implications for increased interaction between curcumin and FAD further confirms that a co-amorphous solid phase has been formed.

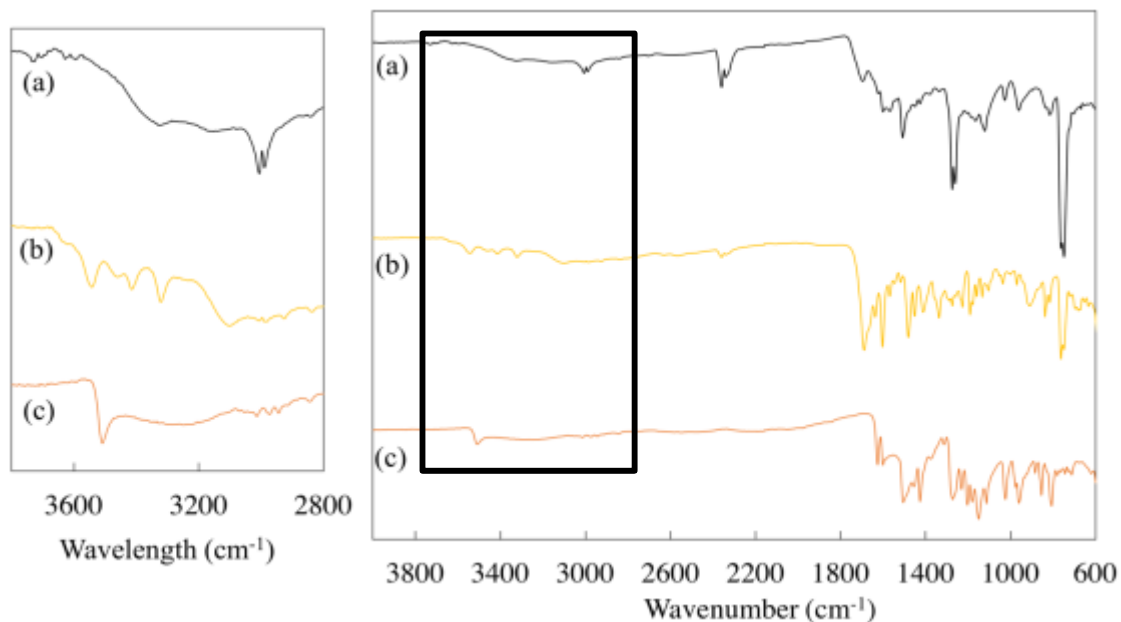


Figure 0.6: FT-IR spectra for (a) CUR-FAD, (b) raw folic acid dihydrate and (c) raw curcumin.

Solubility and Dissolution Rate Tests

Since the objective in forming a new solid state with curcumin was to increase the amount absorbed in the body, powder dissolution rate studies were conducted. Excess amount of CUR-FAD was placed in nine separate vials which were then each filled with 2 mL of 40% EtOH solution at 37°C. Vials were stirred at 3 Hz for up to 4 hours, filtered and diluted, then analyzed using UV-Vis spectrophotometer. Figure 0.7 shows dissolution profiles for raw curcumin and the co-amorphous solid. When compared with curcumin, there is an increase in dissolution rate for the co-amorphous product. The dissolution rate for the co-amorphous product was found to be similar to the pyrogallol co-crystal (about 182 mg of curcumin/L after 4 hours), which has the largest increase in IDR compared to other curcumin co-crystals. Thermodynamic equilibrium solubility studies were also conducted over 24 hours at 37°C by adding excess CUR-FAD to 2 mL of 40% EtOH solution. It was found that 458 ± 25 mg/L and 328 ± 31 mg/L of curcumin and folic acid dihydrate were dissolved, respectively. Using the area under the curve, the amount of curcumin dissolved in four hours from the co-amorphous mixture is 41.2 ± 3.8 g h/L, which is much greater

than that of curcumin form I (12.2 g h/L).²⁵ The PXRD pattern of the remaining powder in solution after 24 hours is shown in Figure 0.8. The overall pattern is still amorphous in nature, but characteristic peaks can be seen at 2θ values of 17.3 and 8.9 for curcumin and 13.0 and 10.9 for folic acid dihydrate. Thus, it can be stated that the co-amorphous mixture is still relatively stable since it remains highly amorphous in nature after 24 hours in solution at an elevated temperature.

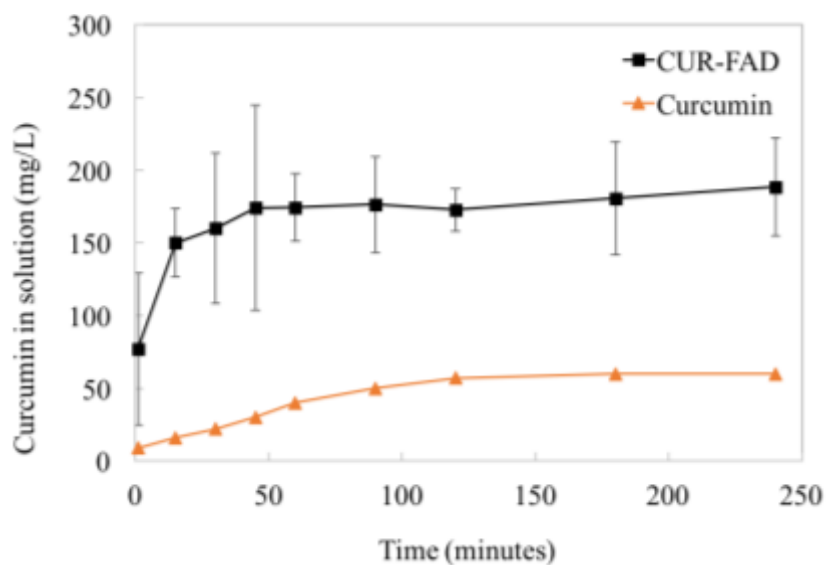


Figure 0.7: Powder dissolution rate studies for CUR-FAD compared with curcumin.²⁵

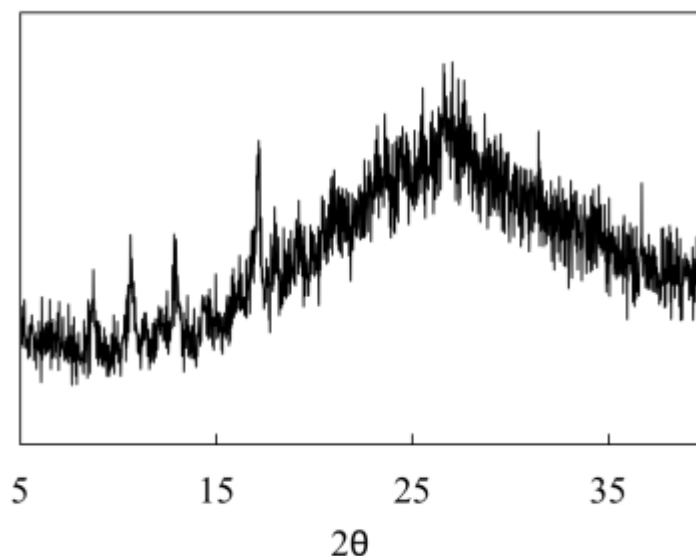


Figure 0.8: PXRD pattern of powder from thermodynamic equilibrium solubility.

Folic acid is a form of the water soluble vitamin B-9, and it is highly encouraged to take during pregnancy for both maternal and fetal health.⁵² Curcumin is also known to reduce placental inflammation, a common symptom of preeclampsia that occurs in up to 8% of pregnancies.^{53,54} When combined, this new drug-drug combination has the potential to be repositioned as a prenatal drug. Both curcumin and folic acid have been shown to be effective in the treatment and pre-treatment of ovarian cancer; once again, this could lead to a reposition of this co-amorphous mixture as a women's health drug and could potentially lead to a lower number of drugs prescribed.^{55,56}

Formation of Curcumin Form II

When performing solution crystallization to synthesize curcumin co-crystals, Form II curcumin crystals were found to grow in the presence of dextrose. Solution crystallization was performed for this pair due to ambiguity in the PXRD patterns (i.e. appeared to show novel peaks). While this was not the initial aim of these experiments, it is still beneficial since this curcumin polymorph has a faster dissolution rate. It is the metastable polymorph, so Form II is generally not stable and will not form easily relative to Form I. Since it is crystallized in the presence of dextrose, this makes the process safer for pharmaceutical

and food applications. Also, this procedure does not involve dimethyl sulfoxide, a difficult to remove solvent, nor cooling like some known processes.⁴⁰ A simple method is proposed from which Form II crystals can be grown via slow evaporation, or by rapid evaporation (i.e. heating the solution close to boiling point of solution), from a solution of 90% methanol with equimolar dextrose present. The crystals grown were of X-ray quality and resulted in the confirmation of Form II curcumin that crystallizes in the orthorhombic space group of $Pca2_1$ (shown in Figure 0.9).⁵⁸ Further research should be conducted to test the validity and feasibility of this method on a larger scale.

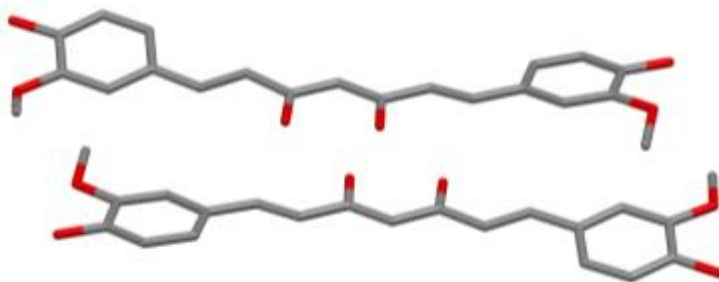


Figure 0.9: Asymmetric unit of Form II curcumin with space group of $Pca2_1$ formed via slow evaporation from 90% methanol in the presence of dextrose. Hydrogen atoms are omitted for clarity. C: grey; O: red.

Conclusion

Curcumin is a natural drug product that is found to have many health benefits; however, its use in industry is limited by its very low aqueous solubility. To increase the bioavailability of curcumin, screening for a novel solid state was conducted. The excipients screened were chosen using a combination of the supramolecular synthon approach, computational molecular complementarity and knowledge of known curcumin co-crystals. It was found that physical mixtures would form with dextrose, *N*-acetyltryptophan, and ibuprofen, while eutectics would form with biotin, carbamazepine, ethyl paraben, paracetamol, suberic acid, succinic acid and L-tyrosine. Of particular interest of this work is the result of screening with folic acid dihydrate. Folic acid dihydrate was chosen due to its approved molecular complementarity with curcumin. A novel solid state of curcumin is presented in this paper as a co-amorphous mixture with folic acid dihydrate (CUR-FAD). Using liquid assisted grinding, the mixture became co-amorphous. This mixture, which can

be repositioned in the pharmaceutical industry as a prenatal, has shown to dissolve faster than curcumin in aqueous solutions. At 60 minutes, 175 mg/L of curcumin is dissolved from CUR-FAD; this is much more efficient than curcumin, which is found to dissolve about 40 mg/L at 60 minutes. The co-amorphous mixture is found to keep its amorphous behaviour after 24 hours in solution at 37°C. Further work should be conducted to see the stability of this mixture. Co-amorphous mixtures have been shown to be more stable than a single amorphous compound but retain the increased solubility and dissolution rates; therefore, more excipients should be screened for this type of solid state. An improved method is given for the formation of metastable curcumin Form II crystals which is industry friendly since it is done in the presence of dextrose and no methanol is included into the molecular structure.

References

- (1) Ak, T.; Gülçin, İ. *Chem. Biol. Interact.* **2008**, *174* (1), 27–37.
- (2) Srimal, R. C.; Dhawan, B. N. *J. Pharm. Pharmacol.* **1973**, *25* (6), 447–452.
- (3) Pourreza, N.; Sharifi, H.; Golmohammadi, H. *Microchem. J.* **2016**, *129*, 213–218.
- (4) Soudamini; Kuttan, R. *Indian J. Pharmacol.* **2016**, *20* (2), 95.
- (5) Cheng, A. L.; Hsu, C. H.; Lin, J. K.; Hsu, M. M.; Ho, Y. F.; Shen, T. S.; Ko, J. Y.; Lin, J. T.; Lin, B. R.; Ming-Shiang, W.; Yu, H. S.; Jee, S. H.; Chen, G. S.; Chen, T. M.; Chen, C. A.; Lai, M. K.; Pu, Y. S.; Pan, M. H.; Wang, Y. J.; Tsai, C. C.; Hsieh, C. Y. *Anticancer Res.* **2001**, *21* (4B), 2895–2900.
- (6) Ravindranath, V.; Chandrasekhara, N. *Toxicology* **1980**, *16* (3), 259–265.
- (7) Wang, Y. J.; Pan, M. H.; Cheng, A. L.; Lin, L. I.; Ho, Y. S.; Hsieh, C. Y.; Lin, J. K. *J. Pharm. Biomed. Anal.* **1997**, *15* (12), 1867–1876.

- (8) Gordon, O. N.; Schneider, C. *Trends Mol. Med.* **2012**, *18* (7), 361-3-4.
- (9) Sekiguchi, K.; Obi, N. *Chem. Pharm. Bull. (Tokyo)*. **1961**, *9* (11), 866–872.
- (10) Gala. *J Dev. Drugs* **2013**, *2* (3), 1–2.
- (11) Duggirala, N. K.; Perry, M. L.; Almarsson, Ö.; Zaworotko, M. J. *Chem. Commun.* **2016**, *52* (4), 640–655.
- (12) Yamamura, S.; Gotoh, H.; Sakamoto, Y.; Momose, Y. *Eur. J. Pharm. Biopharm.* **2000**, *49* (3), 259–265.
- (13) Hancock, B. C.; Parks, M. *Pharm. Res.* **2000**, *17* (4), 397–404.
- (14) Parks, G. S.; Huffman, H. M.; Cattoir, F. R. *J. Phys. Chem.* **1927**, *32* (9), 1366–1379.
- (15) Parks, G. S.; Snyder, L. J.; Cattoir, F. R. *J. Chem. Phys.* **1934**, *2* (9), 595–598.
- (16) Elamin, A. A.; Ahlneck, C.; Alderborn, G.; Nyström, C. *Int. J. Pharm.* **1994**, *111* (2), 159–170.
- (17) CORRIGAN; I., O. *Int. J. Pharm.* **1984**, *18*, 195–200.
- (18) Stagner, W. C.; Guillory, J. K. *J. Pharm. Sci.* **1979**, *68* (8), 1005–1009.
- (19) Yu, L. *Adv. Drug Deliv. Rev.* **2001**, *48* (1).
- (20) Dengale, S. J.; Grohgan, H.; Rades, T.; Löbmann, K. *Adv. Drug Deliv. Rev.* **2016**, *100*, 116–125.

- (21) Löbmann, K.; Laitinen, R.; Grohgan, H.; Gordon, K. C.; Strachan, C.; Rades, T. *Mol. Pharm.* **2011**, *8* (5), 1919–1928.
- (22) Dengale, S. J.; Ranjan, O. P.; Hussien, S. S.; Krishna, B. S. M.; Musmade, P. B.; Gautham Shenoy, G.; Bhat, K. *Eur. J. Pharm. Sci.* **2014**, *62*, 57–64.
- (23) Qian, S.; Heng, W.; Wei, Y.; Zhang, J.; Gao, Y. *Cryst. Growth Des.* **2015**, *15* (6), 2920–2928.
- (24) Löbmann, K.; Strachan, C.; Grohgan, H.; Rades, T.; Korhonen, O.; Laitinen, R. *Eur. J. Pharm. Biopharm.* **2012**, *81* (1), 159–169.
- (25) Löbmann, K.; Grohgan, H.; Laitinen, R.; Strachan, C.; Rades, T. *Eur. J. Pharm. Biopharm.* **2013**, *85* (3), 873–881.
- (26) Jensen, K.; Löbmann, K.; Rades, T.; Grohgan, H. *Pharmaceutics* **2014**, *6* (3), 416–435.
- (27) Heikkinen, A. T.; DeClerck, L.; Löbmann, K.; Grohgan, H.; Rades, T.; Laitinen, R. *Pharmazie* **2015**, *70* (7), 452–457.
- (28) Allesø, M.; Chieng, N.; Rehder, S.; Rantanen, J.; Rades, T.; Aaltonen, J. *J. Control. Release* **2009**, *136* (1), 45–53.
- (29) Good, D. J.; Rodríguez-Hornedo, N. *Cryst. Growth Des.* **2009**, *9* (5), 2252–2264.
- (30) Grifasi, F.; Chierotti, M. R.; Gaglioti, K.; Gobetto, R.; Maini, L.; Braga, D.; Dichiarante, E.; Curzi, M. *Cryst. Growth Des.* **2015**, *15* (4), 1939–1948.

- (31) McNamara, D. P.; Childs, S. L.; Giordano, J.; Iarriccio, A.; Cassidy, J.; Shet, M. S.; Mannion, R.; O'Donnell, E.; Park, A. *Pharm. Res.* **2006**, *23* (8), 1888–1897.
- (32) Childs, S. L.; Chyall, L. J.; Dunlap, J. T.; Smolenskaya, V. N.; Stahly, B. C.; Stahly, G. P. *J. Am. Chem. Soc.* **2004**, *126* (41), 13335–13342.
- (33) Huang, Y.; Zhang, B.; Gao, Y.; Zhang, J.; Shi, L. *J. Pharm Sci.* **2014**, *103* (8), 2330–2337.
- (34) Smith, A. J.; Padmini, K.; Wojtas, L.; Zaworotko, M. J.; Shytle, R. D. *Mol. Pharm.* **2011**, *8* (5).
- (35) Song, J.-X.; Yan, Y.; Yao, J.; Chen, J.-M.; Lu, T.-B. *Cryst. Growth Des.* **2014**, *14* (6).
- (36) Goud, N. R.; Gangavaram, S.; Suresh, K.; Pal, S.; Manjunatha, S.; Nambiar, S.; Nangia, A. *J Pharm Sci.* **2011**, *101* (2), 664–680.
- (37) Cheney, M. L.; Weyna, D.; Shan, N.; Hanna, M.; Wojtas, L.; Zaworotko, M. J. *Pharm Sci.* **2011**, *100* (6), 2172–2178.
- (38) Bak, A.; Gore, A.; Yanez, E.; Stanton, M.; Tufekcic, S.; Syed, R.; Akrami, A.; Rose, M.; Surapaneni, S.; Bostick, T.; King, A.; Neervannan, S.; Ostovic, D.; Koparkar, A. *J. Pharm. Sci.* **2008**, *97* (9), 3942–3956.
- (39) Goud, N. R.; Suresh, K.; Sanphui, P.; Nangia, A. *Int. J. Pharm.* **2012**, *439* (1), 63–72.
- (40) Sanphui, P.; Goud, N. R.; Khandavilli, U. B. R.; Nangia, A. *Cryst. Growth Des.*

- 2011**, *11* (9), 4135–4145.
- (41) Suresh, K.; Mannava, M. K. C.; Nangia, A. *RSC Adv.* **2014**, *4* (102), 58357–58361.
- (42) Gately, S. T.; Triezenberg, S. J. Solid forms of curcumin. WO2012138907 A2, 2012.
- (43) Su, H.; He, H.; Tian, Y.; Zhao, N.; Sun, F.; Zhang, X.; Jiang, Q.; Zhu, G. *Inorg. Chem. Commun.* **2015**, *55*, 92–95.
- (44) Chow, S. F.; Shi, L.; Ng, W. W.; Leung, K. H. Y.; Nagapudi, K.; Sun, C. C.; Chow, A. H. L. *Cryst. Growth Des.* **2014**, *14* (10), 5079–5089.
- (45) Chava, S.; Muppidi, V. K.; Gorantla, S. R. A. Solid forms of curcumin and derivatives thereof. WO2015052568 A2, 2015.
- (46) Vidyulatha, K. T.; Jaganathan, K.; Sambath Kumar, R.; Perumal, P.; Sevukarajan, M.; Aneef, M. Y. *Int. J. Pharm. Dev.* **2012**, *2* (2), 67–76.
- (47) Sekhon, B. S. *Daru* **2012**, *20* (1), 45.
- (48) Fábíán, L. *Cryst. Growth Des.* **2009**, *9* (3), 1436–1443.
- (49) Tønnesen, H. H.; Karlsen, J.; Mostad, A.; Samuelsson, B.; Enzell, C. R.; Berg, J.-E. *Acta Chem. Scand.* **1982**, *36b*, 475–479.
- (50) Lu, E.; Rodríguez-Hornedo, N.; Suryanarayanan, R. *CrystEngComm* **2008**, *10* (6), 665.

- (51) Mohan, P. R. K.; Sreelakshmi, G.; Muraleedharan, C. V.; Joseph, R. *Vib. Spectrosc.* **2012**, *62*, 77–84.
- (52) Varshosaz, J.; Hassanzadeh, F.; Sadeghi Aliabadi, H.; Nayebsadrian, M.; Banitalebi, M.; Rostami, M. *Biomed Res. Int.* **2014**, *2014*, 525684.
- (53) Paul, C. *BJOG An Int. J. Obstet. Gynaecol.* **2016**, *123* (3), 392–392.
- (54) Zhou, J.; Miao, H.; Li, X.; Hu, Y.; Sun, H.; Hou, Y. *Inflamm. Res.* **2017**, *66* (2), 177–185.
- (55) Rahardjo, B. *Biomarkers Genomic Med.* **2014**, *6* (3), 105–115.
- (56) Zheng, L.; Tong, Q.; Wu, C. *J. Huazhong Univ. Sci. Technolog. Med. Sci.* **2004**, *24* (1), 55–58.
- (57) Ward, C.; Acheson, N.; Seymour, L. *J. Drug Target.* **2000**, *8* (2), 119–123.
- (58) Sanphui, P.; Goud, N. R.; Khandavilli, U. B. R.; Bhanoth, S.; Nangia, A. *Chem. Commun.* **2011**, *47* (17), 5013.

Chapter 5

Efforts to Increase the Solubility of Rufinamide

Rufinamide is an active pharmaceutical ingredient (API) that is used to treat a form of childhood epilepsy called Lennox-Gastaut syndrome that is characterized by having multiple seizure types. This API has a broad-spectrum antiepileptic with low adverse effects. Rufinamide is considered a Class IV API by the Biopharmaceutics Classification System, which means that it has low solubility and low permeability. Since patients with Lennox-Gastaut syndrome are usually children and are often taking multiple medications, it would be advantageous to increase the solubility of this drug to reduce the required dosages. To date, there are no salts, co-crystals, solvates, etc. of this drug; its structural polymorphs are the only solid state forms discovered. We attempted to increase the dissolution rate of rufinamide by choosing potential excipients and conducting extensive screening to form co-crystals or other solid state forms. No novel solid states of rufinamide with excipients were produced. The excipients that were chosen all had potential to form intermolecular bonds and passed a computer-based screening test. However, the molecular structure of a metastable polymorph termed modification B of rufinamide was obtained. Also reported is an accelerated procedure to produce modification B in the presence of citric acid.

Introduction

Lennox-Gastaut syndrome is a serious form of childhood epilepsy characterized by multiple seizure types and often cognitive impairment. This syndrome frequently continues into adulthood, and the seizures are generally not responsive to typical antiepileptic drug care.¹ Rufinamide (shown in Figure 0.1) is an anticonvulsant that acts by reducing the firing of sodium dependent action potentials in treating patients with Lennox-Gastaut syndrome.² This API is a broad-spectrum antiepileptic drug with low drug interaction and good adverse event profile.³ While it is proven to be effective, this drug has very poor aqueous solubility and relatively low permeability, so it is considered to be BCS (Biopharmaceutics Classification System) Class IV.⁴

To date, there are no known co-crystals, solvates, eutectics or co-amorphous mixtures involving rufinamide; however, there are multiple polymorphs.^{5,6} A polymorph is *a solid crystalline phase of a given compound resulting from the possibility of at least two different arrangements of molecules of that compound in the solid state.*⁷ Some of these polymorphs are given below in Table 0.1. Modification A is shown to have better thermodynamic stability; Modification C will transform to A or B at room temperature. The molecular structures of these polymorphs are not given in the CSD (Cambridge Structural Database).

Table 0.1: Some polymorphs of rufinamide

Polymorph	Space Group	Crystal System
Modification A	Pna2 ₁	orthorhombic
Modification B	P-1	triclinic
Modification C	P2 ₁ /C	monoclinic

Looking at the chemical structure in Figure 1, there are multiple sites for potential intermolecular bonding between rufinamide and excipient molecules. Supramolecular synthons are *structural units within supermolecules which can be formed and/or assembled by known or conceivable synthetic operations involving intermolecular interactions.*⁸ Since amide groups are known to form both heterosynthons (e.g. with carboxylic acids) and homosynthons, molecules with either type of functional group should be screened for potential novel solid state forms with rufinamide.⁹

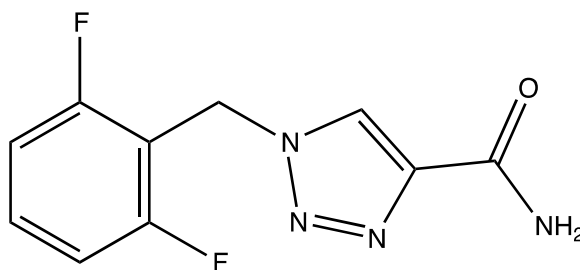


Figure 0.1: Molecular structure of rufinamide.

Materials and Methods

Rufinamide modification A was donated by Apotex Pharmachem Inc. (Branford, Canada). Solvents and excipients were obtained from Sigma Aldrich (Oakville, Canada). Screening of excipients for solid states was done via liquid assisted (ethanol) and neat grinding at various molar ratios for 20 minutes with mortar and pestle. Solution crystallization in various solvent systems was also attempted at varying molar ratios via slow evaporation at ambient conditions or cooling crystallization at a rate of 10 °C /hour. These screenings did not result in novel solid state formation. Bulk modification B was obtained by dissolving citric acid (100 mg) and rufinamide modification A (100 mg) in DMSO (6 mL) at 40°C for 2 hours. The mixture was turbid, so filtration was required and an additional 1 mL of DMSO was added. Next, the solution was left at atmospheric conditions until needle-like crystals formed that were filtered and dried under vacuum at 60°C for three hours. Single crystals were grown via slow evaporation from methanol at ambient conditions, and Bruker Apex II Diffractometer with Mo X-ray radiation was used to obtain the crystal structure. ¹H NMR spectrum was collected on a Mercury VX 400 MHz machine. Powder X-ray Diffraction was obtained from a Rigaku Miniflex instrument with Cu X-ray radiation. Scans were run at a speed of 1.00°/minute for 2θ values over 2° to 40°. Thermogravimetric analysis and differential scanning calorimetry were conducted on the Mettler-Toledo STAR^e 851^e and 822^e instruments, respectively, at a heating rate of 10 °C/minute from 25-350 °C.

Results and Discussion

Since Class IV drugs are undesirable, increasing the solubility of rufinamide was attempted through solid form screening. Co-crystal screening via grinding and solution methods was conducted in an attempt to form novel solid states of rufinamide with a host of excipient molecules. To help choose an appropriate co-former, multi-component screening based on molecular complementarity was conducted via Mercury software.¹⁰ This software uses the shape, polarity and hydrogen bonding potential of the API to determine which excipients (from a list of the most commonly used co-crystal formers) may form a co-crystal based on the statistics of other co-crystal forming pairs. At the time of screening, none of the

molecular structures of rufinamide's polymorphs were available in the Cambridge Structural Database (CSD). While it is not essential to have the molecular structure of the API to use this screening technique (e.g. a 3D drawing of the molecule would suffice), much more accurate results can be obtained if the structure of the API is available. Methyl 1-(2,6-difluorobenzyl)-1H-1,2,3-triazole-4-carboxylate, an intermediate in the synthesis of rufinamide, is accessible in the CSD and contains an ester as opposed to the amide group seen in Figure 0.1. The crystal was shown to form weak intermolecular C-H...O and C-H...N hydrogen bonds that link the molecules into chains along the b-axis.¹¹ This molecular structure was modified by simply changing the functional group to an amide so that it exemplified rufinamide. Once modified, this compound resulted in an extensive list of potential co-formers for co-crystal formation. This list led to many possible excipients to screen, so it was narrowed to include only those approved by the US Food and Drug Administration (FDA) that had strong capability to form intermolecular bonds. Excipients screened included citric acid, urea, thiourea, nicotinamide, sorbitol, L-(+)-histidine, L-threonine, ascorbic acid, 4-aminobenzoic acid, propylene glycol, folic acid dihydrate, L-alanine, L-glutamic acid, mandelic acid, succinic acid, lactose monohydrate, chitosan and L-tyrosine. Many different screening techniques, such as solvent crystallization and the grinding/DSC methods were employed as an attempt to form a novel solid state. Though extensive screening with many excipient molecules was conducted, no novel co-crystals, co-amorphous, solvates or eutectic mixtures were discovered.

Rufinamide Modification B

In order to investigate the underlying reason, successful attempts were made to grow single crystals of rufinamide modification B and its molecular structure was obtained through single crystal XRD (X-ray diffraction). By dissolving rufinamide modification A in methanol and allowing slow evaporation, modification B crystallized out as colorless, needle-like crystals. While this unit cell is known, its molecular structure is not published and, as mentioned, cannot be found in the CSD. The sample was mounted on a Mitegen polyimide micromount with a small amount of Paratone N oil. All X-ray measurements were made on a Bruker Kappa Axis Apex2 diffractometer at a temperature of 110 K. The unit cell dimensions were determined from a symmetry constrained fit of 9962 reflections

with $5.02^\circ < 2\theta < 68.16^\circ$. The data collection strategy involved ω and ϕ scans up to 68.602° (2θ). The frame integration was performed using SAINT.¹² The resulting raw data was scaled and absorption corrected using a multi-scan averaging of symmetry equivalent data using SADABS.¹³ The structure was solved by using a dual space methodology using the SHELXT program.¹⁴ All non-hydrogen atoms were obtained from the initial solution. All hydrogen atoms were introduced at idealized positions and were allowed to ride on the parent atom. The structural model was fit to the data using full matrix least-squares based on F^2 . The calculated structure factors included corrections for anomalous dispersion from the usual tabulation. The structure was refined using the SHELXL-2014 program from the SHELXTL suite of crystallographic software.¹⁵ Graphic plots were produced using the Mercury program suite (Summary of crystal data in Table 0.2).¹⁶

Table 0.2: Summary of Crystal Data of Rufinamide Modification B.

Formula	C ₁₀ H ₈ F ₂ N ₄ O
Formula Weight (<i>g/mol</i>)	238.20
Crystal Dimensions (<i>mm</i>)	0.377 × 0.137 × 0.086
Crystal System	Triclinic
Space Group	P -1
Temperature, K	110
<i>a</i> , Å	5.2943(10)
<i>b</i> , Å	11.936(5)
<i>c</i> , Å	17.121(6)
α , °	71.540(14)
β , °	87.719(9)
γ , °	77.255(8)
<i>V</i> , Å ³	1000.5(6)
<i>Z</i>	4
F(000)	488
ρ (<i>g/cm</i>)	1.581
λ , Å, (MoK α)	0.71073
μ , (<i>cm</i> ⁻¹)	0.133
R ₁	0.0632
wR ₂	0.1131
GOF	1.033
Maximum shift/error	0.001
Min & Max peak heights on final ΔF Map (<i>e</i> ⁻ /Å)	-0.287, 0.519

Modification B of rufinamide was found to crystallize in the space group P-1 with $Z = 4$. The packing in the unit cell is shown in Figure 0.2. Intermolecular N-H \cdots O hydrogen bonding occurs between the amide groups of distinct molecules (Figure 3). There is also N-H \cdots N bonding between amide groups and nitrogen of the triazole. The bond lengths range from 2.890 to 3.057 Å and are representative of strong hydrogen bonding between molecules. The shortest and strongest intermolecular bonds are the N-H \cdots O bonds (i.e. bonds a, b and c in Figure 0.3), which is known to be a convincing homosynthon. Intriguingly, the homosynthon is formed between three distinct rufinamide molecules as opposed to two molecules, which is more common. This is evidently illustrated in Figure 0.4. The presence of an amide strengthens the intermolecular bonding, which is noticeable when compared to the weak hydrogen bonding of the rufinamide derivative mentioned earlier. It is worth mentioning that halogen bonding was observed in the structure of rufinamide between fluorine groups and the aromatic benzene rings of individual molecules. Weak intermolecular bonding is also seen between hydrogen molecules of the CH₂ group and the triazole nitrogen.

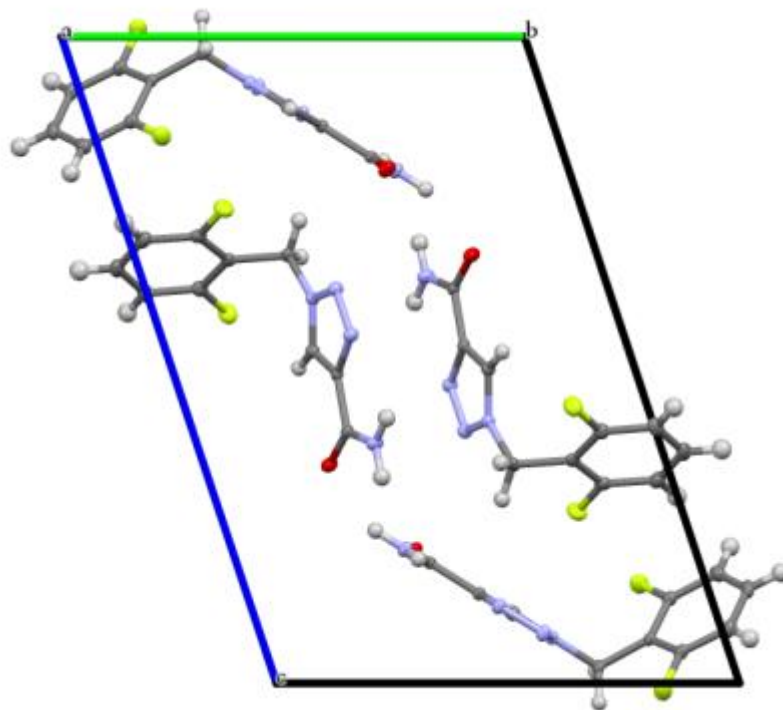


Figure 0.2: Molecules of rufinamide modification B in one unit cell. F: green, O: red, N: blue, C: grey and H: white.

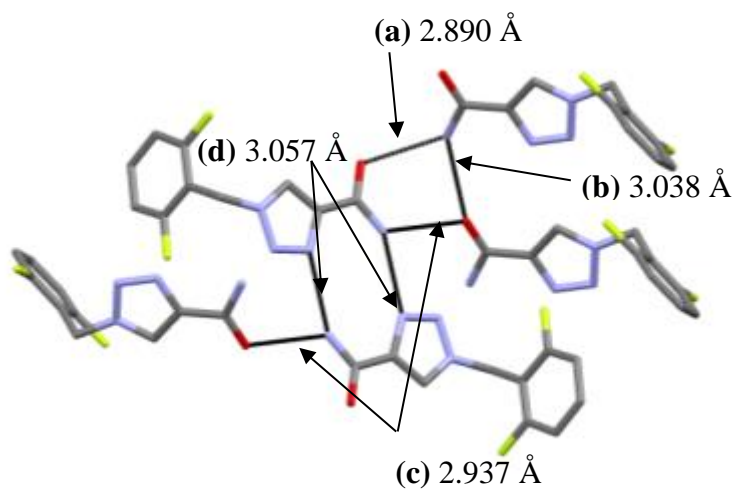


Figure 0.3: Strong hydrogen bonding between the molecules in the lattice are shown in black dotted lines (labelled a-d); hydrogen atoms have been omitted for more clarity. F: green, O: red, N: blue, C: grey.

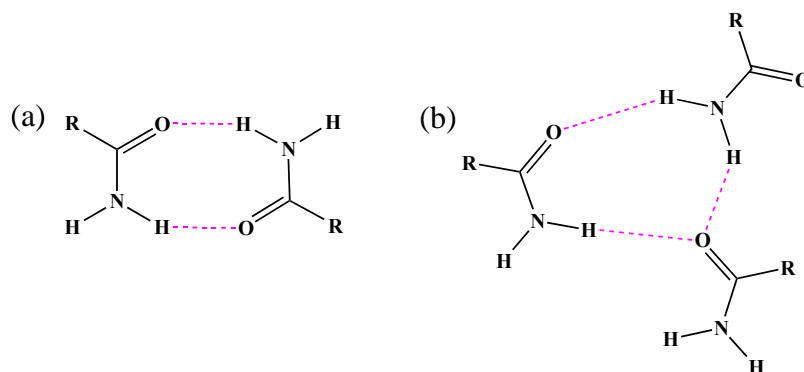


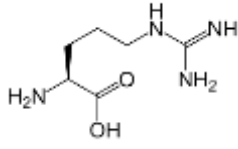
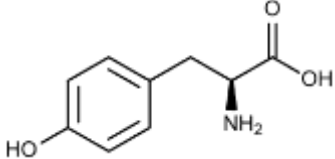
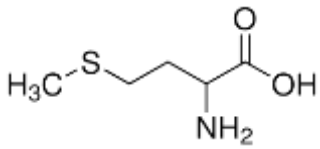
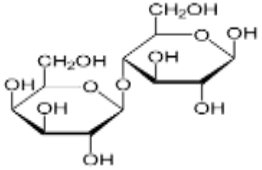
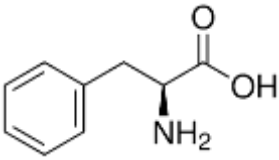
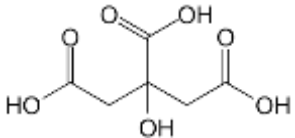
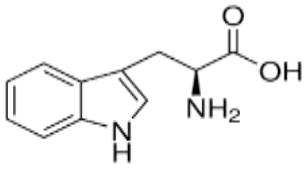
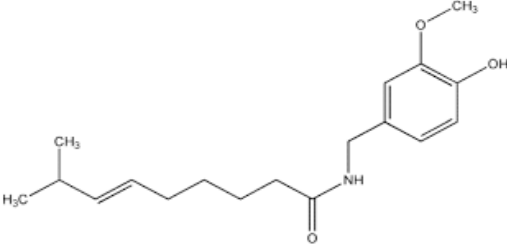
Figure 0.4: Intermolecular homosynthons between (a) two and (b) three amide groups from distinct molecules.

Further Screening

Once the molecular structure of rufinamide modification B was obtained, it was possible to run the multi-component screening through Mercury using the molecular structure of the modification B, instead of a compound with a structure similar to rufinamide, as discussed earlier. A much narrower list of potential co-formers was obtained, which could lead to more accurate screening. For instance, succinic acid was a potential co-crystal former with the modified rufinamide intermediate; however, it did not pass the statistical screening with rufinamide modification B due to issues with shape and size complementarity. The FDA approved list from the second screening computer generated group of suggested co-formers is given in

Table 0.3. Some of the potential co-formers that were suggested for the modified rufinamide derivative showed negative results for co-crystal formation with modification B. This coincides with the statement that co-crystal formation is very dependent on the shape of the molecule, not solely hydrogen bond formation capabilities.¹⁰

Table 0.3: FDA approved co-formers from CSD screening with rufinamide modification B

L-arginine		L-tyrosine	
L-methionine		lactose	
L-phenylalanine		citric acid	
L-tryptophan		capsaicin	

Another extensive screening was conducted, but this time with modification B as the starting solid form of the API and the co-formers listed above; however, still no new solid states were discovered. This was peculiar due to the many potential sites for hydrogen bonding in rufinamide. Also, triazole derivatives have been shown to readily form co-crystals with compounds containing carboxylic acid groups.¹⁷

When analyzing the chemical structure of rufinamide, it seems like a good candidate for incorporating an excipient into the crystal lattice. There are multiple sites for hydrogen bonding (e.g. amide, triazole and halogen functional groups) and its low aqueous solubility makes it an interesting target for co-crystal, co-amorphous, eutectic or solvate formation. Additionally, the Z' value (i.e. the molecules in the asymmetric unit) for rufinamide

modification B is 2, and it has been shown that molecules with a $Z' > 1$ have a stronger tendency to form co-crystals.¹⁸ Furthermore, when screened for potential co-crystal co-formers, many molecules were suggested with eight of them being FDA approved. It has also been previously shown that triazole groups are capable of forming hydrogen bonds with dicarboxylic acids leading to the formation of co-crystals, but rufinamide was unable to form any novel solid state with the molecules listed in Table 3.⁶ It was observed that rufinamide tended to form needle-like crystals and would often form a jelly-like solution during the crystallization process (i.e. a hydrogel). In order for a novel solid state to form, the intermolecular bonding force between API and excipient needs to be stronger than the API-API and excipient-excipient intermolecular bonding force. Perhaps the intermolecular forces between molecules of rufinamide are too strong to overcome by the attempted co-former molecules. As stated, there are no solid states of rufinamide in literature that involve excipient addition into the crystal lattice. Amide-amide bonds are very strong, and it is shown in the crystal structure of rufinamide modification B that this homosynthon is a stabilizing force. The high stability of the rufinamide crystal structure would also explain why grinding did not help in the formation of any new forms: the mechanical forces were not strong enough to break the bonds.

Another suggestion as to why no novel solid states were produced with excipient molecules could be due to solubility issues. Rufinamide has very poor solubility in most solvents and had to be heated to dissolve fully. Often, solvents such as dimethylformamide (DMF), dimethylsulfoxide (DMSO) and dimethylacetamide (DMAC) were used, in which the excipients were very highly soluble. These solubility issues could lead to the fast crystallization of rufinamide before any co-former had the chance to interact with it.

Results from Screening with Citric Acid

While no novel solid state form was obtained through screening with citric acid similar to other employed excipients, some interesting results were observed in the case of citric acid. Crystals were obtained by dissolving citric acid and rufinamide modification A in DMSO; the solution was left at atmospheric conditions until solids were formed. The crystals obtained were filtered and dried under vacuum for solvent removal. When compared with

the starting material (i.e. modification A), seemingly novel powder XRD (PXRD) pattern was recorded; which is illustrated in Figure 0.5 (a). The differential scanning calorimetry (DSC) thermograph (Figure 0.5 (b)) appeared very similar to that of rufinamide modification A, which is not characteristic of co-crystal formation. Solution ^1H NMR (nuclear magnetic resonance) was run to identify the main components of the solid and can be seen in Figure 0.6. The NMR spectrum revealed that rufinamide was present (i.e. the product's spectrum matches that of the starting material), so the experimental conditions did not lead to decomposition of the API. Interestingly, when compared to the spectrum of pure citric acid, this starting material is undoubtedly absent in NMR of the product; indicating that citric acid did not crystallize with rufinamide. These findings led to further analysis of the PXRD pattern, which revealed that the product was the metastable modification B. This was proven by matching the diffraction pattern with the pattern that was simulated from the obtained single crystal results.

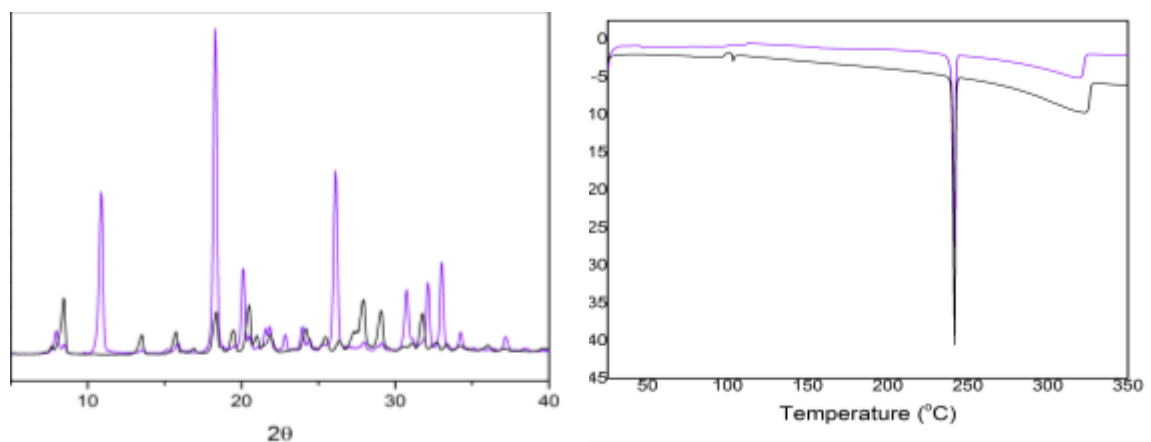


Figure 0.5: (a) PXRD patterns and (b) DSC thermographs for rufinamide modification A (black) and rufinamide modification B obtained from solution (purple).

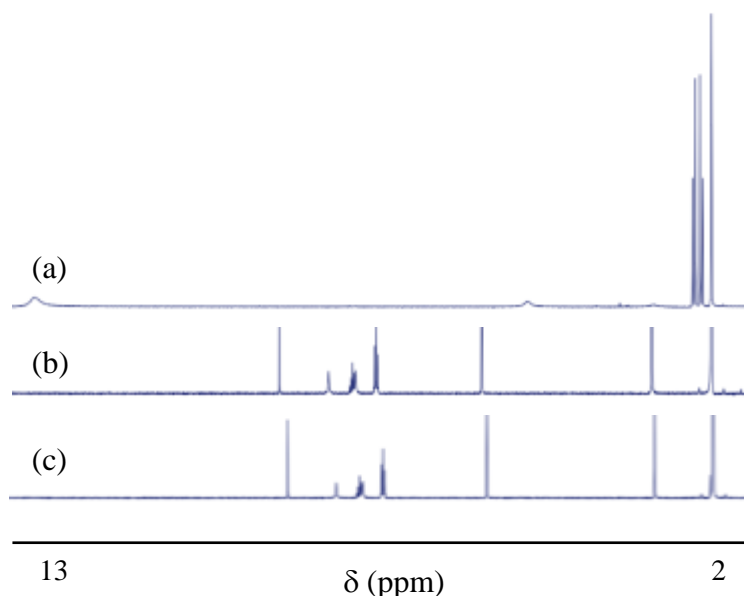
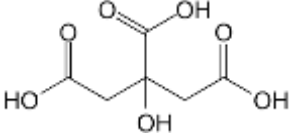
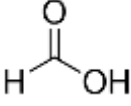
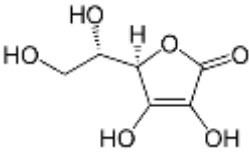
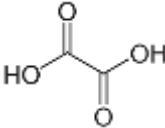


Figure 0.6: ^1H NMR spectra for (a) citric acid, (b) rufinamide modification A and (c) rufinamide modification B in DMSO-d_6 .

The proposed process to obtain modification B is much quicker than slow evaporation and resulted in a more homogeneous product with increased crystallinity. The procedure was replicated by using different acids (summarized in Table 0.4), but the product either did not crystallize or decomposed. Citric acid has a $\text{pK}_{\text{a}1}$ of 3.08, while oxalic acid has a $\text{pK}_{\text{a}1}$ of 1.23. Oxalic acid is much stronger acid and leads to the decomposition of rufinamide. Formic acid and ascorbic acid have $\text{pK}_{\text{a}1}$ values of 3.75 and 4.10, respectively. They are not strong acids and comparable to citric acid. While rufinamide did not decompose using these acids, it resulted in the crystallization of modification A. Next, the solvent type was varied (i.e. DMF, DMAC), but the results could not be duplicated. Clearly, there must be some solvent effects that are present when DMSO is used.

Table 0.4: Attempted acids for synthesis of rufinamide modification B. ¹⁹

Acid	Structure	pKa ₁
Citric Acid		3.08
Formic Acid		3.75
Ascorbic Acid		4.10
Oxalic Acid		1.23

Conclusion

Lennox-Gastaut syndrome is a devastating type of childhood epilepsy that can be treated with the drug rufinamide. This drug has been proven to be effective, but it has a low aqueous solubility that demands higher doses. Screening was conducted using solution and grinding methods to find other solid forms (such as co-crystals, co-amorphous, eutectic mixtures, solvate) to increase rufinamide's solubility and bioavailability. Although screening did not result in the formation of a novel solid state, a novel synthesis of a metastable form of rufinamide, modification B, was discovered. The proposed method depended on solvent and excipient present. The molecular structure of rufinamide B, a poorly soluble antiepileptic drug, was determined and used in computer based co-crystal screening. The lack of novel solid states from the suggested co-formers implies that this method is not entirely reliable if co-crystal formation is challenging and molecular synthon approach should also be employed. Rufinamide is a small molecule with many potential sites for hydrogen bonding, and it has rotation about a CH₂. Therefore, it should not be

disregarded completely for formation of a novel solid state. Also, due to the nature of Lennox-Gastaut syndrome, multiple prescriptions are used; perhaps drug-drug solid states should also be investigated.

References

- (1) Crumrine, P. K. *J. Child Neurol.* **2002**, *17* (1 suppl), S70–S75.
- (2) Bialer, M.; Johannessen, S. I.; Kupferberg, H. J.; Levy, R. H.; Loiseau, P.; Perucca, E. *Epilepsy Research.* 1996, pp 299–319.
- (3) Wheless, J. W.; Vazquez, B. *Epilepsy Curr.* **2010**, *10* (1), 1–6.
- (4) Medicines and Healthcare Products Regulatory Agency. Formulation switching of antiepileptic drugs: A Report on the Recommendations of the Commission on Human Medicines from July 2013 <http://www.mhra.gov.uk/home/groups/comms-ic/documents/websiteresources/con341226.pdf> (accessed Jun 12, 2017).
- (5) Sola, C. L.; Freixas, P. G.; Ceròn, Bertran Jordi Barjoan, P. D. Polymorph of Rufinamide and process for obtaining it. EP2465853 A1, 2010.
- (6) Burkhard, A.; Hofmeier, U. C.; Portmann, R.; Scherrer, W.; Szlagiewicz, M. Crystal modification of 1-(2,6-difluorobenzyl)-1h-1,2,3-triazole-4-carboxamide and its use as antiepileptic. EP0994863 B1, 2003.
- (7) McCrone, W. C. *Polymorphism*; 1965.
- (8) Corey, E. J. *Chem. Soc. Rev.* **1988**, *17* (0), 111–133.
- (9) Adalder, T. K.; Sankolli, R.; Dastidar, P. *Cryst. Growth Des.* **2012**, *12* (5), 2533–2542.
- (10) Fábíán, L. *Cryst. Growth Des.* **2009**, *9* (3), 1436–1443.
- (11) Dong, S.-L.; Cheng, X.-C. *Acta Crystallogr. Sect. E Struct. Reports Online* **2011**, *67* (4), o769–o769.
- (12) Bruker-AXS, Madison, WI 53711, U. **2013**.
- (13) Bruker-AXS, Madison, WI 53711, U. **2012**.

- (14) Sheldrick, G. M. *Acta Crystallogr. Sect. A, Found. Adv.* **2015**, *71* (Pt 1), 3–8.
- (15) Sheldrick, G. M. *Acta Crystallogr. Sect. C Struct. Chem.* **2015**, *71* (1), 3–8.
- (16) C. F. Macrae, I. J. Bruno, J. A. Chisholm, P. R. Edgington, P. McCabe, E. Pidcock, L. Rodriguez-Monge, R. Taylor, J. van de S. and P. A. W. *J. Appl. Cryst* **2008**, *41*, 466–470.
- (17) Remenar, J. F.; Morissette, S. L.; Peterson, M. L.; Moulton, B.; MacPhee, J. M.; Guzmán, H. R.; Örn, A. **2003**.
- (18) Anderson, K. M.; Probert, M. R.; Whiteley, C. N.; Rowland, A. M.; Goeta, A. E.; Steed, J. W. *Cryst. Growth Des.* **2009**, *9* (2), 1082–1087.
- (19) Bruice, P. Y. *Organic chemistry*; Pearson Prentice Hall, 2007.

Chapter 6

Conclusion and Recommendations

There is a clear need in the pharmaceutical industry to increase the solubility of new active pharmaceutical ingredients (APIs), since many of them are considered BCS (Biopharmaceutics Classification System) Class II and IV drugs. Increased solubility and dissolution rate of these APIs will lead to better bioavailability, reduced dosages, less waste and potentially fewer prescriptions; this all suggests savings for the pharmaceutical industry. In this thesis, three low solubility APIs (i.e. esomeprazole magnesium, curcumin and rufinamide) were all investigated for their ability to form novel solid states. This was done by screening with excipients that are approved for use in drugs and would expectantly interact with the API through intermolecular bonding. Formation of solid states was confirmed by a combination of powder and single crystal X-ray diffraction, differential scanning calorimetry, thermogravimetric analysis, solution nuclear magnetic resonance spectroscopy and dynamic vapour sorption. Further screening on these drugs can be conducted to find more novel states.

Conclusions

Esomeprazole magnesium is a low solubility drug used to treat chronic acid reflux. To improve this API, screening was conducted using solution crystallization and grinding techniques. What was obtained was a solvate with both water and 1-butanol present. High quality single crystals of this novel solid state were crystallized and the molecular structures were determined using X-ray diffraction. This is the first single crystal structure reported that displays esomeprazole coordinated to a metal center. The esomeprazole acts as a bidentate ligand, with three molecules coordinated to a single magnesium center. Magnesium cations are also shown to co-ordinate to water molecules, and water is furthermore shown to be filling the channels of the crystal lattice along with non-stoichiometric amounts of butanol molecules. The covalently bonded waters are much more strongly kept in the lattice than those maintained by hydrogen bonding. When heated under vacuum the channel solvents were removed to reveal the dihydrate of esomeprazole

magnesium. This solvate will have similar solubility to the dihydrate since it has the same crystal structure. The discovery of this esomeprazole magnesium solvate could have applicability to the development of improved pharmaceutical solid dosage forms.

Found in a variety of Asian cuisine, turmeric is a common spice that contains curcumin, a natural drug product that is found to have many health benefits. The use of curcumin in the pharmaceutical and food industries is often limited by its lack of aqueous solubility. In this thesis, screening for a novel solid state of curcumin with a variety of excipients was conducted. To narrow the search, a computer-based method was employed to predict which co-formers would form co-crystals with form I (most common and stable) curcumin. Folic acid dihydrate is one these predicted co-formers and was displayed to form a novel solid state with curcumin. After grinding with ethanol, a co-amorphous mixture was obtained and confirmed by PXRD (Powder X-ray Diffraction) and DSC (Differential Scanning Calorimetry). Repositioning of this mixture as a prenatal drug is possible since both folic acid and curcumin are used to treat a variety of pregnancy symptoms. This would save money and reduce the number of prescriptions needed. The co-amorphous mixture is also advantageous because it has improved dissolution rate over curcumin in aqueous solutions. After one hour, 175 mg/L of curcumin is dissolved in 40% ethanol from the co-amorphous mixture. This is a vast improvement over the 40 mg/L of form I curcumin after one hour. This mixture is also shown to be relatively stable and will keep its amorphous behaviour after 24 hours in solution at body temperature. Co-amorphous states in the pharmaceutical industry are relatively new and not well studied. The results confirm the validity of this solid state form as an improvement to APIs with low bioavailability. Additionally, given in this work is an alternative method of forming metastable form II curcumin. Crystals can be synthesized by slow evaporation from methanol in the presence of dextrose. Powder can be obtained from anti-solvent crystallization with water. This method is faster than current methods of producing form II curcumin and give a high purity yield.

Rufinamide is a low solubility API that is used to treat a form of childhood epilepsy call Lennox-Gastaut syndrome that is characterized by multiple seizure types. While this API is proven to be effective, its solubility issues lead to increased dosages to generally young patients. To increase this undesirable characteristic, and essentially its bioavailability,

screening for the formation of a novel solid state was conducted. Many excipients were screened based on the molecular structures of a modified form of rufinamide and the metastable modification B. After extensive screening, no co-crystals, solvates, eutectics or co-amorphous mixtures were discovered. Perhaps the strong intermolecular bonding found in rufinamide is why it was not possible to include another molecule into its crystal lattice. Presented is a novel synthesis route for the crystallization of modification B as well as its molecular structure. This crystallization was found to be very dependent on the solvent (dimethyl sulfoxide) and excipient (citric acid) employed.

Recommendations

The screening of esomeprazole magnesium was successful in finding a novel solvate form; however, it was not practical or necessary to do dissolution rate or solubility studies because of the channel solvates. Since the solvent molecules that were not coordinated to magnesium were only weakly involved in intermolecular bonding, they would be easily removed and not problematic to quantify. This would lead to difficulties in solubility determination because molecular weight would vary for each sample. Also, since the molecular structure so closely matched esomeprazole magnesium dihydrate, it can be assumed to have a similarly improved solubility. Future work can be done to screen this API more thoroughly for other solid states. Perhaps it would be easier to form co-crystals or co-amorphous mixtures with esomeprazole as opposed to the magnesium salt. The molecular structure of the water/1-butanol solvate was very complex and could not be used to help determine a list of potential co-formers from Mercury. If single crystals could be produced that display the binding of the esomeprazole molecules to magnesium without solvent, then perhaps the software could be employed. This would help to narrow the search for potential API-excipient combinations as well as help improve understanding of the conceivable intermolecular interactions. The starting material used in the screening was the amorphous form of the pharmaceutical salt. Screening could possibly be conducted by starting with a crystalline form and comparing the result to screening with the amorphous form.

There were many differences in the predicted co-formers from Mercury software and the co-crystal formers that have been shown to form curcumin co-crystals in literature. If a greater understanding of these differences was made then perhaps it would be easier to know which excipients would be successful. More screening can be conducted with molecules that more closely represent those that have been shown to form novel solid states. Since curcumin is naturally occurring, maybe it can be viewed as an excipient for potential solid states with other drugs. The curcumin-folic acid dihydrate co-amorphous mixture (CUR-FAD) can be further studied. By running Raman and solid state nuclear magnetic resonance, perhaps a proposed bonding mechanism between the two molecules can be given. Stability studies that were not possible due to time constraints should be conducted for CUR-FAD for an extended period of time and under specific temperature and humidity conditions.

There is definitely a need to further investigate the possibility of solid state formation with rufinamide. With its high potential for intermolecular hydrogen bonding and having Z' value greater than 1, it should theoretically be readily available for synthesis of co-crystals, co-amorphous mixtures, eutectics or solvates. A wide range of excipients were attempted based on supramolecular synthons and computational suggestions. Possibly, a lesser emphasis should be placed upon the Mercury generated excipients, and a larger range of pharmaceutically approved excipients should be screened. Perhaps a literature survey of the unsuccessful co-crystallization of APIs should be conducted to further understand why no novel states were formed. Since there are known polymorphs of this API, a different modification could be isolated for attempts at solid state formation. It is also recommended that a wider range of solvents be attempted for crystallization experiments.

Appendices

Appendix A Supporting Information for Chapter 3

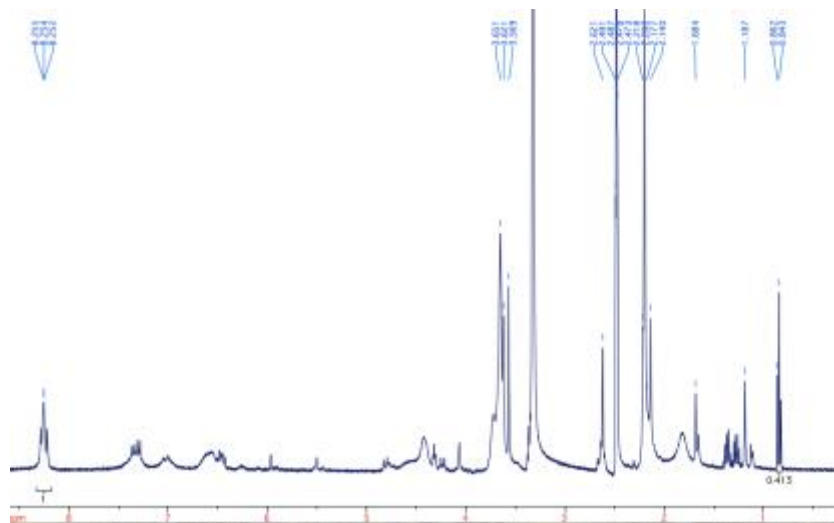


Figure A - 1: ¹H NMR of the esomeprazole magnesium solvate.

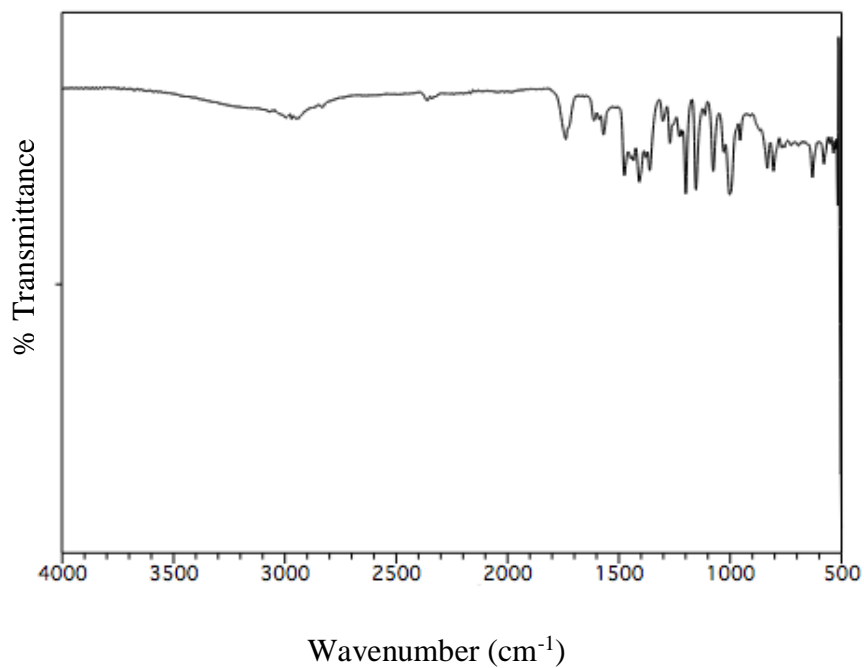


Figure A - 1: FTIR of the esomeprazole magnesium solvate.

Appendix B Calibration Curves for CUR-FAD Dissolution Studies

When doing dissolution studies, UV-Vis is a viable means for determining the concentration of a solution. This technique requires the formation of a calibration curve from known concentrations that utilizes Beer's Law (i.e. $A = \epsilon cl$) to determine an extinction coefficient. This extinction coefficient is then used for the concentration calculation of unknown sample concentrations.

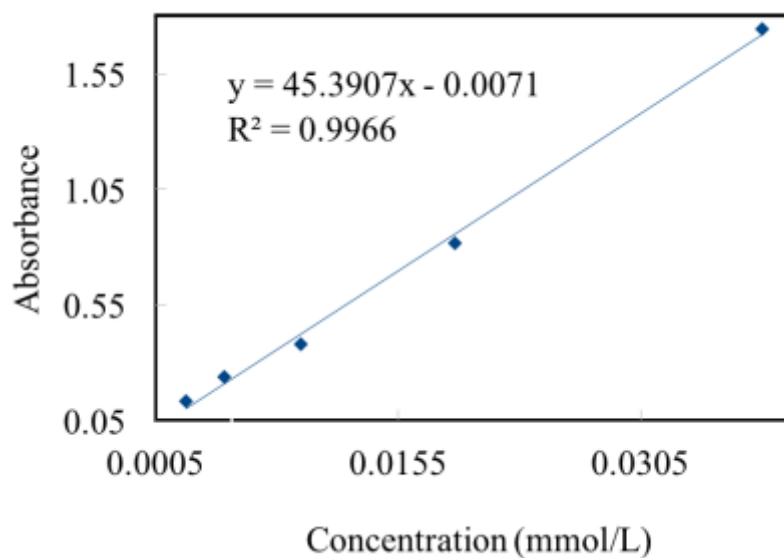


Figure B - 1: Calibration curve and line of best fit for raw curcumin in 40% EtOH.

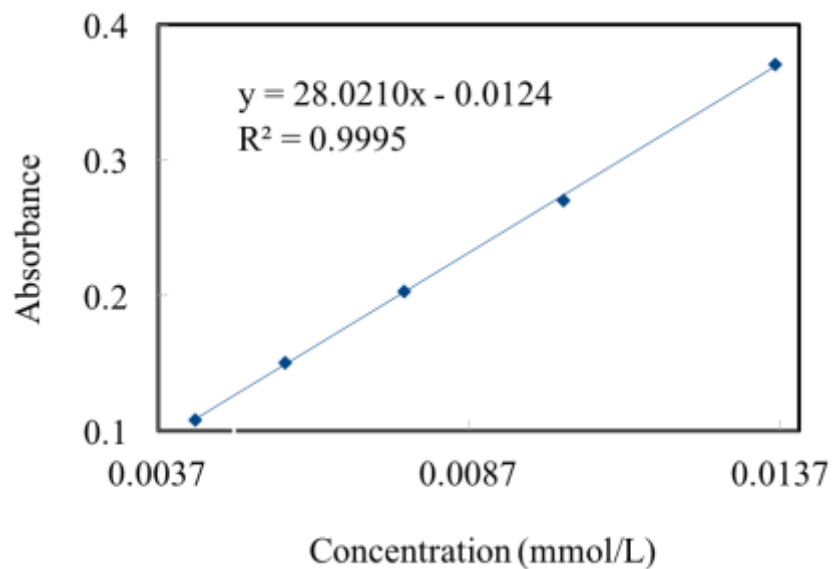


Figure B - 2: Calibration curve and line of best fit for raw folic acid dihydrate in 40% EtOH.

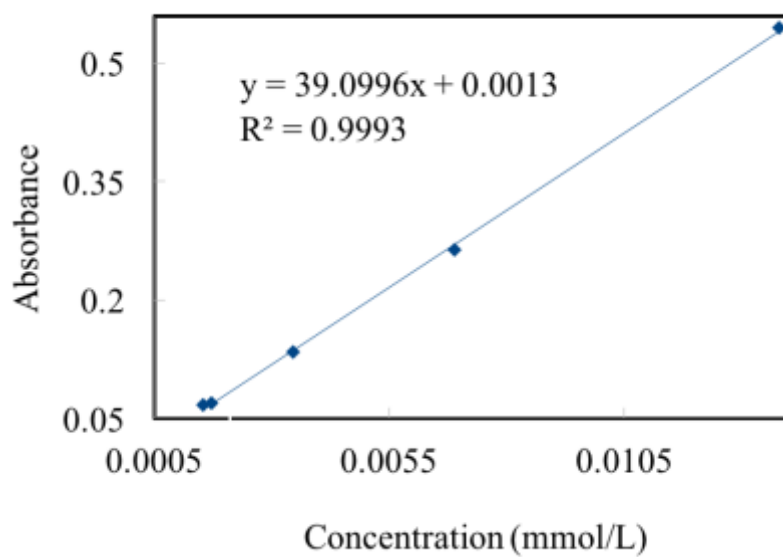


Figure B - 3: Calibration curve and line of best fit for co-amorphous mixture of curcumin and folic acid dihydrate in 40% EtOH.

Curriculum Vitae

Name: Jenna Marie Skieneh

Post-secondary Education and Degrees: University of Windsor
Windsor, Ontario, Canada
2011-2015 B.Sc.

The University of Western Ontario
London, Ontario, Canada
2015-2017 M.ESc

Honours and Awards: Larry Calvert Award
2017

Mitacs Globalink Research Award -MHRD India
2016

Dean's Honour Roll
2014-2015

Related Work Experience Teaching Assistant
The University of Western Ontario
2015-2017

Research Assistant
University of Windsor
2014-2015

Publications:

Published: **Skieneh, J.**; Khalili Najafabadi, B.; Horne, S.; Rohani, S. Crystallization of Eesomeprazole Magnesium Water/Butanol Solvate. *Molecules* **2016**, *21*, 544.

Submitted: **Skieneh, J.**; Rohani, S. A Review of Crystal Engineering via Non-Ionic Excipient Addition in the Crystal Lattice to Increase Drug Solubility and Bioavailability. *Crystal Growth and Design* **2017**.

Submitted: **Skieneh, J.**; Rohani, S. Efforts to Increase the Solubility of Rufinamide. *Journal of Crystal Growth* **2017**.

Submitted: **Skieneh, J.**; Dalvi, S.; Rohani, S. Co-amorphous form of curcumin-folic acid dihydrate with increased aqueous dissolution rate. *Crystal Growth and Design* **2017**.

Conference Presentations:

Skieneh, J.; Sathisaran. I.; Dalvi, S.V.; Rohani, S. (2017). Exploring the co-crystallization of curcumin. 24th Congress of the International Union of Crystallographers

Skieneh, J.; Green, J.R. (2015). The Monitoring of Competitive Nicholas Reactions to Determine Propargyldicobalt Hexacarbonyl Cation Stability. 43rd Southern Ontario Undergraduate Student Chemistry Conference